NN08201,2782

Propositions for the PhD thesis of Alan E. Green:

"The practical application of scintillometers in determining the surface fluxes of heat, moisture and momentum",

Wageningen, 24th January 2000.

1. Absorption scintillations can contribute to the Large Aperture Scintillometer signal if not appropriately high-pass filtered. (Dit proefschrift).
2. The Large Aperture Scintillometer has not changed significantly since the original design of Gerry Ochs in the 1980's. (Dit proefschrift).
3. Because path-averaged absorption scintillations are selectively low-pass filtered due to the magnitude of the sampling volume their spectral energy mainly reflects the large-scale behaviour of the atmosphere.
4. Scintillation presents a ground-based technique with the potential to path-average surface-flux emissions of CO_2, CH_4 and other trace gases at kilometre scales.
5. A 2-D drag anemometer and a 1-D sonic anemometer combination provide comparable measurements of the friction velocity and sensible heat flux to a single 3-D sonic anemometer. (Green et al., 1991).
6. A *kiwifruit volume meter* has a useful role in orchard management through monitoring fruit-size, susceptibility to water stress and predicting final crop yield. (Green et al., 1990).
7. The adage that science should be done for the sake of science is outdated. Although universities should take a fundamental approach to research they must be conscious of opportunities to commercialise any discoveries.
8. Postgraduate research is best performed on the other side of the World to avoid one's turn on the coffee roster

The Practical Application of Scintillometers in Determining the Surface Fluxes of Heat, Moisture and Momentum

De Praktische Toepassing van Scintillometers bij het Bepalen van de Oppervlaktefluxen van Warmte, Waterdamp en Impuls

Alan E. Green

Promotor:

Prof. dr. A. A. M. Holtslag

Hoogleraar in de meteorologie en luchtkwaliteit.

Co-promotor:

Dr. H. A. R. de Bruin

Universitair hoofddocent bij de leerstoelgroep meteorologie & luchtkwaliteit

Samenstelling promotiecommissie:

Dr. F. Beyrich – Deutcher Wetterdienst

Dr. W. Kohsiek – KNMI

Prof. dr. P.A. Troch – Wageningen Universiteit

Prof. dr. H.F. Vugts – Vrije Universiteit Amsterdam

NN08201,2932

The Practical Application of Scintillometers in Determining the Surface Fluxes of Heat, Moisture and Momentum

Alan E. Green

Proefschrift
ter verkrijging van de graad van doctor
op gezag van de rector magnificus
van Wageningen Universiteit,
prof. dr. ir. L. Speelman
in het openbaar te verdedigen
op woensdag 24 januari, 2001
des namiddags te vier uur in de Aula

IM 1604522

CIP- DATA KONINKLIJKE BIBLIOTHEEK DEN HAAG

Green, A. E.

The practical application of scintillometers in determining the surface fluxes of heat, moisture and momentum/ A.E. Green

Thesis Wageningen Universiteit. – With ref. – With summary in Dutch
ISBN 90 5808 336 5
Subject headings: Scintillation / surface flux measurements / large-scale

BIBLIOTHEEK
LANDBOUWUNIVERSITEIT
WAGENINGEN

For my Mother and my Father

Contents

1 Introduction 1

1.1 Background and objectives 1

1.2 Thesis structure 2

1.3 Complementary manuscripts 5

1.3.1 Large-aperture scintillometry: the homogeneous case 5

1.3.2 Scintillometer measurements of sensible heat flux over heterogeneous surfaces 6

1.3.3 Using a large-aperture scintillometer to measure absorption and refractive-index fluctuations 7

1.3.4 Measuring sensible heat flux over pasture using the C_T^2 profile method 8

2 Aspects and applicability of scintillometry in meteorology, hydrology and remote-sensing 11

2.1 Introduction 11

2.2 Comparing the scintillometer to conventional surface. Flux methods 13

2.2.1 The scintillometer 13

2.2.2 Eddy covariance 18

2.2.3 The profile method 20

2.2.4 The Bowen-ratio method 20

2.2.5 The water balance method 21

2.3 Flux measurements over heterogeneous terrain 21

2.4 The scintillometer as a tool for meteorological research 26

2.5 Remote-sensing using the scintillation method 29

2.6 Application of scintillation to water management and hydrology 30

3 The scintillation method 33

3.1 Introduction 33

3.2 Forms of $\Phi_n(\kappa)$ in the variance, inertial-convective and dissipation ranges 34

3.3 Wave propagation 39

3.4 Structure parameters 43

3.5 Estimating the surface fluxes from structure parameters 47

3.6 Summary 50

4 Surface-layer scintillation measurements of daytime sensible heat and momentum fluxes 53

4.1 Introduction 54

4.2 Theoretical background 55

4.2.1 The temperature structure parameter C_T^2 55

4.2.2 Estimation of sensible heat and momentum fluxes 58

4.3 Scintillometer design 61

4.3.1 Laser diode transmitter 61

4.3.2 Receiver 62

4.4 Experimental 63

4.4.1 Site descriptions and weather conditions 63

4.4.2 Instrumentation and data analysis 64

4.5 Results and discussion 66

4.5.1 C_T^2 comparison 66

4.5.2 Sensible heat flux and friction velocity 68

4.6 Summary 71

5 Sensible heat and momentum flux measured with an optical inner scale meter 73

5.1 Introduction 74

5.2 Theory 75

5.2.1 Large-aperture scintillometer (LA) 76
5.2.2 Laser scintillometer 76
5.2.3 The inner scale meter (ISM) 77
5.3 Experimental 80
5.3.1 Site description and weather conditions 80
5.3.2 Deployment of instruments 80
5.3.3 Reference flux instrumentation and supporting climatological measurements 82
5.3.4 Data collection and analysis 82
5.4 Results and discussion 83
5.4.1 Laser and large-aperture scintillometers 83
5.4.2 Inner scale meter 86
5.4.3 Latent heat flux 89
5.5 Summary 89

6 Use of the scintillometer technique over a rice paddy 91
6.1 Introduction 91
6.2 Theory 93
6.2.1 Relating fluctuations in temperature and humidity to the refractive-index 93
6.2.2 Equations for determining surface fluxes from structure parameters 97
6.3 Experiment site and conditions 100
6.4 Instrumentation and data collection 102
6.5 Results and discussion 103
6.6 Summary 107

7 Path-averaged surface fluxes determined from infrared and microwave scintillometers 111
7.1 Introduction 111
7.2 Theory 114
7.2.1 Extracting C_T^2 and C_Q^2 from the scintillometer signals 114
7.2.2 Linking the structure parameters to the surface fluxes 115

7.3 Experimental details 118
7.3.1 Site and weather conditions 118
7.3.2 The microwave scintillometer 120
7.3.3 The infrared scintillometer 120
7.3.4 Eddy covariance instruments 122
7.4 Results and discussion 123
7.4.1 The spectra of $C_{n_{mw}}^2$ 123
7.4.2 The effect of fluctuating Q on $C_{n_{mw}}^2$ and $C_{n_{ir}}^2$ 125
7.4.3 The wavelength dependence of $C_{n_{mw}}^2$ and $C_{n_{ir}}^2$ 128
7.4.4 Comparing the surface fluxes 130
7.4.4.1 Time series 130
7.4.4.2 Half-hour comparison 131
7.5 Summary 133

8 Estimating latent heat flux from a vineyard using scintillometry 135
8.1 Introduction 135
8.2 Theory 137
8.2.1 Structure parameters C_T^2 and C_Q^2 137
8.2.2 Sensible and latent heat fluxes 138
8.3 Experimental 142
8.3.1 Site description and instrumentation 142
8.3.2 Weather conditions and data collection 144
8.4 Results and discussion 145
8.4.1 Near-neutral and advective conditions 145
8.4.2 Unstable conditions 148
8.5 Conclusion 154

Summary 157
Samenvatting 161
References 167
Curriculum Vitae 177

1

Introduction

1.1 Background and objectives

This thesis presents a series of experiments using electromagnetic scintillation to infer the surface fluxes of heat, moisture and momentum. The scintillation technique is of interest to environmental researchers as a remote sensing method because it can provide a path-average of the surface fluxes over kilometre distances. Scintillometers can determine surface fluxes more rapidly than conventional flux measurement techniques and ultimately they may provide a solution to making these measurements over non-homogeneous surfaces.

This treatise asks the question, ***'how successful is the scintillometer method in determining surface fluxes and under what circumstances does it appear to fail?'*** To assist with this exposition a series of experiments conducted over varying surfaces and atmospheric conditions and using different scintillometer configurations are presented and discussed.

The background to this work begins in the early 1990's when the Author was working for the Horticultural Research Institute of New Zealand. The Environmental Physics Group based at Kerikeri began a series of experiments using scintillometers to remotely probe the atmosphere. The long-term objective of this work was to develop a routine monitoring system capable of providing continuous registration of the surface fluxes of heat, moisture and momentum at greater spatial scales than currently achievable by eddy covariance instrumentation. The work would it was hoped, bridge the gap between the canopy scale and meso-scale surface-flux measurements. It was expected the scintillation method would have applications in catchment hydrology and remote sensing validation using satellite thermal imaging. This thesis records experiments where the Author has made a major contribution and represents a sample

of the scintillation experiments undertaken over the last decade of the millennium. There is a time-line of continual instrument development, progressing from a visible semiconductor diode-laser scintillometer, to a HeNe gas-laser scintillometer, a near-infrared large-aperture scintillometer and finally a microwave scintillometer. Experimental results from different sites under a variety of atmospheric conditions have combined to underpin the thesis.

Essentially the purpose of this research was to develop a pragmatic approach for the scintillation method. Unforseen problems in instrument performance, theoretical assumptions and the prevailing atmospheric conditions have at times contrived to make scintillation measurements difficult if not outright impossible. Therein lies the value of this work, which is recognizing and defining some limitations of the method so that future research can be directed into resolving these shortcomings.

The research has had international collaboration with other institutes interested in scintillometry. These included the Royal Netherlands Meteorological Institute (KNMI) and the Meteorology and Air Quality Group at Wageningen University (WUMET) The Netherlands; NIAES, Japan; INRA (Bourdeaux, France); and the CSIRO (Australia). In particular Dr Wim Kohsiek (KNMI) suggested the construction of a microwave scintillometer and was very familiar with the NOAA designed large-aperture near-infrared scintillometer (LAS). This liaison and advice with the Author resulted in several field campaigns with the KNMI and WUMET. The WUMET graduate research program is responsible for scintillometers being installed World-wide in countries such as Turkey, China and Sri Lanka.

1.2 Thesis structure

This thesis consists of one review chapter and five experimental papers selected for their diversity and relevance to scintillation. The Author has contributed to other scintillation experiments and these are briefly summarized in Section (1.3). The experimental research has been progressive, beginning with a simple semiconductor laser-diode employed several meters above the surface and culminating with a two-wavelength scintillometer combination operating at 30 m above a valley floor. A common theme of each experiment is the application of Monin-Obukhov similarity theory (MOST) to determine the surface fluxes from the measured structure parameters of heat and moisture. Each of the experimental chapters have been

submitted for publication or published in scientific journals. Minor modifications have been made to each manuscript for inclusion in this thesis.

The important points and knowledge on scintillometry are presented in Chapter (2). The scintillometer method is reviewed in Chapter (3). Particular attention is given to the important components of the method including the spectrum of isotropic turbulence, wave propagation through this turbulence, the structure parameters of the refractive-index, heat and moisture and the application of MOST. Each of these steps has some approximation or limitation, which may affect the final surface flux calculation. Because scintillation is a subject which encompasses many scientific disciplines stretching from wave propagation theory through to micrometeorology, an experimentalist without a broad overview of the subject should be aware of the potential sources of error in the method. The review of Chapter (3) goes someway to assisting in this regard.

The first of the experimental papers (Chapter 4) discusses the use of a simple and inexpensive laser-diode as a scintillometer. The scintillometer was constructed and tested at a height close to the surface (z = 1.5 m) at two different locations that varied in surface roughness and was found to provide a reliable measurement of the friction velocity, u_* and sensible heat flux, H_{sc} over a propagation pathlength, L = 100 m. The Hill spectra describing isotropic turbulence in the inertial-convective subrange was used to correct the recorded signal log intensity variance, σ_I^2 for the effect of the inner-scale length, l_o. To determine l_o, an estimate of u_* was first taken from a cup anemometer averaged windspeed, u_c and a measure of crop height, h_c. The effect of signal saturation was seen in a comparison of the temperature structure parameter C_T^2 calculated from the scintillometer σ_I^2 and measured using a rapid-response thermocouple.

In Chapter (5) the dependence of a point-source scintillometer (HeNe gas-laser) on l_o was used to determine u_*. This was achieved by combining the HeNe scintillometer signal with the signal from a large-aperture near-infrared scintillometer (LAS). The LAS has minimal l_o dependence. The ratio of signal outputs indirectly provided a path-averaged measurement of u_*. H_{sc} was calculated from the LAS signal. This combination instrument, the Inner Scale Meter, was sensitive to small differences between scintillometer outputs and gave a coarse comparison of u_* to

eddy covariance measurements. The H_{sc} to H_{ec} comparison was reasonable despite using different propagation path-lengths for each scintillometer. As shown previously for the diode-laser scintillometer, a HeNe gas-laser scintillometer's signal could also saturate in strong turbulence. This restricted operation of the Inner Scale Meter to short path-lengths.

The LAS was used over an irrigated rice paddy in Japan during the end of the rice harvest and the approach of the typhoon season. Chapter (6) describes the problems encountered using a scintillometer in the presence of large latent heat, E_{sc} and small sensible heat fluxes. Several problems were encountered. The first of these was that the correlated T-Q fluctuations made a significant effect on the scintillometer signal variance. Secondly absorption scintillations may have increased σ_I^2 and thirdly the LAS can not determine the direction of the sensible heat flux. These factors complicated data interpretation.

Following the less than satisfactory result using a LAS to estimate H_{sc} over a rice paddy, a microwave and LAS were combined as a two-wavelength scintillometer to determine both E_{sc} and H_{sc}. This experiment took place at Ahipara in the far North of New Zealand (Chapter 7). The height above the surface (z = 10 m) and the propagation distance (L = 3 km) were much greater than the previous experiments. The surface was very flat and homogeneous. Comparisons of H_{sc} and E_{sc} made to H_{ec} and E_{ec} (measured at the path midpoint) were reasonable. The method assumed a perfect correlation between T and Q. The effect of low frequency fluctuations in path-averaged Q caused an overestimate in H_{sc} and E_{sc}. The microwave signal displayed inertial subrange behavior and was therefore capable of determining C_n^2 at microwave frequencies. Two LAS receivers placed side-by-side and recording the same signal variance systematically differed by 5%.

The final experiment recorded in this thesis (Chapter 8) built on the previous experience gained using the two-wavelength scintillometer. Now the scintillometer beams were much higher with z = 30 m and propagated across a 2 km wide valley. The valley was well irrigated but the surrounding countryside was very dry. When windspeeds were low agreement between H_{sc} and E_{sc} with H_{ec} and E_{ec} was reasonable. With advection and entrainment of dry and warm air into the valley H_{sc}

and E_{sc} overestimated the eddy covariance measurements. For very unstable conditions E_{sc} and H_{sc} could be calculated without prior knowledge of u_*. As the convective boundary layer (CBL) inversion passed through the scintillometer beam it caused additional signal variance and resulting overestimates in H_{sc} and E_{sc}.

1.3 Complementary manuscripts

The Author has contributed to other scintillation research during this decade. These contributions included involvement in field experiments, instrumentation design and secondary authorship on the subsequent manuscripts. Some of the results have impacted on the understanding and conclusions drawn for the five experiments described in this thesis. A short explanation of each relevant paper is provided.

1.3.1 Large-aperture scintillometry: the homogeneous case

Authors: McAneney, K. J., Green, A. E. and Astill, M. S. Published in the Journal of Agricultural and Forest Meteorology, **76** (1995), 149-162.

The LAS is used in most of the experiments recorded in this thesis but is generally combined with other scintillometer types. In this paper the physical principles and design criteria specific to the LAS were reviewed. A field-test over a pathlength, L = 350 m and at z = 1.4 m gave values of H_{sc} and u_* (cup anemometer) in close agreement with H_{ec} and u_* taken from eddy covariance instruments (Figure 1.1). A maximum pathlength of L = 1.7 km was calculated for a height, z = 2 m before signal saturation became a limiting factor in LAS performance. The shorter averaging times and longer pathlengths that are possible using the LAS compared to laser type scintillometers were discussed. The study clearly demonstrated the path-averaging capabilities of the LAS for the homogeneous surface case.

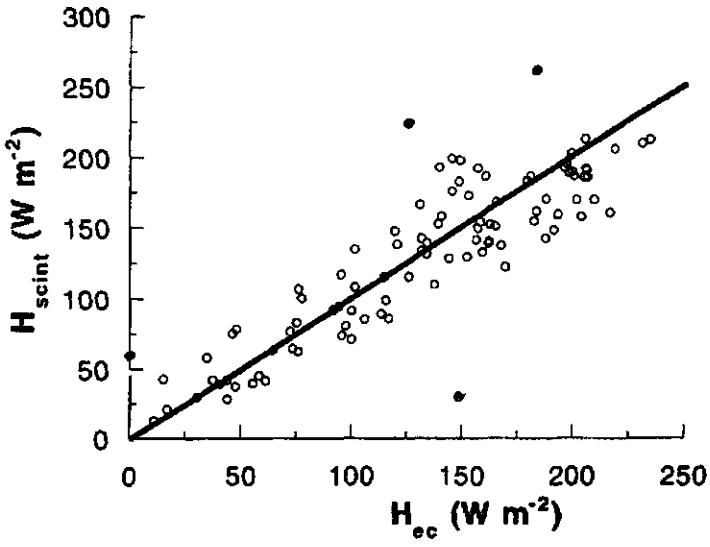

Figure (1.1). A comparison of sensible heat fluxes as measured by scintillation and mean windspeed and by eddy covariance. The solid line indicates the 1:1 relationship.

1.3.2 Scintillometer measurements of sensible heat flux over heterogeneous surfaces

Authors: Lagouarde, J-P, McAneney, K. J. and Green, A. E. Published in the Proceedings; Scaling up in hydrology using remote sensing (1996). Institute of Hydrology, Wallingford, UK.

The experiment reported in this manuscript provided a test of the LAS path-weighting sensitivity. Different LAS apertures and pathlengths were combined over surfaces of varying aerodynamic roughness and surface wetness. Eddy covariance instruments were positioned at points along a two-component path (maize to fallow) and attributed a specific weighting for each directly measured H_{ec}. The average of the H_{ec} was shown to agree very well with H_{sc} indirectly calculated from the LAS (Figure 1.2). The path-averaging capability of the LAS and its response to a simple step change in surface roughness and the different surface energy balance components, is reassuring for any planned research over non-homogeneous terrain.

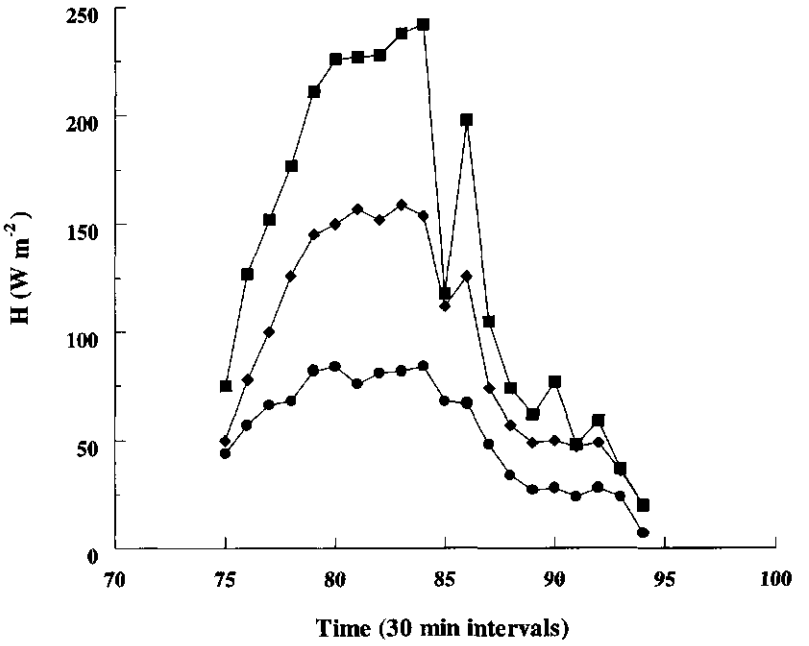

Figure (1.2). Time series of sensible heat derived from the scintillometer (◆) and direct measurements by eddy covariance in the maize (●) and fallow (■) fields.

1.3.3 Using a large-aperture scintillometer to measure absorption and refractive-index fluctuations

Authors: Nieveen, J. P., Green, A. E. and Kohsiek, W. Published in the Journal Boundary-Layer Meteorology, **87** (1997), 101-116.

The LAS measured the contributions of the refractive and absorption fluctuations to the measured scintillations in a near-infrared wavelength region. Because the LAS used an infrared light emitting diode as it's radiative source whose irradiance overlapped strongly absorbing water vapor lines it could be adapted for such measurements. Absorption scintillations did not contribute to σ_I^2 if they occurred outside the scintillation bandwidth of the LAS set by the electronics. The lower cut-off frequency for this bandwidth was 0.03 Hz. Observations taken towards dusk as C_n^2 decreased (Figure 1.3) indicated some absorption scintillations exceeded this cut-off frequency and may have contributed up to 5% of the recorded σ_I^2. This

result goes someway in explaining the dependency of the LAS signal variance to changes in path-averaged Q. Such situations were encountered and described in the experiments of Chapters (6) and (7).

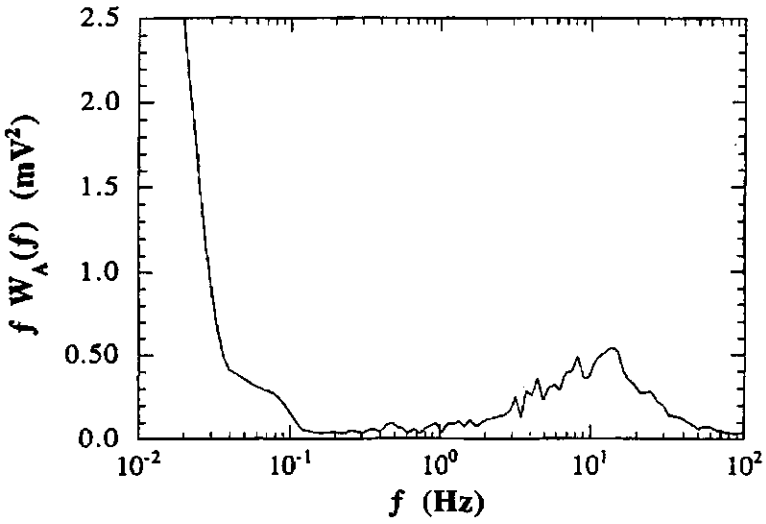

Figure (1.3). The temporal spectral variance. The peak to the right represents the major proportion of refractive energy. Note the intrusion of absorption scintillations and their contribution to the variance at frequencies smaller than 0.03 Hz.

1.3.4 Measuring sensible heat flux density over pasture using the C_T^2 profile method

Authors: Nieveen, J. P. and Green, A. E. Published in the Journal, Boundary-Layer Meteorology, **91** (1999), 23-35.

This experiment was an addition to the test of the microwave scintillometer reported in Chapter (7). Two LAS scintillometer links were set up but at different heights of z = 1.5 m and z = 10 m. C_T^2 scales with increasing height as $z^{-4/3}$ in unstable atmospheric conditions. The ratio of the two LAS signals provided an indirectly calculated stability length scale, L_{mo} from which a path-averaged u_* was determined. H_{sc} was then calculated using u_* and either of the scintillometer signal

outputs. Agreement between final values of H_{sc} compared to H_{ec} was reasonable with a scatter of points about a 1:1 line. A time series of H_{sc} and H_{ec} was presented for the first time using this approach (Figure 1.4). This method provided one solution to obtaining a path-averaged u_* over non-homogeneous surfaces and warrants further investigation.

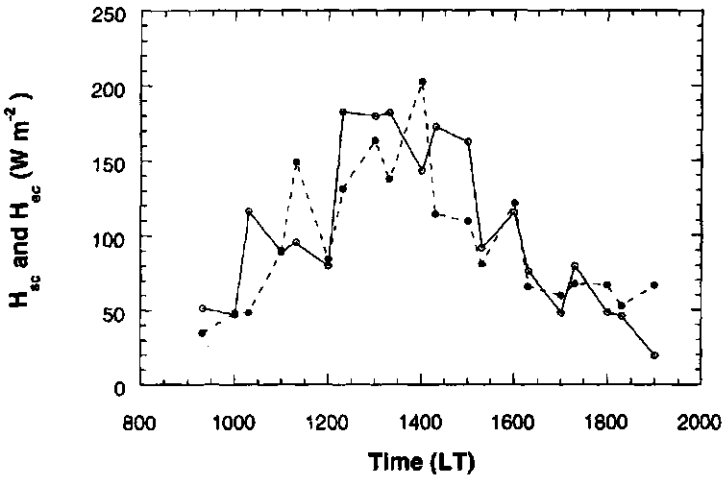

Figure (1.4). Time series of sensible heat fluxes for unstable atmospheric conditions. H_{sc} and H_{ec} are the dashed and solid lines respectively.

2

Aspects and applicability of Scintillometry in Meteorology, Hydrology and Remote-Sensing

2.1 Introduction

Recognising the potential of the scintillation method for inferring the surface fluxes of heat, moisture and momentum is a fairly new and emerging concept. It is not obvious nor is it likely the average boundary-layer meteorologist, hydrologist or remote-sensing expert will have much appreciation of the advantages of the scintillation technique. This unfamiliarity with scintillometry is partly due to its recent rebirth in the last decade but also that the foundations lie in scientific disciplines such as electromagnetic wave propagation, subjects quiet outside their general sphere of interest. From the onset, scientific papers dealing with the scintillation method can be difficult to understand. Some effort is required to appreciate the link between the theory and the pragmatic application of the technique. And although propagationists seek to enlighten the average environmental scientist by publishing their findings in targeted scientific journals the text can still be cumbersome and difficult to comprehend. The papers contained in this thesis fall into this category being technical in content and producing mainly experimental observations. The reason for this bias is primarily historic in origin, as the author of this thesis has spent much time building and testing micrometeorological instrumentation. As mentioned previously, this work instigated collaboration throughout the World with scientists from the Royal Netherlands Meteorological Institute (KNMI) and the Meteorology and Air Quality Group at Wageningen University (WUMET), The Netherlands; The Japanese National Institute of Agro-Environmental Science (NIAES); INRA (Bourdeaux), France; The Observatory at Lindenberg of the German Weather Service (DWD),

Germany and the CSIRO, Australia. This aspect of scintillometer research importantly bridges the gap between the theoretical background and the use of the scintillometer in different experimental configurations. Advances in theory and observations in the field improve the instrumentation and one can not exist without the other. When the point is reached whereby the scintillometer is referred to without need for justification as *the instrument of choice for path-averaging surface fluxes*, then it will have come of age.

It is the objective of this chapter to place the scintillometer alongside the conventional flux gathering methods and explain the pros and cons of each approach. In particular much is made of the ability of the scintillometer to spatial-average the surface fluxes and this is claimed as a distinct advantage over the so-called point measurement methods. Large-scales are attractive to modellers because surface fluxes need to be parameterised at meso-scales to be useful as inputs for their atmospheric process models. Surface verification of satellite remote sensing techniques also requires kilometre pixel resolution and hydrological studies operate at catchment scales. Of course the greater the scale the more heterogeneous the landscape is likely to become. How well the final calculation represents the path-averaged surface flux depends on the theoretical link between what the scintillometer measures and semi-empirical theory that assumes amongst other factors homogeneous terrain. At this stage of the scintillation development making measurements over changing surface roughness and radiation loading is in its infancy and some discussion is warranted.

The role of scintillation in meteorological research and projected future trends for this method are presented within a framework of a simple model for the well-mixed convective Planetary Boundary-Layer (PBL). The ramifications for using scintillometers for modelling and measuring within the Stable Boundary Layer (SBL) are also considered.

Scintillometers are well suited for complementing remote-sensing techniques and some examples of ongoing research in this area will be given. The potential of the scintillometer to provide answers on water usage at large scales impinges on the competition between industry, food production and human consumption. As water becomes a scarce and more valuable resource its management relies heavily on quantitative measurements made at regional scales. The scintillometer in particular the microwave type provides a mechanism to achieve this goal.

2.2 Comparing the scintillometer to conventional surface flux methods

2.2.1 The scintillometer

We preface this section with an outline of the scintillation method and then review its supposedly inherent advantages over the more conventional surface flux techniques. In the first instance we have already made issue of the scintillometer's ability to line-average surface fluxes but we haven't described how this is achieved or any assumptions and limitations of the method. In the discussion that follows we will avoid unnecessarily complicated theory and focus on the primary operation of the scintillometer.

A scintillometer is simple in construction consisting of a source of light of wavelength (λ) that is collimated and directed at a height (z) above the surface under study, to a receiver system positioned at some distance (L). This receiver system collects the light and directs it onto a detector (Figure 2.1). Any changes in intensity or phase that occur as the light wavefront travels through the atmosphere are cumulative, and presented as spatial-averaged changes. These modifications to the fabric of the light signal arise from eddies of heat and moisture refracting the light beam along the path. It is via this theoretically complicated but intuitively simple mechanism that we link the surface fluxes of sensible heat (H) and latent heat (LE) to wave propagation in a turbulent atmosphere. If for instance the light source emits energy in the visible part of the electromagnetic spectrum and the surface heating is strong enough then an observer standing at some distance from the transmitter will see the object distorted or scintillate, a likely origin of the designation *scintillometer*. These eddies represented in Figure (2.1) as circles of various diameters can be blown through the beam or rise vertically from the surface. It is through the large-scale processes of solar heating of the surface and wind shear that large eddies first originate and are broken up to all sizes. They have a known constant energy redistribution within a spatial bandwidth known as the inertial-convective subrange. Turbulence within this subrange is considered to be isotropic and homogeneous, expressively for the purpose of developing theoretical descriptions of the energy redistribution. Such an idealised atmosphere never occurs in nature. The outer-scale length (L_o) provides the lower spatial limit, which is approximately half the

measurement height. Beyond this limit the atmospheric turbulence is governed by large-scale processes and no suitable description of the energy distribution with scale size exists. At the upper limit of the inertial-convective range the inner-scale length (l_o) describes the transition to the dissipation range where kinetic energy of motion is no longer lost through inertia but now dissipated as heat.

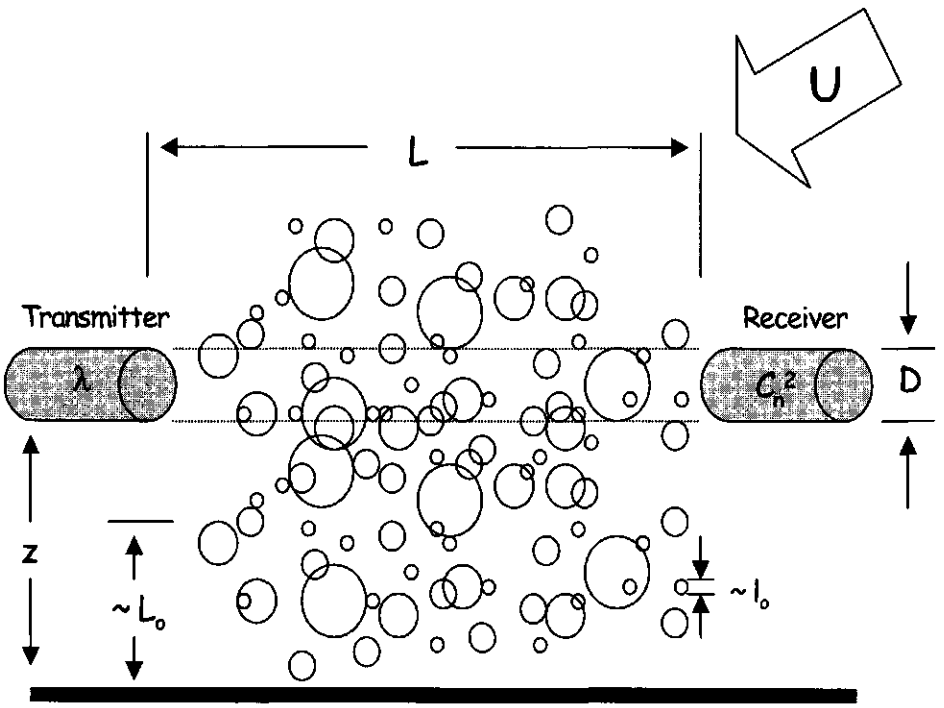

Figure (2.1). Idealised schematic of a scintillometer propagating light of wavelength (λ) over a pathlength (L) in a turbulent atmosphere consisting of eddies of heat and moisture. Surface heating and the wind speed (U) transport a range of eddy sizes (L_o - l_o) through the light beam of a known diameter (D) which distort the signal as it passes over the surface. The strength of this path-averaged refractive turbulence is quantified by the refractive-index structure parameter C_n^2, which is needed to indirectly calculate H and LE.

One obvious shortcoming is that the scintillometer merely reacts to an eddy passing through its beam, it does not distinguish its direction. Because a scintillometer is designed to monitor the logarithmic intensity variance then it does not require an absolute calibration. The implications are clear for routine monitoring as falling power supply levels or dirty optics will not hinder proper data collection and instrument construction is vastly simplified. A point source/detector scintillometer is most sensitive to Fresnel ($F = \lambda L$) sized eddies and a large aperture scintillometer to eddy sizes that are close to its aperture diameter, scales that occur within the inertial-convective subrange. Statistically then a scintillometer extracts information for surface flux calculations at bandwidths centred at higher frequencies than the conventional methods and so in principle can determine a value for surface fluxes within minutes. The perceived advantage here is the ability to respond to atmospheric processes that are happening at these time scales, such as interpreting the energy balance under very stable atmospheric conditions. Certainly as the atmosphere is never truly stationary or homogeneous being able to determine an average surface flux faster than the time scale of large-scale variations is surely of benefit. Care must be taken though that the selection of shorter averaging times does not compromise the time-scale of the turbulent processes under study.

An unfavourable consequence of the sensitivity of the scintillometer to eddy sizes is that at some combination of aperture diameter and propagation distance, signal saturation will occur in strong turbulence. A discussion on the saturation phenomena is presented in Chapter [3] but there are some simple rules constructed around spatial scales that help explain the performance of different scintillometer types as follows. If we first consider laser-type scintillometers then we view them as having point-sized apertures the order of millimetres. They are highly likely to operate at visible to near-infrared wavelengths, which from within the family of scintillometer types is considered the shorter wavelength range. For a visible red laser at 670 nm operating over a path length of 100 m, $F = 8$ mm, a number approaching the magnitude of l_o. The laser scintillometer will require correcting for inner scale effects using the appropriate spectrum of Hill (1978). This functional correction requires knowing l_o, entailing auxiliary micrometeorological measurements to be performed. There are other options such as the Inner Scale Meter of Hill et al. (1992) or the Biochromatic Technique of Thiermann and Grassl (1992) which extract l_o from

a combination of different scintillometers. There is even a commercial type of scintillometer (Thiermann, 1992b) available which uses two beams originating from the one source with the displacement the order of l_o. Being able to correct for l_o is only one factor plaguing laser scintillometers as their small apertures mean they see many eddies and so suffer from signal *saturation* in strong turbulence. Effectively the variation in the strength of the turbulence is no longer log-normal and the theoretical assumptions that lead to a measure of the path-averaged strength of refractive turbulence are invalid. Laser scintillometers are at best only useful near the ground when $L < 200$ m. The refractive-index structure parameter C_n^2 is the spatial statistic used as a measure of the path-averaged strength of refractive turbulence. Because approximately $C_n^2 \propto z^{-4/3}$, then through using the laser scintillometer at tens of metres from the surface the potential for signal saturation can be avoided and there will be a minimal l_o dependence because, $F > l_o$. As an example, Kohsiek (1985) used a CO_2 laser over a distance of 5.9 Km and at a height of 40 m. Here, $F > l_o$ and so the spectrum of refractive turbulence in the inertial-convective range did not require correction for the effect of l_o.

Understandably researchers preferred to avoid saturation leading the way to the invention of the large aperture scintillometer (LAS), Wang et al. (1978). The aperture (D) is large in the dimensional sense it is generally much greater than F and the inner scale. It still operates as a scintillometer but it performs an average of all the small-scale eddies across the aperture and requires no correction for the inner scale. This scintillometer operates in the near-infrared wavelengths, is simple to construct and has enjoyed the greatest popularity being easy to operate over kilometre distances. The LAS signal will eventually saturate if operated over large distances in strong turbulence but again like the laser scintillometer this can be avoided to some degree by increasing the height above the surface. Following McAneney et al. (1995) we present the criterion for field utilisation of the LAS as, $l_o < F << D << z/2$.

For a microwave scintillometer used by Green et al. (2000) an aperture diameter of 0.6 m implies there is little likelihood of signal saturation but there exist other limiting factors. One of these is surface reflection a variable obviously affected by the surface roughness. The microwave scintillometer must be mounted at sufficient height to avoid signal distortion through ground reflection. This is an issue particularly troublesome over water which at microwave wavelengths, acts as a big

mirror to a microwave signal. The cost of a microwave scintillometer, as much as US$50,000 is generally too expensive for the average researcher to consider even though the instrument is a preferred option for determining *LE* as it is most sensitive to humidity fluctuations. At microwaves absorption by water vapour cause low frequency absorption scintillations that must be screened from the refractive scintillations. Absorption scintillations likely have their origin in the low frequency atmospheric structures at scales the order of the pathlength.

Unlike the eddy covariance method the scintillation method indirectly calculates the surface flux from a measurement of the variation in the received signal strength. By itself, C_n^2 is not particularly informative to meteorologists wishing to know the components of the surface energy balance but it provides a starting point. Depending on the operating wavelength then the scintillometer is more or less sensitive to combinations of temperature and humidity fluctuations. At visible to near-infrared wavelengths fluctuations in the refractive-index of the atmosphere are caused mainly by temperature changes. C_n^2 is closely related to the corresponding temperature structure parameter C_T^2 from which a calculation of *H* can be performed. It should be mentioned though that even at these wavelengths when the relative humidity fluctuations become large compared to the temperature fluctuations, such as over irrigated surfaces, a correction incorporating the covariant temperature-humidity fluctautions is necessary. This term tends to originate from point measurements rather than spatial averages. At microwave wavelengths both humidity fluctuations and correlated temperature-humidity fluctuations contribute to C_n^2 with the humidity structure-parameter C_Q^2 and the temperature-humidity structure parameter C_{TQ} becoming the important component parts. This proportioning of the structure parameters depending on their wavelengths can be seen in Table (7.1) of this thesis. A combination of microwave and visible to near-infrared scintillometer is then required to determine *LE*. This procedure assumes temperature and humidity are well correlated in the inertial-convective subrange.

Derivation of turbulent fluxes from scintillation measurements assumes C_T^2 obeys Monin-Obukhov (MO) scaling in the atmospheric boundary-layer. This scaling relationship is semi-empirical and untested over heterogeneous terrain. Scaling C_T^2 using MO restricts measurements to homogeneous terrain and requires a stationary

atmosphere. These are prerequisites that are difficult to achieve in practice particularly over extended pathlengths. Another issue, not unlike the extreme transitions common to the Bowen-ratio method is that as the atmosphere switches state from unstable to stable conditions, for a brief moment, spatial fluctuations in all scalars become very small. Both C_T^2 and C_Q^2 are observed to decrease orders of magnitude and corresponding surface flux calculations are in error.

Unless the atmosphere is very unstable then mechanical mixing through wind shear, along with solar heating of the surface contribute to the flux and both must be accounted for in the calculations. Some method of measuring the friction velocity (u_*) is required which can be extracted from eddy covariance instruments or simpler windspeed measurements and rule of thumb assumptions about the surface roughness.

2.2.2 Eddy covariance

The eddy covariance technique directly measures the turbulent fluxes at a local fixed position. As the majority of the energy is contained at low frequency, temporal integration extends tens of minutes to capture the largest and slowest structures. The time-averaged approach is expected to approximate an ensemble average in the sense of being a spatial average of the turbulent field of eddies being transported past a point in space. This contrasts with the scintillometer method, which spatially averages all the turbulent eddies crossing its path in a very short moment of time. The turbulence sensors required for the wind components are these days robust enough for continuous measurements in all three dimensions. However the instruments to measure the scalar concentrations still struggle with the problems of being delicate, expensive and difficult to calibrate and being fast enough (sampling rate > 10Hz) to see all the eddies contributing to the surface flux. They require skilled technicians to operate, must be cleaned daily and necessitate a range of corrections to the algorithms. In addition the eddy covariance technique requires that the temporal cospectra of the vertical wind component and the scalar fluctuations must extend to very low frequencies. Therefore quite apart from dealing with the low frequency drift associated with many of these instruments the issue of atmospheric stationarity may be compromised over the minimal integrating period of 30 minutes. Compounding their usage is the issue of flow distortion. The very act of placing the sensors in the

wind flow distorts the measurement. The spatial positioning of both the wind and the scalar sensor are vital to ensure an accurate representation of the measured flux ie, they should both see the same eddy together or phase distortions will cause coherence errors particularly in light winds. For stable conditions the percentage error in flux calculations is worse as the cospectra extends past the upper frequency response of the combined instruments. Nevertheless the eddy covariance technique is widespread in usage and has been further adapted for CO_2 and CH_4 fluxes. Unlike a decade ago there is a variety of commercial instruments available to the researcher.

In general, scintillation data show a smoother diurnal course for the sensible heat flux density than the eddy covariance data (see later). An example of this is shown in Figure (2.2), taken from De Bruin (1998).

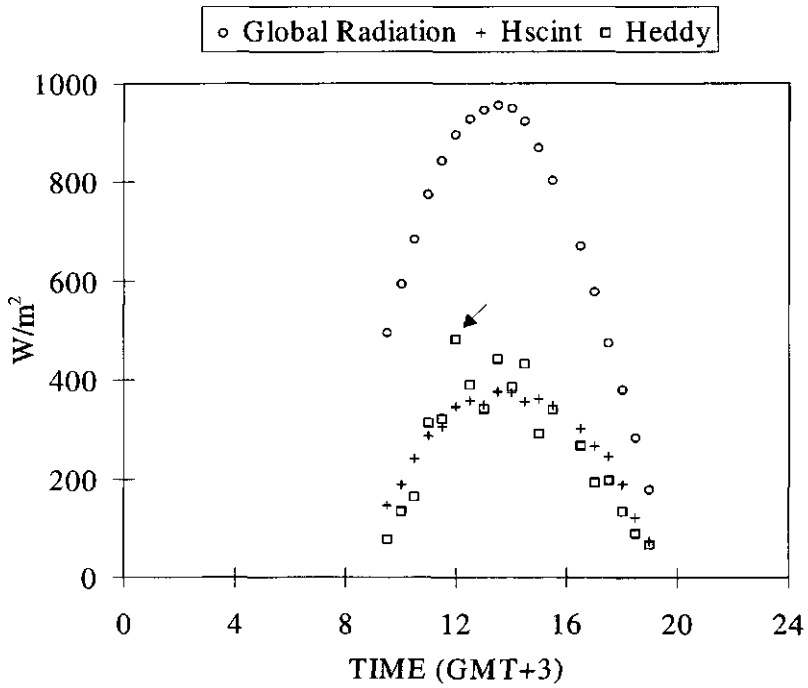

Figure (2.2). Daily course of H_{scint} and H_{eddy} along with the global radiation observed at Creta on 3rd May, 1994. The arrow indicates an eddy covariance data point that is extreme in transition when compared to its scintillometer counterpart. Reproduced from De Bruin, 1998.

This smoothness of the scintillometer data is due to integration over many eddies passing through the beam and measurements made in the inertial-convective subrange are more readily available than the eddy-covariance data.

2.2.3 The Profile method

This method is relatively easy to implement and incorporate into models but requires precise measurements of the vertical gradients of the mean meteorological variables. This method depends on Monin-Obukhov similarity theory for flux calculations and assumes a strong correlation between temperature and humidity fluctuations. The sensors are mounted and vertically displaced on masts that must be centred in the field and satisfy fetch requirements. Note, the measurement accuracy depend on height and is most stringent at the highest measuring level. As a result the profile method is difficult to apply over tall vegetation. Physical disturbance of the measuring field can lead to non-representative fluxes. See for instance Beljaars et al. (1983) who observed significant deviations from the "standard" Monin-Obukhov profiles due to obstacles in an almost perfectly flat polder landscape in the Netherlands. The method is sensitive to small systematic measuring errors, because the vertical differences of temperature and wind speed are small, especially over rough surfaces. The technique is a point-space design requiring an averaging time of tens of minutes to successfully integrate all eddies contributing to the flux.

2.2.4 The Bowen-ratio method

The Bowen-ratio technique is a relatively easy method to implement and it circumvents the need to measure H and LE directly. It is also a profile method, but "fetch errors" might cancel as long as they affect temperature and humidity fields in the same way. Precise measurements of the net radiation (R_n) and the ground heat flux (G) are required, measurements that are not trivial. Furthermore this approach relies on a similarity of the turbulent transfer mechanisms for heat and moisture so that their eddy diffusivity are equal. De Bruin et al. (1999) pointed out that this assumption might be violated for conditions of strong advection or conditions where one of the fluxes is so small that non-local effects play a role. For instance, over a

very flat, extensive, but dry terrain in La Crau (S. France) temperature and humidity appears not to be similar De Bruin et al. (1991). The Bowen-ratio technique works well for *H* and *LE* but the method is not easily applied to other scalar fluxes.

The instrument tends to be expensive and is bulky compared to eddy covariance instruments. Like the latter it also is a point measurement method needing integration periods of 30 minutes duration and requires orientation into the mean wind flow with the masts in the centre field in order to obtain reliable results. To reduce systematic errors in the sensors a mechanical system reverses their vertical alignment every 15 minutes. The method fails when the Bowen ratio is between -1.5 and -0.7, i.e. close to -1. This can occur during the transition hours around sunrise and sunset. It continues to enjoy a degree of popularity with researchers and a commercial system is currently available.

2.2.5 The Water balance method

The hydrological water balance method is useful as it provides catchment scale estimates of evaporation. The method yields evaporation on a large spatial scale, but its main drawback is that this is only possible on large time scales. It also relies on the assumption of sub-surface water flows that are often difficult to verify in practice. It requires a network of stream/river flow recorders and rain gauges that must be maintained and monitored on a regular basis and is typically labour intensive. It is currently the preferred method for the field hydrologists.

2.3 Flux measurements over heterogeneous terrain

Surely the most important feature of scintillometry is that it bridges the gap in spatial scales from the conventional point measurement systems discussed above to the several kilometre pixel resolution demanded by meso-scale atmospheric models, satellite imaging and catchment hydrology. The very act of performing kilometre scale measurements means the scintillometer will be most likely propagating its beam over undulating heterogeneous terrain and through an intermittent turbulent atmosphere. The reader will be asking himself, "how it is now possible to determine *H* and *LE* as the Monin Obukhov similarity theory underpinning the scintillometer method has been compromised?"

Certainly when we review the experiment conducted by Lagouarde et al. (1996) who used a LAS to measure a path-averaged H over a maize to fallow transition (600 m total pathlength) then we see the effect of having similar aerodynamic characteristics but different energy partitioning. In this example the scintillometer was mounted several metres above the surface. Naturally the fallow had the greater H but when averaged with that from the maize and accounting for the scintillometer's bell-shaped weighting curve, the eddy covariance agreement to the path-averaged scintillometer H is excellent (see Figure 1.2). As the experiment continued, then a contrast between the maize and fallow surface roughness developed with the maize reaching 3.3 m high and the fallow filling in with approximately 40% foliage at a 30 cm height. A comparison of path-averaged C_n^2 with the eddy covariance weighted C_n^2 agreed to within 2%, but a scintillometer determined H was not attempted because of the stark contrast in aerodynamic roughness. There was really no justifiable method that could be used to calculate path-averaged H.

Apparently a solution to this dilemma is to operate the scintillometers at a greater height, what has been discernibly labelled the *blending height* (Wieringa, 1986). At this height typically 30 to 50 m, the proposition is that the scintillometer *sees* an area-averaged flux even though the sub-surface fluxes can be markedly different. And, because this height still lies within the surface boundary-layer then Monin-Obukhov similarity theory is expected to be applicable. Operating at height has the disadvantage that stable platforms must be found for the scintillometer transmitter and receiver. De Bruin et al. (1996) and Green et al. (2000) solved this problem by operating their scintillometers across valleys in Crete (z = 70 m) and New Zealand (z = 30 m) respectively. At this height and during daytime atmospheric conditions are considered close to local free convection. The implications are that u_* is a minor player and the fluxes derive principally from the buoyant transport of heat and moisture without mechanical mixing. This markedly simplifies the flux calculations using both LAS and microwave type scintillometers and removes the need to measure u_*.

In what follows we present two examples of the effectiveness of the blending height concept. Firstly, an experiment was conducted in the Flevopolder in Holland (Meijninger et al., 2001). Because this is an area of land recovered from the sea it is particularly flat and has been planted in a chessboard configuration of vegetable crops

having various surface roughness and water demands. Dotted about the landscape are wind turbines providing a perfect means to mount the scintillometers tens of metres above the surface and propagate their beams over kilometres from farm to farm.

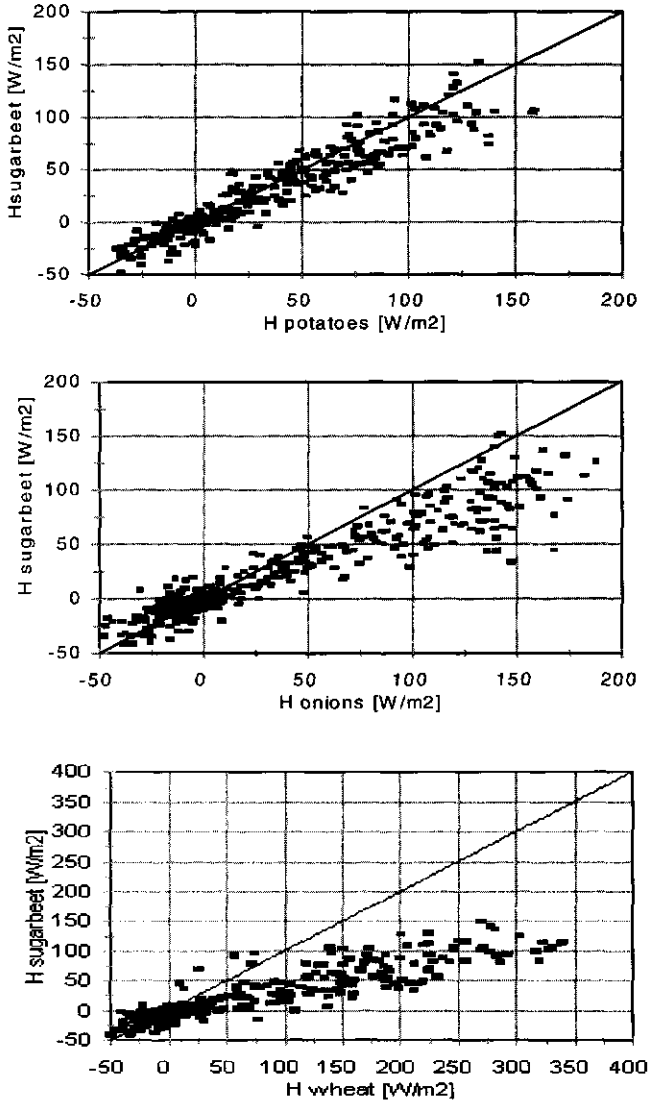

Figure (2.3a). A plot of the measured eddy-covariance fluxes (one crop compared to three others), showed differences in sub-surface sensible heat fluxes. Reproduced from Hoedjes and Zuurbier, 1999.

Eddy covariance instruments placed within the crops directly under the beam calculate the surface fluxes at the source whilst the scintillometer beam at 10 m areal-averaged all the flux sources. Figures (2.3a, 2.3b, 2.3c) show preliminary results from this experiment (Hoedjes and Zuurbier, 1999).

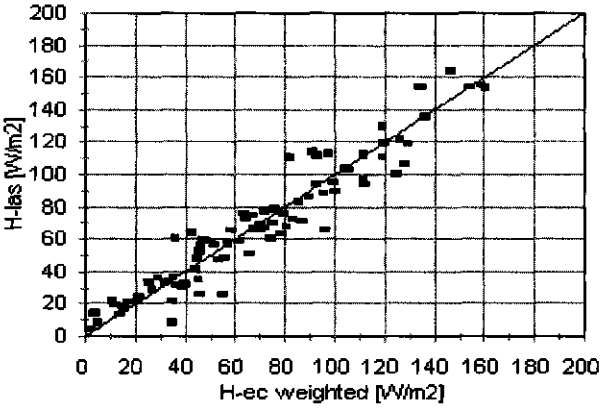

Figure (2.3b). Comparison of the path-weighted, averaged eddy covariance and LAS sensible heat fluxes. Reproduced from Hoedjes and Zuurbier, 1999.

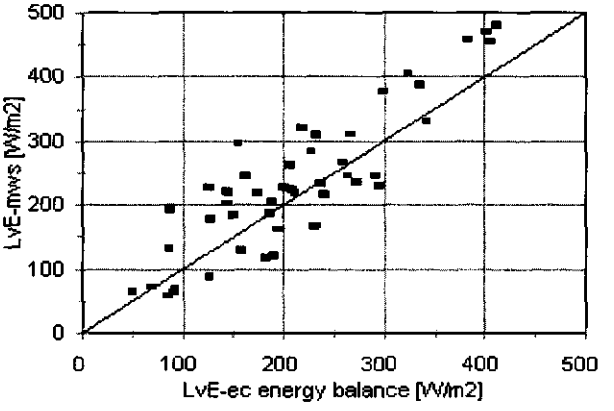

Figure (2.3c). A comparison of estimated path-averaged evaporation using the microwave scintillometer and the weighed mean of the eddy covariance results (LE = R_n - G- H). Because the energy balance did not close, no plot of the microwave scintillometer LE versus LE eddy covariance is presented (from Meijninger et al., 2000).

The LITFASS experiment, see Beyrich et al., (2000a) provided a further test of the blending height concept over slightly undulating terrain near Lindenberg (Germany) that varied from forest, agricultural fields to lakes (Figure 2.4).

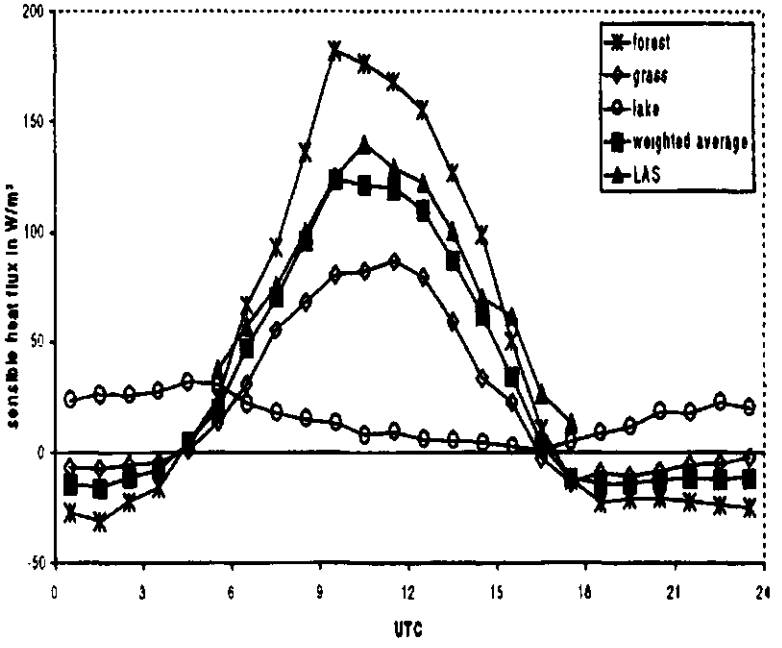

Figure (2.4). Mean diurnal cycle of the sensible heat flux over main land-use classes, as a land-use, weighed average and from the LAS measurements in the LITFASS experiment (taken from Beyrich et al., 2000a).

In both experiments the weighted-averaged measured fluxes are in good agreement with those taken from the LAS. The experimental indications are that this is a workable solution to measuring fluxes over heterogeneous terrain. This is not the case for close to the surface measurements.

2.4 The scintillometer as a tool for meteorological research

What does scintillometry offer to the discipline of meteorology and how is it any advantage over conventional methods? In general, meteorology deals with processes on a spatial scale of 1 km or more. This applies to research on the planetary boundary layer (PBL), developing models for weather forecasting and climate (change) research. In the last decades it is generally acknowledge that the atmosphere-land interactions play a dominant role in atmospheric processes. In its turn, the sensible heat flux on spatial scale of 1 km or more appears to be an important "driving force" in meteorological models. It is outside the scope of this thesis to discuss these features in detail but they can be clarified using the following expression describing the evolution in time of the height of the convective PBL (see e.g. Garratt ,1992)

$$h = \sqrt{\frac{2(1+2c_e)}{\gamma_\Theta}(I-\delta_0)}, \tag{2.1}$$

where, h is the height of the PBL, γ_θ is the vertical temperature gradient, c_e is a constant which is 0.2, $\overline{w'\Theta'}_s = H/\varrho c_p$, with H the mean sensible heat flux at the surface on a scale of at least 1 Km, $I = \int_{t_0}^{t} \overline{w'\Theta'}_s(t')dt$, with t the time, t_0 the time net radiation becomes positive and δ_0 is determined by the initial conditions at $t = t_0$. This formula follows from the so-called well-mixed *slab model* for the PBL. Although this model is certainly too simple to be applicable under all daytime conditions, it appears to describe the main lines of the PBL evolution fairly well (for recent developments in PBL research see Holtslag and Duynkerke, 1998). This illustrates the importance and the need for independent data of area-mean, sensible heat flux at the surface in PBL research. Considering the evidence presented in the previous sections only scintillometry appears to be a promising tool for this purpose.

Another feature of scintillometers is that they require short averaging times. In some cases the averaging time required for the eddy-covariance method exceeds the time the turbulent atmosphere is stationary. An example is the very stable conditions in the PBL. Note that under these conditions the Monin-Obukhov similarity theory is violated, which also causes problems in current numerical general atmospheric

circulation models (see Beljaars and Viterbo, 1998). An important point is that turbulence in the very stable surface layer is very often intermittent and related to short bursts. These intermittent flows occur on such a short time scale that the eddy-covariance method is compromised. New observational approaches are required and scintillometry appears to be a very promising experimental tool.

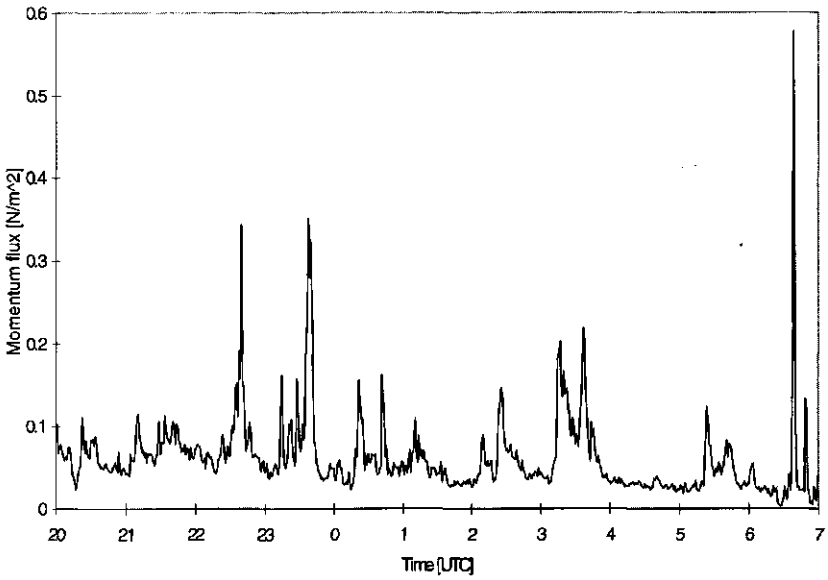

Figure (2.5). Momentum flux determined with a dual beam scintillometer during nighttime over a frozen ice sheet in the Baltic. The intermittent events can be seen very clearly.

An example of atmospheric intermittency detected with a scintillometer is given in Figure (2.5), which depicts observations with a dual-beam laser scintillometer over the frozen Baltic in 1998, within the framework of the international project NOPEX-WINTEX (http://www.hyd.uu.se/nopex). Recently, the international community recognized the significance of intermittent turbulence in the stable atmospheric boundary layer. See for instance the special issue of Boundary Layer Meteorology (Nappo and Johansson, 1999). Among other activities, this interest resulted in the organisation of an international field experiment Co-operative Atmosphere-Surface

Exchange Study – October, 1999 (hereafter denoted as CASES-99) in which WUMET contributed.

Large eddy simulation (LES) models for atmospheric turbulence resolve all scales except the sub-grid-scale (see Moeng, 1998). From the output of LES models one can construct line-averaged values of the structure parameters of temperature and humidity. This implies that scintillometry can be used to check the LES output, because essentially, scintillometers measures the line-averages of these structure parameters. This idea is the object of future research.

2.5 Remote-sensing using the scintillation method

The requirements for remote sensing and routine monitoring at large-scales entails the establishment of reliable scintillometer links that operate continuously without malfunction. Such system configurations would be difficult to maintain with conventional flux gathering methods, the manpower input and expense being simply too great. Even eddy covariance aircraft measurements that are the next best alternative are extremely expensive. From these long-term scintillation experiments comes a pool of experimental data of area-averaged surface fluxes in different climatological regions. The major use of this data is to verify and improve existing flux parameterisation schemes for land surface fluxes with the obvious spin-offs for modelling and improving the management of water resources.

Some mention has already been made of the ability of scintillometers to continuously operate without needing constant calibration. This feature is a definite advantage for portable installations requiring solar panel charging of battery supplies. WUMET have carried out several experiments designed for remote sensing using the scintillometer method. These include such diverse locations as Mexico, (see Hartogensis ,1997; Chehbouni et al, 1999; Hoedjes and Suurbier, 2000), China, Spain and Turkey (Meijninger and De Bruin, 1999) being installed with LAS (networks). Importantly these experiments demonstrate the long-term operational capability of the LAS. Until this work research had concentrated on getting a result from a scintillometer and not addressing the issue of whether routine monitoring was possible.

A good example of the effectiveness of the scintillometer to perform are the results obtained for sensible heat fluxes over irrigated areas in western Turkey, 1998.

(Meijninger and De Bruin, 1999). In this case two LAS were set up, one over a valley and the other over a cotton field. The scintillometers provided values of H for the entire growing season and valuable ground truth data. Particularly impressive from an operational perspective was that the scintillometers could remain unattended going about their business of collecting turbulence data.

Data gathered within the framework of an international experiment EFEDA by WUMET and the KNMI, was used to test the scintillation method over a dry vineyard area in the region of La Mancha, Spain for June 1991. The scintillometer was mounted at 3.3 m height and operated over 875 m (which is about the pixel size of a NOAA-AVHRR image) propagation length. Consequently, the LAS can be used as verification of models with which surface heat fluxes are derived from satellite images. An example of this application is given in Roerink et al. (2000) who compared a method, called ***S-SEBI,*** to derive surface fluxes from LANDSAT-TM, with the flux derived from a LAS installed by WUMET. This refers to a heterogeneous site south of Sienna in Tuscany (Italy). In this case the path length of the LAS was 4.7 km.

An important result from this work (De Bruin et al., 1995) was apparently only a coarse estimate of u_* is required to assist in the calculation of H. And since mechanical turbulence decreases with increasing height it is deemed useful to install the LAS at sufficient height such that H is considered to be due solely to free convection. This simplifies calculations of H as a measurement of u_* is now not required.

2.6 Application of scintillation to water management and hydrology

Water is becoming an expensive and a scarce commodity. The competition for water resources amongst industry, agriculture and human consumption is forcing authorities to improve their management techniques. However, to do so they require factual data on the water balance and how the hydrological processes are operating at the catchment scale (Bloschl and Sivapalan, 1995). The users of the resource are charged for access and volume discharge be it from rivers, aquifers or irrigation systems. Growers are keen to optimise water application per plant requirement and more than ever prepared to invest in technology that assists them. Local authorities are charged with the responsibility of allocating the resource fairly. In all situations a basic

understanding of the areal water usage is required at catchment scales (Commission of the European Communities, 1996) and scintillometry is well suited to this task. In many cases the people charged with the above tasks are hydrologists used to monitoring runoff, stream flow and rainfall. Simulation models have been developed to estimate catchment fluxes (Beven, 1989). These have relied on point measurements as inputs which fail at delivering robust areal estimates, so it is little wonder the concept of an areal-averaged evaporative figure is attractive to the average hydrologist and modeller (Batchelor et al., 1998).

Within this thesis are two minor examples of how scintillometry can assist better water management. The first concerns Chapter [6] the Japanese rice paddy experiment conducted outside Tsukuba in 1996. In Japan there is fierce competition for water resources and land with rice paddies using a fair proportion of the Japanese lowlands. The aim was to use the LAS to help determine the evaporative flux from the well-irrigated rice paddies. The NIAES were interested in the project because long-term the scintillometer technique offered a method to optimize water usage and this fitted well within their environmental brief. Installation and monitoring of the LAS was straightforward however data interpretation was fraught with problems mainly from measuring over a surface where fluctuations in humidity were large and $H < LE$. Additionally and unknown at the time was that absorption scintillations were intruding into the operating bandwidth of the LAS and distorting the final calculations of H. Despite these problems which ultimately improved the scintillometer method and the instrument design and the fact a typhoon destroyed all of the NIAES eddy covariance gear whilst leaving the LAS unscathed, the scintillometer demonstrated a capability to provide useful surface flux data.

The work in Chapter [7] developing the combination of microwave and LAS scintillometers led to a application of the scintillometers over a valley of irrigated grapes (Chapter [8]). The purpose of the experiment was to install the scintillometers on opposite valley ridges to monitor the latent heat flux from the valley floor. The vineyard 30 metres below the scintillometer beams, was a commercial operation with a management curious about scintillometry as an irrigation tool. These producers are committed to managing the application of water to maximise yield and tune the grape sugar content. Every drop applied to each grape was paid for at the farm gate. This part of New Zealand experiences severe summer droughts pushing up the competition for water draw-off during the summer months. Several interesting results came from

this work. It was possible to calculate and monitor the valley evaporative flux using the scintillometer technique, a heartening result for remote sensing applications. The data set showed evidence of the effects on the scintillometer signal during the development of the CBL and also the strong entrainment of advected dry air into the valley. For free convective conditions the calculation of H and LE was simplified as u_* was not required. This formulation showed an excellent comparison with eddy covariance measurements.

De Bruin (1998) suggested an example of a way to use scintillometry in water management, based on the data analysed from the Crete-project (De Bruin et al., 1996). In Figure (2.7) the diurnal course of the scintillometer sensible heat flux is depicted for a day in May 1995 and in September 1995.

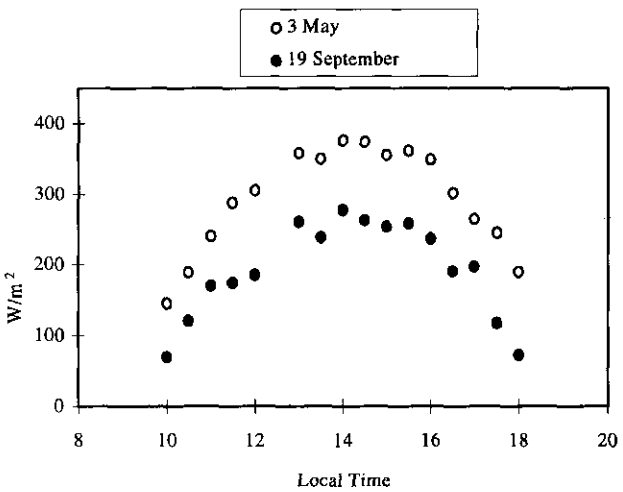

Figure (2.6). Diurnal course of sensible heat flux measured with the scintillometer on 3 May and 19 September 1995.

It is noted that there was no rainfall in the area since March 1995, so one would expect that the sensible heat flux would increase during the season by virtue of the fact the surface dried out and thus evaporation decreased with time. The opposite is observed, indicating that evaporation certainly did not drop during April to

September, which can be due only to irrigation. Note that direct measurements of actual evaporation carried out by the Free University of Berlin confirm this picture: in September 1994 more evaporation was measured than in April/May 1995. One of the problems in this area is that for irrigation purposes too much water has been extracted from the ground and the ground water table has dropped more than 25 m in the last decade. The example illustrates a possible application of the long-path scintillometer. It can serve as a tool for a governmental body to independently check the total water use of an entire area with a relatively low-cost instrument.

3

The Scintillation Method[1]

Abstract

The important components of the scintillation method are discussed including the spectrum of isotropic turbulence; wave propagation through this turbulence; structure parameters vital for interpreting the propagation statistics and MOST the link between these parameters and the surface fluxes of heat, humidity and momentum. Because of the vastness of this subject and the variety of scientific disciplines involved the review focuses on the issues, problems and the inevitable compromises related to extracting the fluxes using scintillometry.

3.1 Introduction

There are currently more scintillometers than ever before being applied in boundary-layer meteorology studies. This is partly due to a renaissance of scintillometry, the commercial availability of saturation-resistant optical scintillometers plus the advent of laser-diode scintillometers. And, as these scintillometers are used over longer distances, at greater heights and over varying terrain we question whether their measurements are reliable if they are used outside the envelope of current knowledge? It is our opinion that the depth and breadth of understanding needed to make accurate surface flux measurements requires an appreciation of the approximations and limitations built into the scintillometer method. It is detailing these understandings that motivates this review.

Hill (1992b) published a comprehensive review article tabulating the background, recent progress and future trends in optical scintillation. Andreas (1990)

[1] Green, A. E., De Bruin, H. A. R. and Meijninger, W., *to be submitted to an atmos. journal*

turbulence. Both these works are particularly valuable reading and source of references. In 1997, Hill motivated by the resurgent interest in scintillometry published a detailed description of the algorithms for obtaining atmospheric surface-layer fluxes using scintillometers. Our review of this subject takes a different approach. As wave propagation in a turbulent medium covers many disciplines from theoretical physics through to boundary-layer meteorology and the application of scintillometers requires competence in opto-electronics and microwave engineering we summarise the important features of the scintillometer method from a pragmatic perspective.

This review consists of four overlapping components. Firstly, the reader is introduced to the importance of accurately describing the energy associated with random fluctuations in the refractive-index of air. Next, this spatial description of turbulent energy is incorporated within the theory of propagating electromagnetic (EM) energy with respect to small changes in amplitude and phase. The structure parameters are a measure of the strength of refractive turbulence associated with these amplitude and phase changes and they are discussed in the third section. Finally, we outline how similarity theory links the structure parameters to the surface fluxes and some problems associated thereof.

Concluding, ideally the reader will have an overview as to the chain of events leading from a presumably accurate scintillometer measurement through to a surface flux calculation.

3.1 Forms of $\Phi_n(\kappa)$ in the variance, inertial-convective and dissipation ranges

Understanding the form of the three dimensional, spatial power spectrum of the refractive-index $\Phi_n(\kappa)$ is very important for determining scintillation statistics, in particular C_n^2 and l_o. The effect of random fluctuations in the refractive-index on the EM radiation propagating through a turbulent atmosphere is quantified by $\Phi_n(\kappa)$. It has been the habit of propagationists to describe $\Phi_n(\kappa)$ using mathematical models.

Fluctuations of the temperature, humidity and therefore the refractive-index are advected by the mean wind field. All have similar spatial-power spectra in the *inertial-convective* range (Hill, 1978a), a range characterised by isotropic and

homogeneous turbulence. Turbulent kinetic energy is introduced into this range through the large-scale processes of wind shear and solar heating of the ground which break up the large eddies and mix them to all sizes. Within the inertial-convective range the kinetic energy is redistributed at a constant rate, the kinetic energy dissipation rate (ε), down to a lower limit designated by a wave-number, $\kappa_m = 2\pi/l_o$. l_o is the inner-scale length beyond which energy is dissipated as viscous heat in the *dissipation range*. The spatial wavenumber, $\kappa_o \approx 2\pi/L_o$ where L_o is outer-scale length, defines the lower limit for the inertial-convective range. At smaller wavenumbers, $\kappa < \kappa_o$, turbulence is likely neither homogeneous nor isotropic. This is the *variance* range, the range where the majority of the energy is contained. A form of $\Phi_n(\kappa)$ is shown in Figure (3.1) with κ_o and κ_m demarcating the transitions.

Kolomogorov (1941) hypothesied the shape of $\Phi_n(\kappa)$ in the inertial-convective range. His theoretical model took the form,

$$\Phi_K(\kappa) = 0.033\, C_n^2 \kappa^{-11/3}. \tag{3.1}$$

C_n^2 may be interpreted as a measure of the strength of the refractive turbulence. However, the $\kappa^{-11/3}$ proportionality overestimated $\Phi_K(\kappa)$ in the dissipation range. Tatarskii's mathematical remedy (1961) was to apply a Gaussian cutoff to $\Phi_K(\kappa)$ at the high spatial wavenumbers giving,

$$\Phi_T(\kappa) = \Phi_K(\kappa)\exp(-1.56\kappa^2\eta^2). \tag{3.2}$$

From Hill and Clifford (1978b) we know the Kolmogorov microscale, $\eta = l_o/7.5$, where,

$$l_o = 7.4(\nu^3/\varepsilon)^{1/4}, \tag{3.3}$$

and ν is the kinematic viscosity of air. Experimental data was to later show $\Phi_T(\kappa)$ required a more gradual descent in the dissipation range (Time, 1972).

Careful measurements by Williams and Paulson (1977) and Champagne et al. (1977) revealed a *bump* in $\Phi_T(\kappa)$ between the inertial-convective and dissipation ranges. Equation (3.2) is inadequate to describe $\Phi_n(\kappa)$. Nevertheless, both experimentalists and theorists persist with its application.

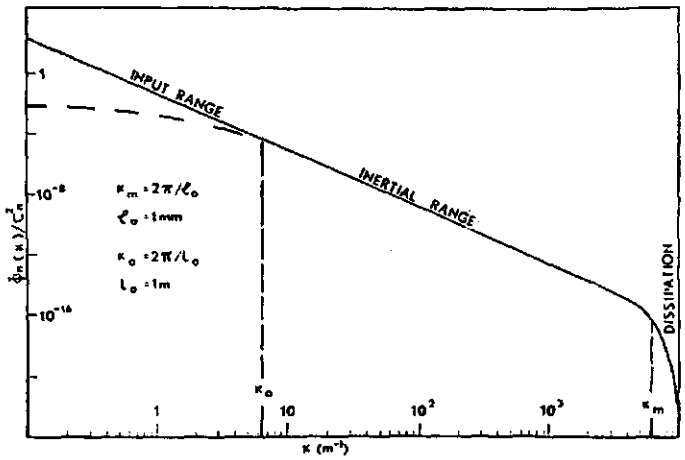

Figure (3.1). A spectrum of the refractive-index fluctuations. The solid line is the Tatarskii spectrum and the dashed line the von Karman spectrum in the variance-containing range. Reproduced from Clifford and Strohbehn (1970).

Hill and Clifford (1978b) described a sub-range of the inertial-convective range, the *viscous convective* range and developed a theoretical spectrum for the inertial-convective through to the dissipation range. This took the form of the solution to a second-order differential equation. Hill gave the analytical approximation to their spectrum (Churnside, 1990) as,

$$\Phi_H(\kappa) \approx \Phi_K(\kappa)\left[exp\left(-70.5\kappa^2\eta^2\right) + 1.45exp\left(-0.97(ln\kappa\eta + 1.55)^2\right)\right]. \tag{3.4}$$

Equation (3.4) is simplified so that,

$$\Phi_H(\kappa) \approx \Phi_K(\kappa) f(\kappa\eta). \tag{3.5}$$

The Hill spectrum deviates less than a few percent from measured values at high wavenumbers. Figure (3.2) is the Hill spectrum normalised by $\Phi_K(\kappa)$ clearly showing the bump in the viscous-convective range. The Hill spectrum was derived from temperature fluctuations assuming they dominate refractive-index fluctuations at optical wavelengths. Hill (1978a) showed the refractivity spectrum also has a viscous-convective range but the shape depended on the relative contributions from the temperature spectrum, humidity spectrum and temperature-humidity co-spectrum.

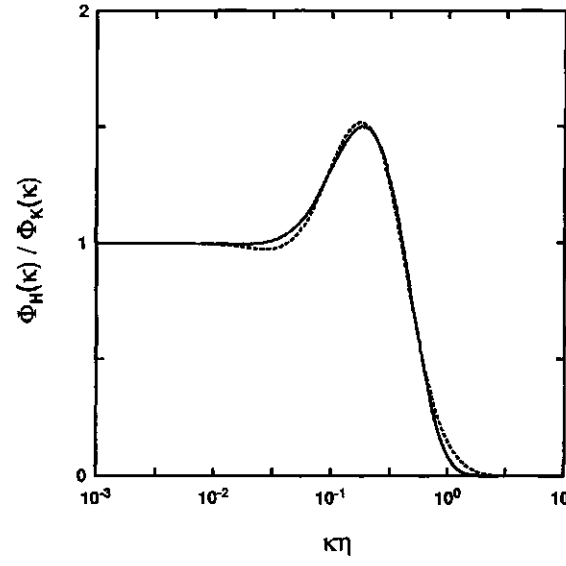

Figure (3.2). The ratio of $\Phi_H(\kappa)$ to $\Phi_K(\kappa)$ plotted against $\kappa\eta$. The numerical values (solid line) and the analytical approximation (dashed line) are presented. Reproduced from Churnside (1990).

At wave-numbers smaller than κ_0, $\Phi_n(\kappa)$ will change shape (see Figure 3.1). The form of the spectrum is not known nor is it predictable below κ_0 (Clifford and Strohbehn, 1970). The von Karman spectrum is often used to describe the variance–containing and inertial-convective ranges and is expressed as,

$$\Phi_V(\kappa) = 0.033\, C_n^2 \left(\kappa^2 + L_o^{-2}\right)^{-11/6}. \qquad (3.6)$$

$\Phi_V(\kappa)$ does not recognise the existence of the viscous-convective sub-range and fails to describe the dissipation range. For $\kappa >> 1/L_o$, $\Phi_V(\kappa)$ approximates the Kolomogorov spectrum and becomes constant for $\kappa << 1/L_o$. L_0 depends on the height above the surface and local conditions and may vary from a fraction of a metre to 100 metres or more. Equation (3.6) implies $\Phi_V(\kappa)$ depends exclusively on L_0 in the variance range. This is incorrect as atmospheric behaviour depends on many spatial scales. Nevertheless, propagation theorists continue with $\Phi_V(\kappa)$ in describing the variance-containing range and sometimes the inertial-convective range even though the atmosphere behaves quiet differently (Hill, 1992b). Additionally, phase scintillations are sensitive to the amplitude range of $\Phi_n(\kappa)$ and optical phase data by Hill et al. (1988) shows disagreement with the von Karman spectrum.

At low wavenumbers absorption fluctuations may enhance $\Phi_n(\kappa)$ and contribute significant energy to the variance-containing range if they are not filtered from the refractive fluctuations (Nieveen et al., 1998).

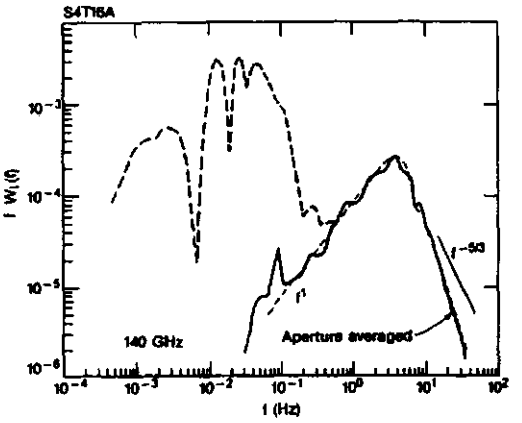

Figure (3.3). Intensity spectrum from clear-air turbulence conditions (solid line) illustrating the effect of a change in absorption during the data run (dashed line). Reproduced from Hill et al. (1990).

A scintillometer propagating EM radiation about the absorption wavelengths of not just water molecules but any gas species may be affected by line-averaged

attenuation. Microwave scintillometers are most susceptible to absorption fluctuations showing a deviation from scattering theory at low κ (Hill, 1988). When absorption fluctuations dominate scintillation then the spectral density function of the intensity variance becomes bimodal. Figure (3.3) demonstrates the effects of low-frequency absorption fluctuations on the temporal energy spectra of the intensity variance obtained using a microwave scintillometer. The absorption fluctuations comprise most of the energy, the absorption spectrum is not described by existing theory and the von Karman spectrum is unusable.

3.3 Wave propagation

As EM radiation travels through the atmosphere fluctuations in the density of the air induce fluctuations in the wave-front. Significant variation in amplitude and phase will occur for random spatial and temporal fluctuations in the refractive-index. The spatial distribution of this energy is described by $\Phi_n(\kappa)$. For the purpose of obtaining an averaged description of the effects of this propagation and in order to preserve the form of $\Phi_n(\kappa)$, a horizontal, statistically homogeneous and isotropic atmosphere is assumed. In reality and particularly over distance only a degree of these statistics are realisable.

There have been several approaches in describing the general problem of wave propagation in a random medium (Lawrence and Strohbehn, 1970). One solution has been to directly solve the vector wave-equation using the Rytov method. The method substitutes an expression for the log-amplitude χ and phase into a simplified form of the wave equation. This transformation is then solved for small fluctuations in amplitude and phase. It is required that, $\lambda << l_o$ and $\lambda^3 L/l_o^4 << 1$, where λ is the wavelength of the EM radiation. These conditions are easily met for optical wavelengths. For microwave propagation Clifford and Strohbehn (1970) showed this approach was still valid if $\lambda \geq l_o$.

The statistic of most interest to us is the variance of χ, σ_χ^2 in a plane perpendicular to the direction of propagation because it is related to the log-intensity variance σ_I^2 of the received EM radiation ($\sigma_I^2 = 4\sigma_\chi^2$). Application of the Rytov method leads to a normal probability distribution for χ ($= ln(A/A_o)$).

Solution for the general case of σ_χ^2 gives (Lawrence and Strohbehn, 1970),

$$\sigma_\chi^2 = 4\pi^2 K^2 \int_0^L dz \int_0^\infty d\kappa \kappa \Phi(\kappa) \sin^2\left(\frac{\kappa^2 z(L-z)}{2\kappa L}\right) \tag{3.7}$$

The optical wavenumber $K = 2\pi/\lambda$. The physical interpretation of the sin^2 path weighting function is a symmetrical bell-shaped curve tapering to zero at either end. This will reduce the influence of flow field distortions by transmitter and receiver mountings (Thiermann and Grassl, 1992a).

Substituting for the accurate spectrum of Hill (1978) $\Phi_H(\kappa)$ into Equation (3.7) and integrating over the pathlength and wavenumber κ yields a solution similar to that obtained by Thiermann and Grassl (1992),

$$\sigma_\chi^2 = 0.124 C_n^2 K^{7/6} L^{11/6} f_a\left(l_o/\sqrt{\lambda L}\right) \tag{3.8}$$

In Figure (3.4) the function $f_a\left(l_o/\sqrt{\lambda L}\right)$ is plotted against the inner-scale length normalised by the Fresnel-zone, $F = \sqrt{\lambda L}$. This is a significant result for spherical wave propagation. Laser scintillometers are sensitive to F sized turbulent eddies. To avoid saturation L is generally chosen to be less than several hundred metres which forces the fraction $l_o/\sqrt{\lambda L}$ to occur on the steep portion of the curve in Figure (3.4). Therefore the scintillometer operates within the viscous-convective range which requires the accurate spectrum $\Phi_H(\kappa)$ to be used in propagation calculations.

For microwave propagation $\lambda > l_o$ and without inner-scale dependence Equation (3.8) reduces to,

$$\sigma_\chi^2 = 0.124 C_n^2 K^{7/6} L^{11/6} . \tag{3.9}$$

The Rytov approximation is valid when perturbations in the refractive-index are small, $\sigma_\chi^2 \leq 0.3$. As the strength of refractive turbulence increases the scintillations saturate and any scintillometer whose performance is based on the proportionality σ_χ^2

and C_n^2 will fail (Wang et al., 1978). For optical scintillometers both saturation and l_o can affect the path weighting.

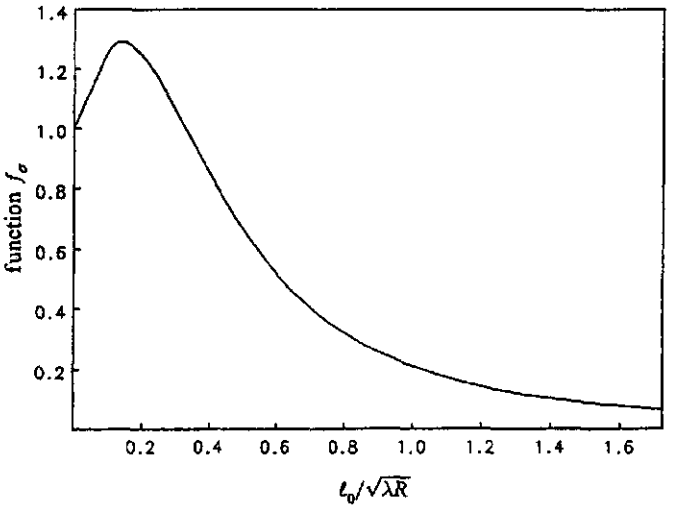

Figure (3.4). The function f_o describing the log-amplitude variance at a point detector as a function of the inner scale l_o, for the refractive-index spectrum $\Phi_n(\kappa)$ and a spherical wave. l_o is normalised by the Fresnel-zone, $\sqrt{\lambda R}$. Note here $R \equiv L$. Reproduced from Thiermann and Grassl (1992a).

Clifford et al. (1974) extended the perturbation theory for saturation of optical scintillation by strong turbulence with their model using linear filtering of σ_χ^2. Churnside (1992) gives the expression for a finite-aperture, diameter (D) scintillometer,

$$\sigma_\chi^2 = 4\pi^2 K^2 \int_0^L dz \int_0^\infty d\kappa \kappa \Phi(\kappa) \sin^2\left(\frac{\kappa^2 z(L-z)}{2\kappa L}\right)\left(\frac{2J_1[0.5\kappa Dz]}{0.5\kappa Dz} x \frac{2J_1[0.5\kappa D(1-z)]}{0.5\kappa D(1-z)}\right)^2 \quad (3.10)$$

J_1 is the zero-order Bessel function of the first kind and $z = s/L$ is the distance from the transmitter (s) normalised by the pathlength L. When $D \to 0$ then the J_1 functions approach unity and we have the point transmitter/receiver case. At high wavenumbers

the denominators reduce the integrand. The point at which this reduction begins is of the order $\kappa D \cong 1$, and therefore the scintillometer is not sensitive to l_o provided $D >> l_o$. When $D >> F$ the signal is averaged and σ_χ^2 is reduced so the Rytov method can be applied over greater L for the condition $\sigma_\chi^2 \geq 0.3$. Numerical results from their model agreed with observations in strong turbulence.

Frehlich and Ochs (1990) observed that over sufficiently long propagation paths (L = 1 km) the aperture-averaged variance is affected by strong scattering. Their recommendation was that D should be kept sufficiently large so that only the inertial-convective portion of $\Phi_n(\kappa)$ is sensed and the effect of the inner scale is minimised.

Wang et al. (1978) designed an optical wavelength scintillometer to avoid the saturation and inner scale effects. They did not consider the Hill spectrum in their analysis. Their scintillometer used spatially incoherent receiver and transmitter optics greater than a Fresnel-zone in diameter $(D > F)$, which biased the refractive-turbulence towards larger sized eddies.

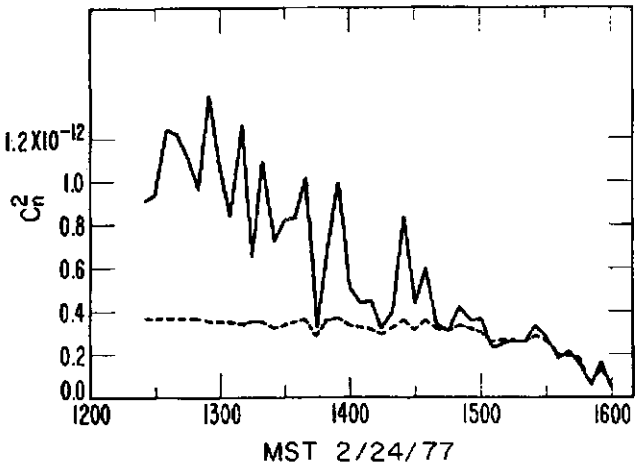

Figure (3.5). Comparison of C_n^2 ($m^{-2/3}$) measurements made with the saturation-resistant optical scintillometer and with a laser scintillometer on a 500 m optical path 1.5 m above the ground. Each point is a 5 min. average. The differential saturation-resistant system used 15 cm diameter optics; the laser system used a spherical wavefront which irradiated a 1 mm diameter receiving system. Reproduced from Ting-i Wang et al. (1978).

Figure (3.5) compares the performance of the saturation-resistant scintillometer with a laser scintillometer in calculating 500 m line-averaged C_n^2. The benefits of the large-aperture scintillometer (LAS) are obvious. When C_n^2 varies spatially along the propagation path the LAS path weighting is determined by the sin^2 function and the two Bessel functions. By changing the ratio of transmitter to receiver aperture diameters the shape of the path weighting will change.

Another method, that of spatial filtering (Churnside et al., 1988), was shown to spatially resolve refractive turbulence strength to within 4.5 m over selected portions of a 110 m propagation path.

3.4 Structure parameters

Structure functions are the basis for scintillation measurements of surface-layer fluxes (Hill, 1997). Structure functions or cross-structure functions may be defined for any scalar or combination of scalars such as temperature, humidity, pressure or the refractive-index. For spacing r in the inertial-convective range the refractive-index structure function is (Tatarskii, 1961),

$$D_n(r) = \left\langle [n(x) - n(x+r)]^2 \right\rangle = C_n^2 r^{2/3}. \tag{3.11}$$

The < > brackets denote an ensemble average although in practice a temporal average is generally made. The structure parameter C_n^2 is a proportionality factor but it may vary several orders of magnitude. Similarly the T, Q and T-Q correlation structure functions are defined by,

$$\begin{aligned} D_T(r) &= \left\langle [T(x) - T(x+r)]^2 \right\rangle = C_T^2 r^{2/3} \\ D_Q(r) &= \left\langle [Q(x) - Q(x+r)]^2 \right\rangle = C_Q^2 r^{2/3} \\ D_{TQ}(r) &= \left\langle [T(x) - T(x+r)]\ [Q(x) - Q(x+r)] \right\rangle = C_{TQ}^2 r^{2/3} \end{aligned} \tag{3.12}$$

Equations (3.11) and (3.12) are at times said to obey the Kolomogorov 2/3-law. Within the dissipation range of $\Phi_n(\kappa)$, $D_n(r) \propto r^2$. The inner-scale l_o is the spacing at which the $r^{2/3}$ and r^2 asymptotic forms equate and at which $D_n(r)$ begins to decrease because of viscous dissipation (Hill and Clifford, 1978b).

The structure parameters can be measured directly using spatially displaced, sensors (Lawerence and Strohbehn., 1970, Kohsiek, 1982b). Other spectral based approaches have been developed. For instance the inertial-convective form of the one-dimensional refractive-index spatial-power spectrum is (Wyngaard and Le Mone, 1980),

$$\Phi_n(\kappa_1) = 0.25 C_n^2 \kappa_1^{-5/3}. \tag{3.13}$$

κ_1 is the stream-wise component of the wavenumber. Taylor's frozen-field hypothesis (Wyngaard, 1971a) assumes turbulent eddies are carried by a mean windspeed $\overline{U}$ and change only slowly as the move past a fixed position. $\Phi_n(\kappa_1)$ is the Fourier transform for the frequency spectrum of temporal fluctuations n (= $\kappa_1 \overline{U}/2\pi$) measured at this position. Equation (3.13) may be then solved for C_n^2. Similar equations exist for C_T^2, C_Q^2 and C_{TQ} (Wyngaard and LeMone, 1980),

$$\begin{aligned} \Phi_T(\kappa_1) &= 0.25 C_T^2 \kappa_1^{-5/3} \\ \Phi_Q(\kappa_1) &= 0.25 C_Q^2 \kappa_1^{-5/3} \\ Co_{TQ}(\kappa_1) &= 0.25 C_{TQ}^2 \kappa_1^{-5/3} \end{aligned} \tag{3.14}$$

Corrsin (1951) proposed an expression for the one-dimensional spatial-power spectrum of temperature and humidity fluctuations in the inertial-convective subrange to be,

$$\begin{aligned} \Phi_T(\kappa_1) &= \beta_1 \varepsilon^{-1/3} N_T \kappa^{-5/3} \\ \Phi_Q(\kappa_1) &= \beta_1 \varepsilon^{-1/3} N_Q \kappa^{-5/3} \end{aligned} \tag{3.15}$$

N_T and N_Q are dissipation rates for the T and Q and β_1 is known as the Kolmogorov constant. Kaimal et al. (1972) confirmed the temperature and velocity spectra have a well defined –5/3 power-law behaviour, consistent with isotropic turbulence and that L_o was governed by the combined effects of shear and buoyancy as predicted by Kolomogrov.

Wyngaard and Clifford (1978) proposed the T-Q cospectra also obeyed a –5/3 power-law. Careful high frequency measurements by Kohsiek (1984) and Priestley and Hill (1985) later confirmed this relationship,

$$Co_{TQ}(\kappa_1) = \gamma_1 \varepsilon^{-1/3} N_{TQ} \kappa^{-5/3} \tag{3.16}$$

N_{TQ} is the dissipation rate for the T-Q covariance and γ_1 is the Kolmogorov constant for T-Q. Equation (3.16) was an important result as without experimental evidence it had been assumed C_{TQ} obeyed the 2/3-law.

Spatial fluctuations in the refractive-index, $[n(x) - n(x+r)]$ are due to fluctuations in T, Q and P about their average value. Ignoring the negligible pressure fluctuations the structure parameters are equated using (Hill et al., 1980),

$$C_n^2 = \frac{A_T^2}{\overline{T}^2} C_T^2 + 2\frac{A_T A_Q}{\overline{TQ}} C_{TQ} + \frac{A_Q^2}{\overline{Q}^2} C_Q^2 \tag{3.17}$$

The constants A_T and A_Q are functions of wavelength, and the mean values of T, Q and P. Calculated A_T and A_Q are given by Hill et al. (1980) from radio to infrared wavelengths and by Andreas (1989) for visible through to microwave wavelengths.

A similar expression to Equation (3.17) equates the scalar spectra (Andreas, 1987) using Equations (3.13) to (3.16),

$$\Phi_n(\kappa_1) = \frac{A_T^2}{\overline{T}^2}\Phi_T(\kappa_1) + 2\frac{A_T A_Q}{\overline{TQ}} Co_{TQ}(\kappa_1) + \frac{A_Q^2}{\overline{Q}^2}\Phi_Q(\kappa_1). \tag{3.18}$$

A direct consequence of Equation (3.15) is that $\beta_1 = \gamma_1 = \beta_n \cong 0.4$, where β_n is the Kolmogorov constant for the refractive-index.

Equation (3.14) has been solved for C_n^2 using micrometeorological measurements (Hill et al., 1988). If structure parameters C_T^2, C_Q^2 and C_{TQ} are required, three independent measurements of C_n^2 are needed by scintillation or other means. Three different wavelength scintillometers were used to solve for C_T^2, C_Q^2 and C_{TQ} but unfortunately this was unsuccessful (Kohsiek, 1982b) because of technical problems.

If the surface is dry and scintillation measurements are made at visible to near-infrared wavelengths then Equation (2.17) may be simplified to,

$$C_n^2 = \frac{A_T^2}{\overline{T}^2} C_T^2 . \tag{3.19}$$

Measuring over wetter surfaces Equation (3.17) becomes,

$$C_n^2 = \frac{A_T^2}{\overline{T}^2} C_T^2 \left(1 + \frac{0.03}{\beta} \right)^2 \tag{3.20}$$

$\beta = H/E$, the Bowen-ratio, is the ratio of sensible to latent heat flux. Measurements made at different scales have been combined. A line-averaged scintillometer value for C_n^2 and a micrometeorological measurement of β are used to solve for C_T^2. However, incorporation of β is equivalent to rearranging Equation (3.17) using the relationship (Kohsiek, 1982),

$$\beta = \left(\frac{\varrho C_p}{L_E} \right) \left(\frac{C_T}{C_Q} \right) \tag{3.21}$$

The implication is that the value of β used in Equation (3.21) is equivalent to the line-averaged value given by Equation (3.20). Also, and not so obvious is that the formulation of Equation (3.17) assumes a perfect correlation between the T and Q fluctuations in the inertial-convective range (Hill et al., 1988) so that,

$$C_{TQ} = \pm\sqrt{\left(C_T^2 C_Q^2\right)} \tag{3.22}$$

Hill (1988) provided the solution for C_T^2 and C_Q^2 using the relationship of Equation (3.22) and two different λ scintillometers operating at microwave and near-infrared wavelengths (subscripts $_m$ and $_i$ respectively) for,

$$\begin{aligned} C_Q^2 &= \left(A_{T,m}^2 C_{n,i}^2 + A_{T,i}^2 C_{n,m}^2 + 2SA_{T,m}A_{T,i}\sqrt{C_{n,m}^2 C_{n,i}^2}\right)/(TD)^2 \\ C_T^2 &= \left(A_{Q,m}^2 C_{n,i}^2 + A_{Q,i}^2 C_{n,m}^2 + 2SA_{Q,m}A_{Q,i}\sqrt{C_{n,m}^2 C_{n,i}^2}\right)/(QD)^2 \end{aligned} \tag{3.23}$$

where, $D = \left(A_{T,m}A_{Q,i} - A_{T,i}A_{Q,m}\right)/TQ$ and S is the sign of the T-Q correlation.

Andreas (1989) performed a sensitivity analysis for the two-wavelength method. He concluded the combination of a visible to near-infrared wavelength with a microwave wavelength gave roughly the same accuracy as the eddy covariance method.

3.5 Estimating the surface fluxes from structure parameters

Turbulence similarity theory relates the structure parameters to surface fluxes. Monin-Obukhov (1954) similarity theory (MOST) is generally used for the atmospheric surface layer, which to a first order approximation is treated as being a constant flux layer. For treating surface-layer similarity of C_T^2, C_{TQ} and C_Q^2, MOST scaling requires a stationary and horizontally homogeneous boundary-layer. The implications of using MOST for scalar quantities including the refractive-index, was discussed in detail by Hill (1989) and a recent publication by Hill (1997) reviews the algorithms for obtaining the surface fluxes.

Andreas (1989) made a particularly pointed observation, *'since horizontal homogeneity is fundamental to the assumptions of MOST and therefore required to analyse path-averaged measurements, what advantages does path-averaging have?'* The scintillometer procedure becomes more convoluted when point measurements, for example of u_*, are substituted for path-averaged values. Andreas (1989) justifies the continued application of MOST, firstly because there is no other theoretical

framework available and the scintillation method should be first tested for accuracy in horizontally homogeneous conditions. Secondly, experimental evidence suggests flux-profiles can be used to model the turbulence provided the surface does not have significant undulations or marked roughness changes (Andreas, 1996).

Priestley and Hill (1985) suggested that departures from MOST were caused by large-scale dynamics of the boundary-layer. Kaimal et al. (1976), Wyngaard and LeMone (1980) showed entrainment effects caused MOST to deviate in the mid- and upper regions of the convective boundary-layer.

Recently Peltier and Wyngaard (1995) addressed the problem of substantial turbulent intermittency in EM propagation. The intermittency caused the probability distribution of the refractive-index fluctuations to deviate from Gaussian. The structure parameters are better viewed as being local flow variables rather than ensemble averages. In so doing and through redefining the structure parameters as being driven by local values of N_T and N_Q the predicted C_T^2, C_{TQ} and C_Q^2 compared well with measurements.

Wyngaard and Clifford (1978) gave a mathematical treatment to compute *H*, *LE* and u_* from structure parameters. Hill (1997) gave the latest and in his opinion the most suitable MOST equations,

$$\begin{aligned}
\frac{C_T^2 z^{2/3}}{T_*^2} &= f(\zeta) \\
\frac{C_Q^2 z^{2/3}}{Q_*^2} &= af(\zeta) \\
\frac{\kappa z \varepsilon}{u_*^3} &= h(\zeta)
\end{aligned} \tag{3.24}$$

L_o is the buoyancy length scale (corrected for humidity effects) included in the expression for atmospheric stability,

$$\zeta \equiv \frac{z}{L_o} = \frac{\kappa g z T_* \cdot (1 + 0.07/\beta)}{u_*^2 T} \tag{3.25}$$

g is gravitational acceleration, and T_*, and Q_* are the temperature and humidity scaling parameters. The constant a, was proven by Hill (1989) to be unity because if T and Q obey MOST scaling then non-dimensional functions of C_T^2 and C_Q^2 must be equal.

Many MOST functions have been proposed for $h(\zeta)$ and $f(\zeta)$. The original forms derive from the Kansas data (Wyngaard, 1973). Based on supporting data Hill (1997) suggested the preferred versions should be,

$$f(\zeta)=\begin{cases}6.34\left(1-7\zeta+75\zeta^2\right)^{-1/3}, & \zeta<0\\ 6.34\left(1-7\zeta+20\zeta^2\right)^{1/3}, & \zeta\geq 0\end{cases}$$
$$h(\zeta)=\begin{cases}\left(1-3\zeta\right)^{-1}-\zeta,, & \zeta<0\\ \left(1+4\zeta+16\zeta^2\right)^{1/2}, & \zeta\geq 0\end{cases} \qquad (3.26)$$

Implementing $h(\zeta)$ and $f(\zeta)$ requires knowing a value for ζ. The procedure adopted by Hill et al (1992a) is to solve ζ iteratively by equating the measured parameters to the dimensionless functions via the relationship,

$$\zeta^2 f(\zeta)[h(\zeta)]^{-4/3}=\frac{g^2\kappa^{2/3}z^{4/3}C_T^2}{T^2\varepsilon^{4/3}} \qquad (3.27)$$

Surface fluxes H and E are then calculated from the values of the scaling parameters defined in Equation (3.24) and the other parameters determined from the scintillation measurements,

$$H=-\rho C_p u_* T_*$$
$$E=-L_E u_* Q_* \qquad (3.28)$$

Both the Inner Scale Meter (Hill et al., 1992a) and the Displaced-beam scintillometer (Thiermann, 1992b) measure l_o directly from which ε is then calculated using Equation (3.3). In the absence of direct measurement of l_o alternative methods

include taking u_* directly from eddy covariance instruments or estimating u_* from average windspeed and a measure of surface roughness.

H can be obtained from C_T^2 alone without u_* (or l_o or ε) in the very unstable limit when $f(\zeta) \propto \zeta^{-2/3}$ (Hill et al., 1992a). If the conditions of local free convection are met then from De Bruin et al. (1995),

$$H = 0.57z\left(\frac{g}{T}\right)^{1/2}\left(C_T^2\right)^{3/4}\rho C_p, \tag{3.29}$$

and from Green et al. (2000),

$$E = L_E z\left(\frac{C_Q^2}{2.5}\right)^{3/4}\left(\frac{gC_T}{TC_Q}\right)^{1/2} \tag{3.30}$$

De Bruin et al. (1995) found that although Equation (3.29) would generally underestimate when compared to the eddy covariance method, the free convection component dominated. This implied that a rather rough estimate of u_* was required to account for the effect of mechanical turbulence on H. Wyngaard and Clifford (1978) and results from Green et al. (1997) show that the fractional error in the momentum flux is approximately twice that of the measured structure functions whereas scalar fluxes are much less sensitive for an unstable atmosphere.

3.6 Summary

The important steps in the scintillation method have been reviewed. The Hill spectrum for $\Phi_n(\kappa)$ provides the most accurate description in the inertial-convective and dissipation ranges but needs to be adopted more widely. An accurate $\Phi_n(\kappa)$ does not exist for the variance-containing range but experimentalist and theorists continue to use the von Karman spectrum. The current approach to describing wave propagation in a turbulent atmosphere is an approximation that failed to describe large spatial and temporal fluctuations in the refractive-index until the perturbation theory was extended for saturation conditions. This advance led to optical scintillometers being designed to operate successfully in strong saturation. Current technology

allows the accurate determination of the structure parameters C_T^2, C_{TQ} and C_Q^2 and l_o be they derived from single or multiple scintillometers. These structure parameters have associated spatial power spectra that obey a –5/3 power-law in the inertial-convective subrange. A three-wavelength scintillometer has yet to successfully determine these parameters and the assumption $C_{TQ} = \pm\sqrt{\left(C_T^2 C_Q^2\right)}$ is used instead. The preferred two-wavelength scintillometer combination is one that operates at visible to near-infrared wavelengths with one operating at radio wavelengths. MOST is the only theoretical framework available to relate C_T^2, C_{TQ} and C_Q^2 to the surface fluxes. The current view is that departures from MOST are due to large-scale atmospheric processes such as entrainment. Intermittency and non-stationarity are also important. Explanations must be found and MOST must be tested over semi-homogeneous terrain to extend the scintillometer method.

4

Surface-layer scintillation measurements of daytime sensible heat and momentum fluxes[1]

Abstract

Line-averaged measurements of the structure parameter of refractive index (C_n^2) were made using a semiconductor laser diode scintillometer above two markedly different surfaces during hours of positive net radiation. The underlying vegetation comprised in the first instance a horizontally homogeneous, pasture sward well-supplied with water, and in the second experiment, a sparse thyme canopy in a semi-arid environment. Atmospheric stability ranged between near neutrality and strongly unstable ($-2 \leq \xi \leq 0$). The temperature structure parameter C_T^2 computed from the optical measurements over four decades from 0.001 to 2 $K^2\ m^{-2/3}$ agreed to within 5% of those determined from temperature spectra in the inertial sub-range of frequencies. Spectra were obtained from a single fine thermocouple sensor positioned near the midway position of the 100 m optical path and at the beam propagation height (1.5 m). With the inclusion of cup anemometer measurements, rule-of-thumb assumptions about surface roughness, and Monin-Obukhov similarity theory, path-averaged optical scintillations allow calculation of surface fluxes of sensible heat and momentum via a simple iterative procedure. Excellent agreement was obtained between these fluxes and those measured directly by eddy covariance. For sensible heat, agreement was on average close to perfect over a measured range of 0 to 500 W m^{-2} with a residual standard deviation of 30 W m^{-2}. Friction velocities agreed within 2% over the range 0 - 0.9 m s^{-1} (residual standard deviation of 0.06 m s^{-1}). The results markedly increase the range of validation obtained in previous field experiments. The potential of this scintillation technique and its theoretical foundation are briefly discussed.

[1] Green, A. E., McAneney, K. J. and Astill, M. S., *Boundary-layer Meterology 68, 357-373, 1994.*

4.1 Introduction

There is an innate attractiveness about using optical scintillation to obtain turbulence information. Early interest in this subject was motivated by communication and astrophysical considerations (e.g. Strohbehn (1968) and Hufnagel and Stanley (1964)) because of distortion to electromagnetic signals caused by refractive-index irregularities which arise from turbulent fluctuations in air temperature and water vapour. Interest in the inverse problem of using optical propagation measurements to infer turbulence information is more recent with Wesely (1976a) being one of the first to attempt to derive estimates of the sensible heat flux (H). From a micrometeorological perspective, much of the appeal of optical techniques derives from the opportunity for spatial averaging and the requirement of only short averaging periods to give statistically reliable measurements (Wyngaard and Clifford, 1978). For reviews of the observational and theoretical progress in scintillation methods, readers are referred to Hill (1992) and to the collection of milestone papers compiled by Andreas (1990). The latter includes early Russian contributions to the literature.

In principle, optical measurements of turbulence promise several advantages over more conventional techniques. Firstly, flow distortion effects are minimised due to intensity fluctuations being path-weighted in a parabolic manner with a maximum midway and tapering to zero at either ends of the optical path (Ting-i Wang et al., 1978). Secondly, and depending on source characteristics and measurement height, path-averaging is possible up to several kilometres (Kohsiek and Herben, 1983), a range which offers possibilities for testing remote sensing estimates of sensible heat (Seguin et al., 1989, Lagouarde and McAneney, 1992). Thirdly, reliable statistical data are obtainable after several minutes (Wyngaard and Clifford, 1978), and finally, no absolute instrument calibration is required. The latter arises because the quantity measured is the variance of the logarithmic signal intensity so that any multiplicative calibration factors cancel and constant terms are removed by band-pass filtering at scintillation frequencies. Despite the above, and the fact that a commercial instrument now exists (Thiermann, 1992b), convincing proof that these features can be exploited in practice to measure surface fluxes routinely has yet to be realised. The current study provides a step in this direction.

The optically most active eddies have sizes of the order of the first Fresnel zone ($= \sqrt{\lambda L}$, where λ is the optical wavelength and L the path length). Since these small scale eddies are likely to be in equilibrium with the local terrain, it might appear that scintillation techniques allow some relief from the general fetch restrictions on micrometeorological measurements and thus provide averaging over horizontally inhomogeneous terrain. Andreas (1989) expresses some optimism in this regard. However scintillation methods depend on Monin-Obukhov similarity theory to link measurements in the dissipation or inertial subrange of frequencies to the entire range of eddy sizes contributing to turbulent transport. Unfortunately larger eddies adjust only slowly to changing surface conditions and therefore reflect terrain and surface features well upstream of the measurement position (Panofsky et al., 1982; Højstrup, 1981). Extending Monin-Obukhov similarity to deal with heterogeneous surfaces remains an objective for future research.

To date, scintillometers have mainly used either He-Ne and CO_2 lasers (e.g. Kohsiek, 1985) and/or high intensity incoherent light from infrared-emitting diodes (e.g. Hill et al., 1992a). Semiconductor laser diodes, as used in this paper, now provide cheaper and low power coherent scintillation sources, although at shorter optical pathlengths ($L < 200$ m) (Thiermann, 1992a) because of saturation and power limitations. The principal aim of this paper is to compare sensible heat and momentum fluxes estimated from mean windspeed and scintillation measurements with those obtained directly by eddy covariance. Measurements by eddy covariance are taken as providing unbiased, best estimates of the fluxes. The theoretical framework supporting the optical measurements is discussed.

4.2 Theoretical background

4.2.1 The temperature structure parameter C_T^2

For optical propagation, the variance of the logarithm of the intensity perturbations (σ_I^2) of a spherical wave front originating from a point source (eg., a laser) as seen by a point receiver is related to the refractive-index structure parameter C_n^2 by the following relationship:

$$\sigma_I^2 = 0.496K^{7/6}L^{11/6}C_n^2\Phi\left(l_o/\sqrt{\lambda L}\right) \qquad (4.1)$$

This is valid provided that the integrated amount of scintillation over the optical path is small ($\sigma_I^2 \leq 1.2$) to avoid saturation (Ting-i Wang et al., 1978). For a given optical wavenumber $K=2\pi/\lambda$, the variance depends upon fluctuations in refractive-index changes described by C_n^2 and the inner scale (l_o) via the function $\Phi\left(l_o/\sqrt{\lambda L}\right)$. The inner scale marks the transition from the inertial-convective to the viscous-convective range and is a measure of the approximate dimensions of the small-scale viscous motions in which turbulent energy is converted into heat (Tennekes and Lumley (1972). Hill and Clifford (1978) give l_o as:

$$l_o = 7.4\left(\nu^3/\varepsilon\right)^{1/4} \tag{4.2}$$

where, ν is the viscosity of air and ε is the rate of turbulent kinetic energy dissipation. Function $\Phi\left(l_o/\sqrt{\lambda L}\right)$ is shown in Figure (4.1). For ease of computation and $l_o/\sqrt{\lambda L} \geq 0.2$, we describe $\Phi\left(l_o/\sqrt{\lambda L}\right)$ by the following polynomial:

$$\Phi(x) = 1.867 - 3.337x + 2.109x^2 - 0.447x^3, \tag{4.3}$$

where, $x = l_o/\sqrt{\lambda L}$. At this point, it should be clear that $\Phi\left(l_o/\sqrt{\lambda L}\right)$ (and hence l_o) is a prerequisite for extracting C_n^2 from measurements of σ_I^2. We return to the determination of l_o in later discussion.

At visible to mid-infrared wavelengths, it is fluctuations in temperature that are primarily responsible for atmospheric scintillation with humidity fluctuations having only a minor role. For optical scintillation such as the twinkling of laser beams, Weseley (1976b) showed that provided temperature and humidity fluctuations are strongly correlated, the temperature structure constant C_T^2 is related to C_n^2 by:

$$C_n^2 = C_T^2\left(\frac{\gamma P}{T^2}\right)^2\left(1+\frac{0.03}{\beta}\right)^2 \tag{4.4}$$

The refractive index for air (γ) is 7.9 x 10^{-7} K Pa^{-1} at λ = 0.67 μm, T is the average air temperature (K) and P the atmospheric pressure (Pa). The last bracketed term is a correction for the effect of humidity and depends upon the Bowen-ratio (β). This

equals the ratio of the sensible (H) to latent heat flux (LE) and serves as an indication of surface wetness. For well-watered vegetation, the evaporative flux is often given by the Priestley and Taylor (1972) formula which predicts a β of around 0.2 (at 20 C) and a correction term in Equation (4.4) of about 35%.

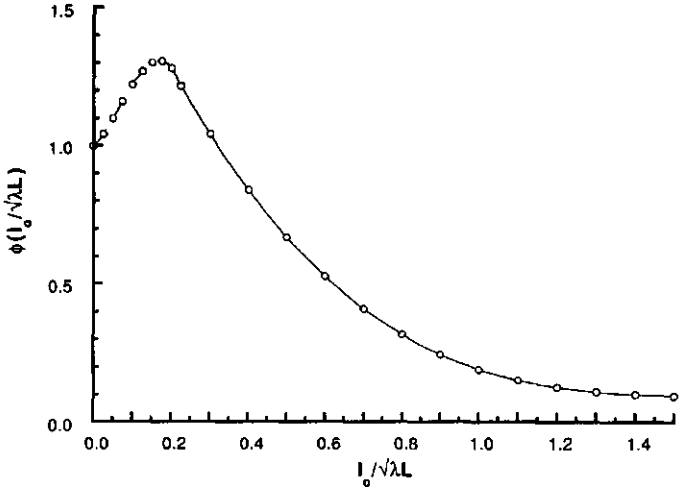

Figure (4.1). The relationship between the function, $\Phi\left(l_o/\sqrt{\lambda L}\right)$ and the inner scale normalised by the first Fresnel zone. Open circles derive from the spectrum for refractive-index fluctuations of Hill (1978). The continuous line is a 3rd order fit given in the text.

As soil water is depleted, latent heat becomes a decreasing component in the surface budget (see for example Figures 2 and 3 of Lagouarde and McAneney (1992)) and β increases. When β equals 0.6 the correction factor is 10%. For a dry surface Equation (4.4) simplifies to,

$$C_T^2 = C_n^2\left(T^2/\gamma\, p\right)^2 \tag{4.5}$$

In subsequent analyses, we will ignore the Bowen-ratio correction and use Equation (4.5).

C_T^2 can also be determined directly. Kohsiek, (1982a), for example, used spatially separated temperature sensors, a procedure which follows directly from the definition of a structure parameter (Panofsky and Dutton 1984). Alternatively C_T^2 can be obtained from spectral measurements with a single temperature sensor and invoking Taylor's 'frozen field' hypothesis, a process adopted in the current study. The one-dimensional spatial spectral density $S_T(k)$ of temperature in the inertial subrange of frequency (n) is given by:

$$S_T(k) = 0.25\, C_T^2\, k^{-5/3} \tag{4.6}$$

where, $k = n/U$ and U is the mean windspeed. We will present data using spectral densities from a very fine thermocouple for comparison with those derived from optical measurements of σ_I^2 and Equations (4.1) to (4.5).

4.2.2 Estimation of sensible heat and momentum fluxes

Equation (4.1) indicates that the measured signal from a low power laser contains information not only on sensible heat flux but also on mechanical turbulence under the guise of l_o. Hill et al. (1992a), Thiermann and Grassl, (1992a) and Thiermann (1992b) adopt various elegant optical methods of determining l_o. Our approach is closer to that of Wesely (1976a) who inferred the momentum flux from measurements of mean windspeed and an estimate of surface roughness. Since the sensible heat and momentum fluxes determine atmospheric stability, which also influences turbulent transport, an iterative procedure is necessary to untangle H from measurements of σ_I^2 and mean windspeed. This procedure is as follows.

We begin by defining a temperature scale:

$$T_* = -H/\varrho\, C_p u_* \tag{4.7}$$

where, ρ is the density of air, C_p is the heat capacity at constant pressure, and u_* is the friction velocity. Following Panofsky and Dutton (1984) and Hill et al. (1992a), we write C_T^2 and ε in dimensionless forms, which are assumed to be universal functions of ξ ($= z/L_{mo}$, where L_{mo} is the Monin-Obukhov length):

$$C_T^2/T_*^2 z^{-2/3} = f(\xi) = 4.9\left(1+7|\xi|\right)^{-2/3}, \quad \xi \le 0 \tag{4.8}$$

$$\kappa z\varepsilon / u_*^3 = h(\xi) = \left(1+0.5|\xi|^{2/3}\right)^{3/2}, \quad -2 \le \xi \le 0 \tag{4.9}$$

and

$$L_{mo} = -u_*^3 \varrho\, c_p T/Hg\kappa\,, \tag{4.10}$$

where von Karman's constant κ is taken as 0.4, g is the acceleration due to gravity and z is the height above ground or the zero plane displacement height for a vegetative surface. The empirical functions $f(\xi)$ and $h(\xi)$ derive from Wyngaard et al., (1971) and Wyngaard and Coté (1971b) respectively.

In order to evaluate $f(\xi)$ and $h(\xi)$, we first need an estimate for ξ which in turn depends on both u_* and H. Following Hill et al. (1992a), we define

$$G(\xi) = g^2 \kappa^{2/3} z^{4/3} C_T^2 / T^2 \varepsilon^{4/3} = \xi^2 f(\xi)\left[h(\xi)\right]^{-4/3} \tag{4.11}$$

Although the right-hand-side of Equation (4.11) looks complicated, we find that over the range of stabilities $-2 \le \xi \le 0$, $G(\xi)$ can be simply parameterised as follows:

$$G(\xi) = 0.00227 - 0.5184\xi\,. \tag{4.12}$$

This relation is shown in Figure (4.2). Using Equation (4.12), we then solve Equation (4.11) explicitly for ξ:

$$\xi = -1.929\left[\left(g^2 \kappa^{2/3} z^{4/3} C_T^2/T^2 \varepsilon^{4/3}\right) - 0.00227\right]. \tag{4.13}$$

The right-hand-side of Equation (4.13) still includes two ξ dependent terms, C_T^2 and ε. The former requires an optical measure of σ_I^2 as well as estimates of ξ and u_* in order to calculate the correction factor $\Phi\left(l_o/\sqrt{\lambda L}\right)$.

The approach adopted in this paper is to solve for ξ iteratively using values of ε estimated from measurements of mean windspeed (U) and an assumed initial value

for ζ. For unstable conditions, the vertical profile of mean wind velocity is given by the following expression:

$$U = u_* [ln((z-d)/z_o) - \psi_m(\zeta)]/\kappa \ , \qquad (4.14)$$

where z_o is a measure of the surface roughness, d is the zero plane displacement and ψ_m is the commonly used integrated stability correction for the diabatic wind profile (Panofsky and Dutton, 1984).

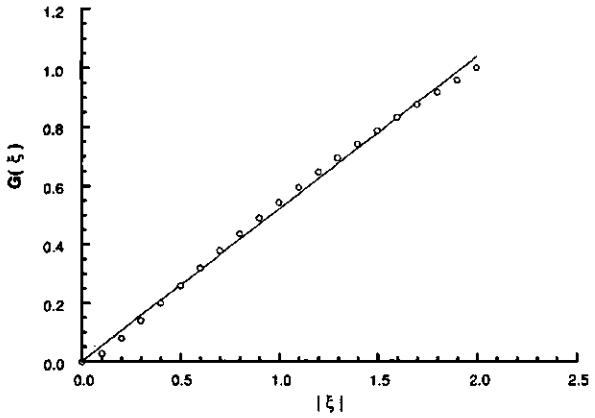

Figure (4.2). $G(\xi)$ as a function of ξ for $\xi \leq 0$ (open circles). The straight line is described by Equation (4.12).

For vegetative surfaces z_o and d can be taken as simple fractions of the vegetation height (h_C) ($d \approx 0.65 h_c$ and $z_o \approx 0.13 h_c$ after Stanhill (1969) and Tanner and Pelton (1960) respectively).

Equation (4.14) allows u_* to be determined given a measurement of U and estimates of z_o and d, together with an initial guess for ζ. This in turn permits calculation of ε and l_o, which allow C_T^2 to be calculated from the measured optical

signal of σ_I^2. This procedure, which calculates a value for u_*, and hence ε and l_o, *en route*, is repeated until the estimated and calculated values for ξ converge. In our experience this convergence occurs rapidly after a maximum of 3 to 4 iterations. H then follows from Equation (4.10).

Lastly we note that calculation of the *LE* could also be included in the above iterative process for little additional effort using the energy budget equation

$$LE = (R_n - G) - H,$$

requiring additional measurements of the available *energy A* ($=R_n - G$; where R_n is the net radiation and G the soil heat flux). This option was not pursued in the present study.

4.3 Scintillometer Design

4.3.1 Laser diode transmitter

A low cost semiconductor laser diode module (Radio Spares: #564-504) was selected to provide a point source of coherent radiation. Power output was 1 mW, operating at 0.67 μm wavelength with a collimating lens producing a 0.5 mrad diverged (full angle) beam with a pointing stability of 0.05 mrad. The beam is polarised and has a 6 mm diameter exit aperture. Typical power consumption is 1.5 W. Figure (4.3) shows a block diagram representation of the scintillation transmitter-receiver hardware.

A 100 KHz square wave excited the laser diode for ambient light discrimination at the receiver optics. The process served to increase the signal-to-noise ratio at the receiver sensor and avoided the need for mechanical choppers and narrow band-pass filters. To facilitate beam alignment the laser module was fixed to the side of a theodolite that was itself mounted on a surveyor's tripod. This arrangement allowed up to a 2 m beam propagation height and three dimensional alignment of the beam onto the point receiver 100 m away. Because of expansion and contraction of the tripod due to changes in air temperature, and misalignment of the optical signal that can result, future experiments will use a concrete support.

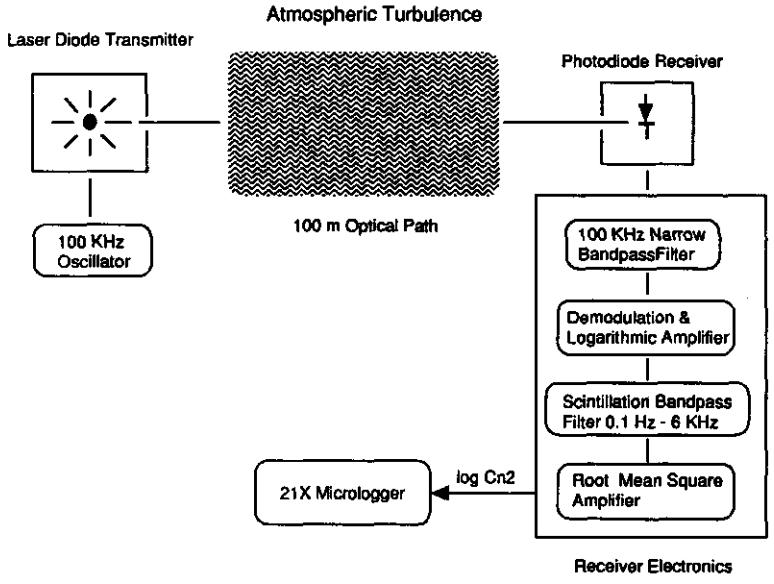

Figure (4.3). Block diagram representation of the scintillometer transmitter and receiver hardware.

4.3.2 Receiver

Receiver electronics are essentially those described by Ochs and Cartwright (1980) with some modifications to demodulate and band-pass filter the carrier wave. The receiver uses a high-speed photodiode (BPX 65) with an active surface area of 1 mm^2 mounted 3 mm behind a 1 mm diameter aperture. The unit is considered a point receiver as the aperture diameter is roughly an order of magnitude less than the first Fresnel zone ($\sqrt{\lambda L}$ = 8 mm). Coarse alignment is made using the theodolite telescope to focus onto the receiver aperture. Fine adjustments are performed using an oscilloscope to obtain the maximum signal amplitude.

The photodiode is housed in a plastic tube with pre-amplification electronics and was also mounted on a surveyor's tripod. The photodiode is configured within a trans-impedance amplifier and produces a voltage output proportional to the

irradiance on its active area. The signal is band-pass filtered centred on the carrier frequency and then demodulated to recover the scintillations. Further signal conditioning outputs the root-mean-square (variance) value of the logarithm of the intensity fluctuations in the scintillation bandwidth (0.1 - 6,000 Hz). Conditioning the signal in this manner has the added benefit that no absolute instrument calibration is needed and thus there are no problems associated with any electronic signal drift.

A logarithmic output is then chosen because of the large dynamic range of C_n^2 which typically spans from 10^{-15} to 10^{-12} $m^{-2/3}$. The root-mean-square circuit has an integrating time constant of approximately 2 sec so as to include the full bandwidth of scintillations. This time constant also means that rapid sampling of the analog output is unnecessary.

4.4 Experimental

4.4.1 Site descriptions and weather conditions

The first experiment took place under heavily overcast conditions over a flat, exposed pastoral site on the Purerua Peninsula, Bay of Islands (lat. 35° 16' S; long. 173° 55' E) in November 1992. The pasture had been grazed by sheep 3 - 4 weeks earlier and by the time of the experiment had an average foliage height around 0.13 m. The pasture composition was variable with predominantly clover and ryegrass species. Heavy rain several weeks prior to the experiment ensured that transpiration was unrestricted by soil water limitations. Windspeeds varied between 3.8 and 6 ms^{-1} and this together with the heavy cloud cover ensured that atmospheric stability remained very close to neutral ($\xi \approx 0$). Bowen ratios (β) averaged around 0.5. Minimum fetch was about 1 km.

The second experiment was carried out in mid-summer (February 1993) on a large, flat, dissected river terrace above the township of Clyde in Central Otago (lat. 45° 11' S; long. 169° 20' E.). This area of the South Island typically experiences very hot, dry summers and provided us with an opportunity to test the scintillometer under conditions of high sensible heat flux. Vegetation consisted of thyme (*thymus vulgaris*), an introduced plant, which has successfully adapted to the semi-arid climate of Central Otago. Under these conditions, the plant grows as a small shrub with

clumps, 0.3 to 0.4 m in height, interspersed with patches of bare ground and lichen. Ground cover was estimated visually at about 50%.

A wide variety of atmospheric conditions was encountered with day-time air temperatures on occasions exceeding 30 C and as low as 5 C at other times when snow fell on surrounding hills. On some days, data had to be rejected when air temperature changes caused movement in the laser mountings. Windspeed ranged up to 13 m s^{-1}. No substantial rain had fallen for several months and Bowen ratios were consistently high ($\approx$ 7) with the surface dry and dusty underfoot. The minimum streamwise fetch over thyme was of the order 1 km. Overall 6 days of data were obtained with ζ ranging between 0 and - 1.8.

4.4.2 Instrumentation and data analysis

For both experiments an optical path of 100 m was employed. The beam was aligned at heights above ground level of 1.2 and 1.5 m at Pureua and Clyde respectively. Efforts were made to ensure that the wind blew roughly at right angles to the optical path so that the eddies causing the scintillation were essentially being averaged over two directions.

Near the midway position and at the same height of the optical path, a simple stayed mast supported eddy covaraince instruments (Figure 4.4) consisting of a 1-dimensional sonic anemometer (10 cm path length), a fine thermocouple (13μm diameter), and a Krypton hygrometer (all from Campbell Scientific Inc., Utah, USA). These provided measurements of the fluctuations in vertical wind velocity, temperature and water vapour. A 2-dimensional drag anemometer (Green et al., 1992) gave absolute values for the fluctuating stream-wise and lateral windspeed components as well as mean windspeed and wind direction. The equipment was reorientated into the wind following any major wind shift.

Sampling frequency for the eddy covariance measurements was 10 Hz and data was processed on-line using a portable datalogger (Campbell Scientific Inc., Utah, USA) programmed to output 30-minute averages of covariances between the different variables and statistics required for the calculation of energy budget components, u_*,

and other derived variables. Calculation of $u*$ required a horizontal co-ordinate rotation.

On a second mast, mean wind speed was measured with a sensitive cup anemometer (stalling speed 0.2 m s^{-1}). Also measured were net radiation (Q^*6.1; Radiation Energy Balance Systems, Seattle, USA), air temperature (Campbell Scientific Inc., type 107 probe enclosed within a naturally ventilated radiation shield), and atmospheric pressure (SenSym, model SCX30AN).

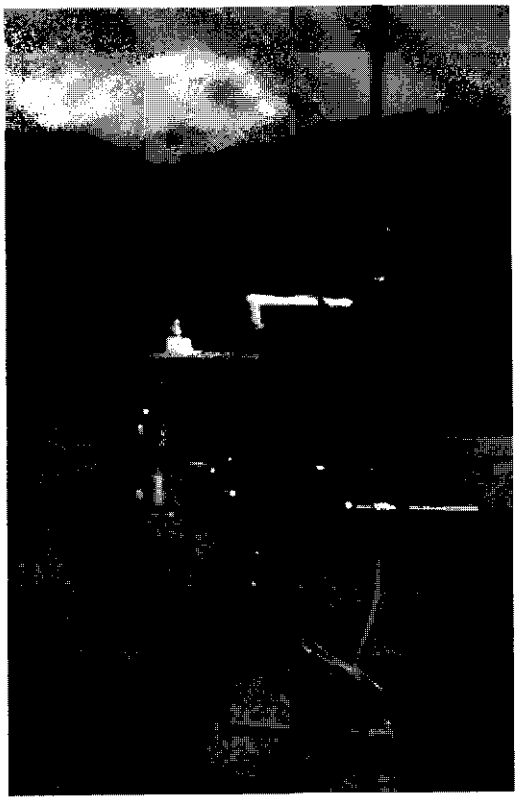

Figure (4.4). Eddy covariance instruments. The drag anemometer is in the background with the krypton hygrometer positioned below the sonic anemometer-thermometer in order to minimize wind blockage and to maximize the acceptance angle for wind direction.

These instruments were sampled each minute and 30-min averages or totals stored in a second 21X datalogger.

A third 21X datalogger with Fast Fourier Transform software (FFT) was dedicated to obtaining spectral measurements from the fine thermocouple. The 13 μm diameter junction has a frequency response exceeding 30 Hz (Tanner et al., 1985). A sequence of 2048 measurements of the fluctuating temperature was made at 20 Hz and an FFT calculated on-line. This procedure was repeated 13 times for each 30 minute period with the results stored as a running average. Bin averaging was used to output spectral energy values at 63 frequencies in the range of 0.156 to 9.81 Hz. A four term Blackman-Harris taper was applied to each data sequence to reduce leakage. Initial tests showed no evidence of aliasing and so no filtering was employed. As all equipment was operated from batteries, there was no contamination from mains frequencies.

4.5 Results and Discussion

4.5.1 C_T^2 comparison

Spectral estimates of C_T^2 were calculated by first fitting by eye a -5/3 line to inertial sub-range frequencies on a log-log graph (see Figure 4.5) and then taking spectral densities from this line usually at $k = 1$ (i.e. when $n = U$) to simplify Equation (4.6). We can expect inertial subrange behaviour for frequencies (n) greater than $2U/z$ (Kaimal et al. 1972; Fairall et al. 1980) and accordingly data was discarded if $U > 8$ m s^{-1} as we could not be confident the inertial sub-range extended far enough back into the measured range of frequencies. Recall that the nyquist frequency is fixed at n=10 Hz for a 20 Hz sampling rate.

The results of half-hourly C_T^2 comparisons are presented in Figure (4.6). The lower limit of the optical measurements is set by instrument noise and equates to a C_T^2 of 0.001 K^2 $m^{-2/3}$. All of the data (from both sites) presented in Figure (4.6) exceeds this threshold. The upper limit is set by the onset of saturation, which is usually taken to occur for $\sigma_I^2 \geq 1.2$ (Ting-i Wang et al. 1978). For λ = 0.67 μm wavelength and a 100 m pathlength, this value is approximately $C_T^2 \approx 6$ K^2 $m^{-2/3}$.

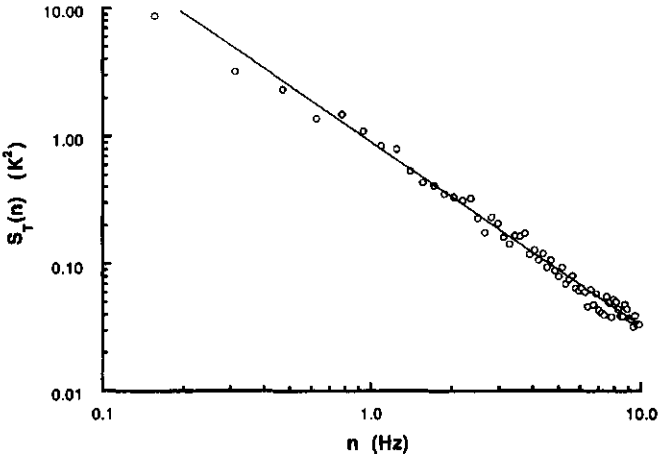

Figure (4.5). A typical half-hourly averaged temperature spectrum ($U = 4.7$ ms^{-1}). The line has a –5/3 slope indicative of an inertial subrange.

The plateau, which occurs at values beyond 2 K^2 m$^{-2/3}$ in Figure (4.6), is consistent with this limit. In practice, and in its current configuration (height and pathlength), this would result in an upper limit for H of around 500 W m^{-2}. This will vary a little depending on atmospheric stability.

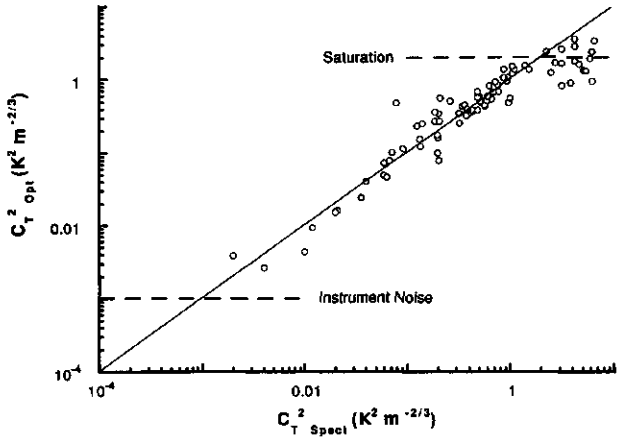

Figure (4.6). Comparison of optical and point measurements of C_T^2 for Pururua and Clyde cites. The line represents the 1:1 relationship.

For values below the onset of saturation, the modest scatter about the 1:1 line shows no obvious bias and linear regression analysis yields:

$$C^2_{Topt} = 1.05(\pm 0.036) C^2_{Tspect}$$

for the 72 data points. This relationship is not statistically different from the 1:1 line and demonstrates remarkable good agreement over a 4 decade range.

4.5.2 Sensible heat flux and friction velocity

To the authors' knowledge, there have been few detailed comparisons of surface fluxes derived from scintillation with independent measurements. Thiermann and Grassl (1992a) and Thiermann (1992b) show encouraging agreement between time series of sensible heat flux as measured by both optical and eddy covariance methods although the range for this comparison is limited ($H \leq 150$ W m^{-2}). For u_* there appeared to be systematic differences of the order of 30% between these two methods but again the range was limited ($u_* < 0.5$ m s^{-1}).

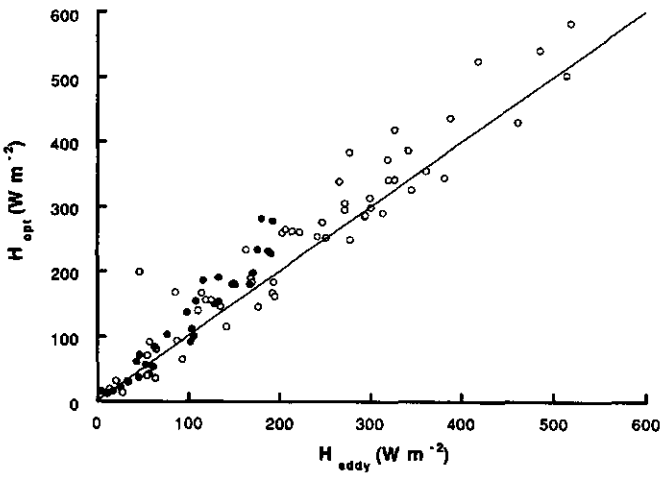

Figure (4.7). Sensible heat computed from optical scintillation and mean windspeed measurements compared to eddy covaraiance reference measurements for Pureua (•) and Clyde (o) sites. The line represents the 1:1 relationship.

Hill et al. (1992a) also present data over a similar range for H and u_*, but according to the authors very little of this data was collected for wind directions within the acceptance angle for the 3 -dimensional sonic anemometer.

Figure (4.7) shows our comparison of sensible heat fluxes as determined from optical scintillation and windspeed measurements, and those measured directly by eddy covariance. Regression analysis of the combined data (91 data points) from both sites, excluding those from Clyde when $C_T^2 > 2$ K^2 m$^{-2/3}$, resulted in the following relationship:

$$H_{opt} = 1.03(\pm 0.034) H_{eddy} + 19.55(\pm 6.888), \qquad r^2 = 0.93.$$

The residual standard deviation is 30 W m^{-2}. The optical method appears to over-estimate in the case of the higher-valued data points from Purerua: Thiermann (pers. comm.) suggests that spatially filtering the laser diode output to obtain a Gaussian irradiance profile may overcome any bias due to additional fluctuations in intensity near the perimeter of the beam. Nevertheless, the overall result implies near perfect average agreement. No correction for the Bowen ratio (Equation 4.3) was applied. For the Clyde data, this correction is trivial, whereas for Purerua, it would amount to about 10%.

The comparison presented above was carried out using 30-min estimates of sensible heat flux. This choice was made to reduce the statistical uncertainty in the eddy covariance measurements, which are taken as giving unbiased estimates of the fluxes. The statistical error in these reference covariance measurements is proportional to the square root of the ratio of the integral time scale and the duration of sampling (Wyngaard, 1973). For meteorological conditions typical of our experimental conditions, Wyngaard suggests a sampling uncertainty of around 5% for 30 min samples of sensible heat flux. In the case of optical scintillation, the time average approaches the ensemble average much more rapidly (Wyngaard and Clifford 1978) since it is time scales associated with eddy sizes near $\sqrt{\lambda L}$ that determine the sampling statistics. These scales are between a 100 and a 1000 times smaller that the integral time scale which is of the order of z/U.

The comparison between the friction velocities obtained from eddy covariance (sonic and drag anemometers) and the combination of optical scintillation and mean windspeed measured with a cup anemometer is shown in Figure (4.8). Regression analysis gives:

$$u_{*opt} = 0.98(\pm 0.039)u_{*eddy}, \qquad r^2 = 0.94.$$

The offset was non-significant. Under our experimental conditions, Wyngaard (1973) suggests a statistical uncertainty in eddy covariance measurements for u_* of around 13%. This would explain most of the residual standard deviation about the regression line of 0.062 m s^{-1} - this figure is equivalent to a percentage error of 12% for an average u_* of 0.5 m s^{-1}.

Errors in U due to say cup overspeeding would result in approximately proportional errors in u_*. Under our conditions this should not exceed 5 % (Coppin 1982). H is also sensitive to such errors - a 5% overestimate in U resulting in a 2.5% underestimate in H. Calculations of u_* are also sensitive to the choice of z_o, and to a lesser degree, d.

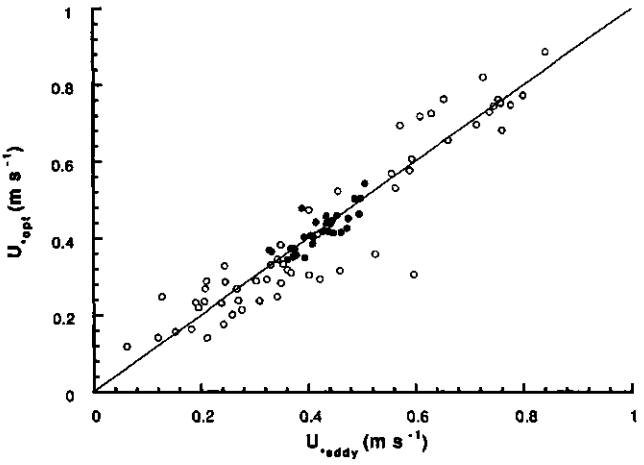

Figure (4.8). Comparison of friction velocities from the scintillometer and eddy covariance instruments at the Purerua (•) and Clyde (o) sites. The line represents the 1:1 relationship.

Both of these surface characteristics have been parameterised here as simple fractions of the crop height and for both experimental surfaces, the estimated values agreed very closely with those calculated independently from Equation (4.14) using eddy covariance values of u_*, and U from the drag anemometer.

In some ways this was a surprising result for the thyme canopy, which had a significant proportion of bare soil ($\approx 50\%$), and implies it is the height of the major roughness elements, rather than their spatial distribution, that is the important from a momentum flux point of view.

4.6 Summary

To date optical methods of measuring surface fluxes have not been widely exploited in boundary-layer studies although their theoretical foundation is established. The excellent results obtained in this study for both sensible heat and momentum fluxes estimated using a combination of optical scintillation and mean windspeed measurements provide a good test of this theory and suggest that optical scintillation can be used to provide routine estimates of these surface fluxes. The requirement for a cup anemometer is hardly less restrictive than the need for supporting measurements of air temperature and pressure. Extending the iterative procedure to estimate the latent heat flux would involve no additional computational cost provided that measurements of net radiation and soil heat flux were available. Further theoretical work to extend Monin-Obukhov similarity relations to non-homogeneous situations would be valuable and enable the path-averaging characteristics of scintillation to be fully exploited.

5

Sensible heat and momentum flux measured with an optical inner scale meter[1]

Abstract

Path-averaged measurements of sensible heat (H) and momentum fluxes (u_*) were made under unstable conditions ($|\xi| < 0.1$) above pasture using an inner scale meter (ISM), an instrument which employs in tandem both a diverging laser beam - point detector scintillometer and a second instrument using a large-aperture (15 cm) incoherent source and receiver of the same diameter. By distorting the beam, refractive turbulence along the optical path creates intensity fluctuations or scintillations at the receiver; eddies with spatial scales of the order of the beam diameter are most effective at this so that while the laser responds to the smaller eddies in the flow, the large aperture instrument is sensitive to inertial subrange turbulence. By combining signals from these two instruments, it is in principle possible to calculate H and u_* explicitly and independent of assumptions about surface roughness. Pathlengths were 100 m for the laser and 292 m for the large-aperture instrument. The site was chosen with the expectation of providing a homogeneous test surface.

Fluxes were first derived from a measurement of mean windspeed and either scintillometer operating independently, and, in line with previous experience, these agreed very closely with reference eddy covariance measurements. The worst case was when winds blew down the propagation path and H derived from the large aperture differed on average from reference measurements by 11%. We suspect that this systematic difference was real and that spatial non-uniformities in the surface energy budget combined with the pathlength differences meant that the two scintillometer beams experienced slightly different path-averaged refractive turbulence under some wind directions. Whatever the reason, this discrepancy engendered quite unrealistic ISM

[1] Green, A. E., McAneney, K. J. and Lagouarde, J-P., *Ag. & Forest Meteorol., 85, 259-267, 1997*

estimates for u_*, which depend very sensitively on the difference in the scintillometer output voltages. After excluding such data, ISM estimates and direct eddy correlation measurements of H agreed within 2%, but the error in $u*$ was still unacceptably high (residual standard deviation = 0.09 m s^{-1}). A sensitivity analysis confirms that the ISM estimate of H is relatively robust compared with u_* and we conclude that while the ISM does provide an alternative methodology for the measurement of sensible heat, it yields only a coarse estimate of the momentum flux.

5.1 Introduction

Apart from their operational simplicity, the main appeal of scintillation techniques in boundary-layer physics is their promise of providing spatially-averaged fluxes at scales of the order of several kilometres. Information at these scales is currently sought for a variety of hydrological and meteorological applications (Stewart et al., 1996). Briefly, scintillation methods work by transmitting a beam of electromagnetic radiation and measuring intensity variations or scintillations in the received signal and in this manner provide a direct measure of the strength of refractive turbulence - or more strictly the structure parameter for refractive-index (C_n^2) - along the path. At visible or near-infrared wavelengths, atmospheric scintillation is primarily the result of fluctuations in air temperature so that C_n^2 is closely linked to the sensible heat flux.

To date, determination of sensible heat flux (H) and/or friction velocity ($u*$) by scintillometry has usually required an ancillary measurement of the average windspeed (U) and estimates of surface roughness (z_o) and the zero plane displacement (d_o); fluxes are then derived via an iterative procedure based on Monin-Obukhov similarity described by Green et al. (1994) and McAneney et al. (1995). This approach has worked extremely well above homogeneous surfaces for which z_o and d_o can be prescribed as simple fractions of the crop height but presents some problems when the optical path traverses surfaces of widely varying surface characteristics (Lagouarde et al., 1996). De Bruin et al. (1995) also report good results after combining a scintillometer measure of C_n^2 and independent measures or estimates of $u*$.

Another option is to invoke the free convective limit, conditions under which H becomes independent of mechanical turbulence and follows directly from a scintillation measurement of C_n^2 and the mean air temperature (Wyngaard and Clifford, 1978). This approach should work increasingly well as the height of measurement increases but are often inappropriate near the surface.

Other possibilities for measuring H and u_* by scintillation include the bichromatic technique (Thiermann and Grassl, 1992a) or a commercially available displaced-beam scintillometer (Thiermann, 1992b). Both methods use visible lasers and will saturate in the sense that the signal variance will no longer increase linearly with C_n^2 as the strength of the refractive turbulence increases above a certain threshold (Clifford et al., 1974). In practice this feature limits their use to distances of the order of 100 -150 m for near-surface measurements.

In this paper we examine the efficacy of yet another method first suggested by Hill et al. (1992a) and called the Inner Scale Meter (ISM). In principle, this approach allows both H and u_* to be determined explicitly from optical measurements without the requirement for ancillary measurements or assumptions about the underlying surface or the atmosphere. The method, as we implement it, employs both a solid-state HeNe laser (0.63 μm wavelength) scintillometer and a large-aperture instrument (0.94 μm wavelength) in tandem. The ISM makes use of the dependence of the signal variance of the laser upon u_* and the fact that the large-aperture is insensitive to this variable. By combining signal variances from these two instruments both H and u_* can be determined unambiguously; Hill et al. (1992a) report encouraging results for a minimal data set. It is the purpose of this paper to test the ISM over a wider range of field conditions and to discuss its operational merits and limitations. The use of a laser scintillometer means our configuration is also limited to relatively short distances.

5.2 Theory

We concentrate here only on those details of the instruments important to their use as part of the ISM; for fuller details of their physical foundation and *modus operandi* the

reader is referred to Green et al. (1994), McAneney et al. (1995) and the literature cited therein.

5.2.1 Large-aperture scintillometer (LA)

The LA provides a direct measure of structure parameter for refractive turbulence C_n^2. For the case of equal transmitting and receiving apertures, this quantity is weighted by a symmetrical bell-shaped curve with a maximum at the centre (Wang et al., 1978; Lagouarde et al., 1996). After Wang et al. (1978), the relationship between the variance of the logarithm of the aperture-averaged signal intensity (σ^2_{LA}), C_n^2, aperture diameter (D), and the pathlength (L_{LA}) between transmitter and receiver, is:

$$\sigma^2_{LA} = 0.892\,\overline{C}_n^2\,D^{-7/3}\,L_{LA}^3 \tag{5.1}$$

The over-bar indicates a path-averaged value and in what follows, we may omit this without ambiguity. The general form of Equation (5.1) can be deduced from geometric optics (Tatarski, 1993) where D is the relevant length scale of the turbulent inhomogeneities most effective at causing large changes in intensity at the receiver.

At visible to mid infrared wavelengths, the temperature structure constant C_T^2 is related to C_n^2 by:

$$C_n^2 = C_T^2\left(T_a^2/\gamma\, p\right)^2\left(1+0.03/\beta\right)^2 \tag{5.2}$$

T_a is the average absolute air temperature, and p, atmospheric pressure. At the 0.94 μm peak wavelength of the LAS source, the refractivity of air (γ) equals 7.9 x 10^{-7} K Pa^{-1}. The correction for the Bowen-ratio ($\beta \neq 0$) in Equation (5.2) accounts for the minor influence of humidity fluctuations. Equation (5.2) assumes that temperature and humidity fluctuations are strongly correlated (Weseley, 1976a) consistent with Monin-Obukhov similarity (Hill, 1989).

5.2.2 Laser scintillometer

The equivalent relationship to Equation (5.1) for the logarithm of the signal intensity of a spherical wave propagating through the atmosphere and measured by a point detector is given by (e.g Thiermann and Grassl, 1992a):

$$\sigma_{lu}^2 = 0.496 C_n^2 \left(2\pi/\lambda\right)^{7/6} L_{lu}^{11/6} \Phi(l_i/F) \qquad (5.3)$$

where $F = \sqrt{\lambda L_{lu}}$ is called the first Fresnel zone and gives the scale of diffractional spreading; λ is the optical wavelength. The function $\Phi(l_i/F)$ is an analytical approximation for the behaviour of the inner scale at small wavenumbers (Hill and Clifford, 1978b). At a path length of 100 m, F is comparable in size to the inner scale (l_i) and it is these small eddies which are largely responsible for distorting the beam. The use of the term 'inner scale' to denote the smallest length scales in turbulent flows derives from the Russian literature where it has been commonly employed in place of the Kolmogorov microscale:

$$\eta = \left(\nu^3/\varepsilon\right)^{1/4}$$

η is determined by dimensional analysis from the dissipation rate per unit mass ε (m^2s^{-3}) and kinematic viscosity ν (m^2s^{-1}) (Tennekes and Lumley 1972). Hill and Clifford (1978) define l_i as the spatial scale characterising the transition between inertial-convective and dissipation ranges of the refractive index spatial power spectrum and show that the ratio of the l_i and η to be 7.4 (see Equation (5.6)).

Equation (5.3) holds provided that the field is weakly scattering; however, for $\sigma_{lu}^2 > 1.2$ the signal saturates in the sense that σ_{lu}^2 no longer increases linearly with C_n^2 (Clifford et al., 1974; Green et al., 1994). It is easily shown by substitution of typical values in Equation (5.3), and Equation (5.5), Equation (5.6) and Equation (5.9) which follow, that when C_n^2 is high, ie. ~ 10^{-12} $m^{-2/3}$, laser scintillometers are limited to distances not much over 100 m. This range could be improved by using longer wavelength lasers and operating at a greater height (Kohsiek, 1985); but not indefinitely - in the limit of l_i/F approaching zero with increasing L, $\Phi(l_i/F)$ approaches unity (Hill and Clifford, 1978) and the sensitivity of laser scintillation to l_i, as required for the ISM, vanishes.

5.2.3 The Inner Scale Meter (ISM)

Assuming the laser and large aperture scintillometers operate at the same beam height (z) and see the same refractive turbulence, then it follows from Equation (5.1) and Equation (5.3) that

$$\Phi(l_i/F) = \left[1.79(\lambda/2\pi)^{7/6} L_{LA}^{3} L_{la}^{11/6} D^{-7/3} \sigma_{la}^{2} / \sigma_{LA}^{2}\right] \tag{5.4}$$

and hence the function $\Phi(l_i/F)$ (and thus l_i,) depends on the ratio of the measured scintillometer log intensity variances for a given experimental configuration.

Further progress depends on the availability of an accurate model for the high frequency portion of the temperature spectrum. Hill and Clifford (1978) present a theoretical model for this spectrum that agrees with experimental measurements and explore its implications for optical propagation. For ease of computation, we parameterise their model as follows:

$$l_i = 0.30489F - 1.0389F \log \Phi(l_i/F) \tag{5.5}$$

This equation is simply an empirical fit for computational convenience and implies no theoretical foundation. It is appropriate for $l_i > 0.2F$ = 1.6 mm, a condition not violated in the present experiment. From l_i follows the rate of dissipation of turbulent kinetic energy (ε) (Hill and Clifford 1978):

$$\varepsilon = v^3 (7.4/l_i)^4 \tag{5.6}$$

The dissipation rate is closely related to u_* via Monin-Obukhov similarity (see below).

C_{nLA}^2 and $\Phi(l_i/F) C_{nla}^2$ are presented at the receiver outputs as scaled voltages V_{LA} and V_{la} of the form,

$$10^{(V_{LA}-14)} = C_{nLA}^2$$

and

$$10^{(V_{la}-14)} = \Phi(l_i/F) C_{nla}^2$$

Over a homogeneous surface, $\overline{C}_n^2 = C_{nLA}^2 = C_{nla}^2$, from whence it follows that

$$\Phi(l_i/F) = 10^{(V_{la}-V_{LA})} \tag{5.7}$$

The function $\Phi(l_i/F)$ is substituted into Equation. (5.5) to solve for l_i which can now be combined with C_{nLA}^2 to estimate u_{*op} and H_{op} as explained below.

Having determined both C_T^2 and ε, the former from the LA and the latter from both scintillation instruments, ISM estimates of H_{op} and u_{*op} are now calculated using the procedure outlined by Hill et al. (1992a). Both C_T^2 and ε are written in dimensionless form as universal functions of ξ (= z/L_{mo}, where L_{mo} is the Obukhov length):

$$\left(C_T^2\right)_{LA} z^{2/3} / T_*^2 = f(\xi) = 4.9\left(1+7|\xi|\right)^{-2/3} \tag{5.8}$$

$$\kappa z \varepsilon / u_*^3 = h(\xi) = \left(1+0.5|\xi|^{2/3}\right)^{3/2} \tag{5.9}$$

and the temperature scaling parameter is defined by,

$$T_* = -H/\rho\, c_p u_* \tag{5.10}$$

where ρ is the density of air, c_p the heat capacity at constant pressure and von Karman's constant κ is taken to be 0.4. Empirical functions $f(\xi)$ and $h(\xi)$ derive from Wyngaard et al. (1971).

To solve Equation (5.8) or Equation (5.9) for T_* and u_* respectively, and thus H, first requires knowing ξ. Here we follow Green et al. (1994) in linearising the equivalent equation from Hill et al. (1992a) for ξ in terms of known constants and the measured optical variables,

$$\xi = -1.929\left|\left(g^2 \kappa^{2/3} z^{4/3} \left(C_T^2\right)_{LA} T^2 \varepsilon^{4/3}\right) - 0.00227\right|. \tag{5.11}$$

g is the acceleration due to gravity (9.81 m s^{-2}). T_{*op} and u_{*op} now follow from Equation (5.8) and Equation (5.9) and H_{op} from Equation (5.10), where the subscripts refer to variables determined from the ISM.

Lastly we estimate the latent heat flux (L_vE_{op}) as a residual in the energy budget equation:

$$L_v E_{op} = (R_n - G) - H_{op} \tag{5.12}$$

where (R_n-G) is the available energy equal to the difference between the net radiation receipt by the surface (R_n) and the soil heat flux (G), and L_v is the latent heat of vaporisation of water. If desired, a value for β can be calculated and used iteratively to correct C_T^2 in Equation (5.2).

5.3 Experimental

5.3.1 Site Description and Weather Conditions

Field measurements were undertaken during the months of February and March, 1995 over pasture on the Purerua Peninsula, Bay of Islands (lat. 35° 16' S; long. 173° 55' E). For all wind directions except from the north-west, the minimum fetch was 1km; for north-westly winds, it was about 200 m beyond which the terrain became gently sloping. The pasture comprised a clover-ryegrass sward, which was maintained in a well-watered condition by episodic rainfall events throughout the summer. These surface conditions were reflected in low values of β (= H/L_vE) which averaged around 0.6 and crop height (h_c) increasing from 6 to 12 cm as grass grew over the duration of the experiment.

Both the laser scintillometer and the LA propagation paths were aligned in a NW-SE orientation (Figure 5.1) in order to take maximum advantage of daytime sea breezes. Daytime air temperatures averaged around 20 C with moderate windspeeds between 1 and 6 m s^{-1}. Conditions were often cloudy with R_n rarely exceeded 500 W m^{-2} and $|\zeta|$ mostly less than 0.1.

5.3.2 Deployment of instruments

Each scintillometer comprised a transmitter and receiver unit mounted on solid concrete block plinths set at opposite ends of the optical paths. The scintillometer beams were offset laterally by 0.5 m at a fixed height of 1.6 m above the surface. For ease of data collection both receiver units were situated side by side on a single concrete tower at the NW end.

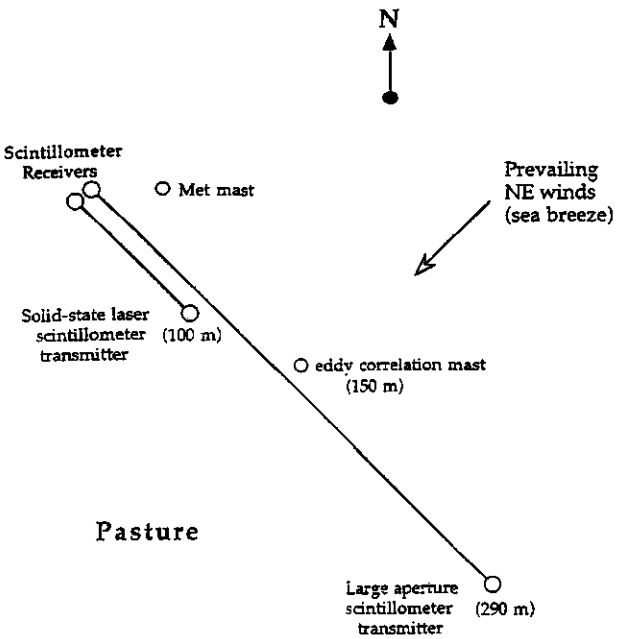

Figure (5.1). Schematic diagram showing the deployment of instruments

Originally, the pathlengths for each instrument were identical but the laser's optical path was shortened once the possibility of saturation was recognised. In retrospect, the same pathlength should have been employed for both scintillometers and data rejected when the variance of the log intensity of the laser signal, exceeded the saturation limit (Section 5.2.2). Final pathlengths for the laser scintillometer and

the LA were 100 and 292 m (Figure 5.1). In view of the sensitivity of both instruments to this variable ($L^{11/6}$ for the laser and L^3 for the LA), an infrared surveying range finder was used to establish the propagation pathlengths to an accuracy of several centimetres.

Whereas the LA instrument was identical to that described by McAneney et al. (1995), the laser scintillometer (Green et al., 1994) had been modified by the use of a 10 mW class IIIb (Model 29272, ORIEL Corp., Stratford, CT., USA) solid-state laser with a rated 5 mW output power for the transmitter. The beam is unpolarized, has a 1 mrad beam divergence, and emits continuous coherent radiation at 0.6328 μm. The laser was mounted within a radiation shield of white stainless steel tubing similar to that used for the LA.

The laser receiver unit comprised an optical head also mounted within a radiation shield and connected by shielded cabling to signal conditioning electronics. The head had been machined from plastic rod, contained a high speed photodiode (BPX65) and amplifying electronics, and was mounted directly behind a line interference filter (Model 52730, Oriel Corp.). This filter restricts incoming light to a 10 nm spectral band centred at the HeNe peak wavelength. A 1mm circular aperture in front of this filter acts as a point receiver for the incoming radiation. Electronic processing included band-pass filtering and the calculation of the variance of the logarithm of the signal intensity fluctuations (Ochs et al. 1990).

5.3.3 Reference flux instrumentation and supporting climatological measurements

Eddy covariance instruments were mounted as described in previous publications (eg. McAneney et al., 1995) on a simple stayed mast off to one side of the midpoint position of the LA path (Figure 5.1) and at the same height (1.6 m) as the optical beams. These instruments provided reference measurements for momentum (u_{*ec}), sensible (H_{ec}) and latent heat ($L_v E_{ec}$) fluxes. Instruments were orientated into the streamwise flow by rotating the mast following any major windshifts. Sensors for T_a (107 thermistor probe: Campbell Scientific Inc., Logan, Utah), R_n (Radiation Energy Balance Systems, Seattle), windspeed and direction were all measured from a second

mast nearer the scintillometer receivers. The averaging time for all calculations was 30 min.

5.3.4 Data collection and analysis

Data were downloaded from portable dataloggers (21X, Campbell Scientific Inc., Logan, Utah) at sunset each day and transferred to a computer spreadsheet for further manipulation. This involved first rejecting data for: (1) periods of rain; (2) poor angle of attack for the eddy correlation instruments; (3) when major wind shifts occurred during the integration period; (4) $R_n < 0$; (5) if energy budget closure for the eddy covaraince measurements was not achieved within 15% of R_n - G with the soil heat flux being assumed to be a fixed proportion (10%) of R_n.

Horizontal coordinate transforms were applied to the wind components prior to calculating u_{*ec}. Friction velocities and sensible heat fluxes were then calculated for each scintillometer as well as from the ISM and the results compared with eddy covaraince fluxes.

5.4 Results and Discussion

5.4.1 Laser and Large Aperture Scintillometers

The two scintillometers were first used independently to calculate sensible and momentum fluxes with the same cup anemometer measurements of U, and with z_o and d_o estimated from crop height (z_o = 0.13h_c and d_o = 0.65 h_c). Results for u_* from either scintillometer gave almost identical results and in the interests of brevity we only display the comparison of u_{*La} to u_{*ec} (Figure 5.2). Regression analysis indicates a slope of 1.04 (±0.011) and a residual standard deviation (RSD) of 0.03 m s^{-1}. Data for this comparison represents all wind directions including occasions when the wind blew down the scintillometer path. The corresponding sensible heat comparisons are presented in Figure (5.3a) and Figure (5.3b) and open circle symbols distinguish 'cross-path' (wind directions in excess of 45° of the optical path) and 'down-path' conditions (wind direction roughly aligned with the scintillometer paths). In the case of the LAS, H_{LA} was higher than H_{ec} on average by 8% for cross-path winds, whereas under down-path conditions, it underestimated by 11%; RSDs amounted to 27 W m^{-2} and 11 W m^{-2} respectively. H_{La}, on the other hand, shows little dependence on wind

direction and regression lines are not statistically different from the 1-1 relation. Scatter was again reduced for the case of down-path winds: RSD of 15 vs 23 W m^{-2}.

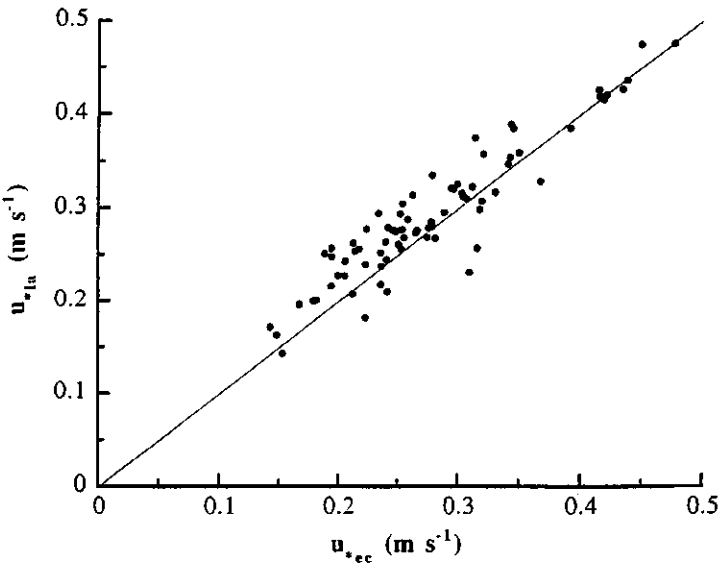

Figure (5.2). Comparison of the friction velocities from the laser scintillometer and the eddy covariance instruments for all wind directions. The straight line drawn is the 1:1 line.

The agreement between either scintillometer and eddy correlation measurements is in good accord with previous experience (Green et al., 1994; McAneney et al., 1995) and perhaps it would be optimistic to expect two independent flux measuring techniques, relying, as they do, on such different physical principles, to do much better. None the less, the effect of wind direction on the LA is curious, and at this juncture, not completely understood. Some attention to this issue is warranted as the apparent differences in refractive turbulence seen by the two scintillometers create problems for the ISM. We recall first that the windspeed and roughness characteristics of the surface were common to both instruments and so that any differences must result from the different estimations of C_n^2.

One line of thought concerns differences in sampling statistics as a consequence of the different pathlengths and the different sized eddies influencing the signal

variances of the two scintillometers. Whereas the laser responds to eddies near the Fresnel zone (approximately 1 cm), the LA reacts to eddies of size similar to the aperture diameter (15 cm).

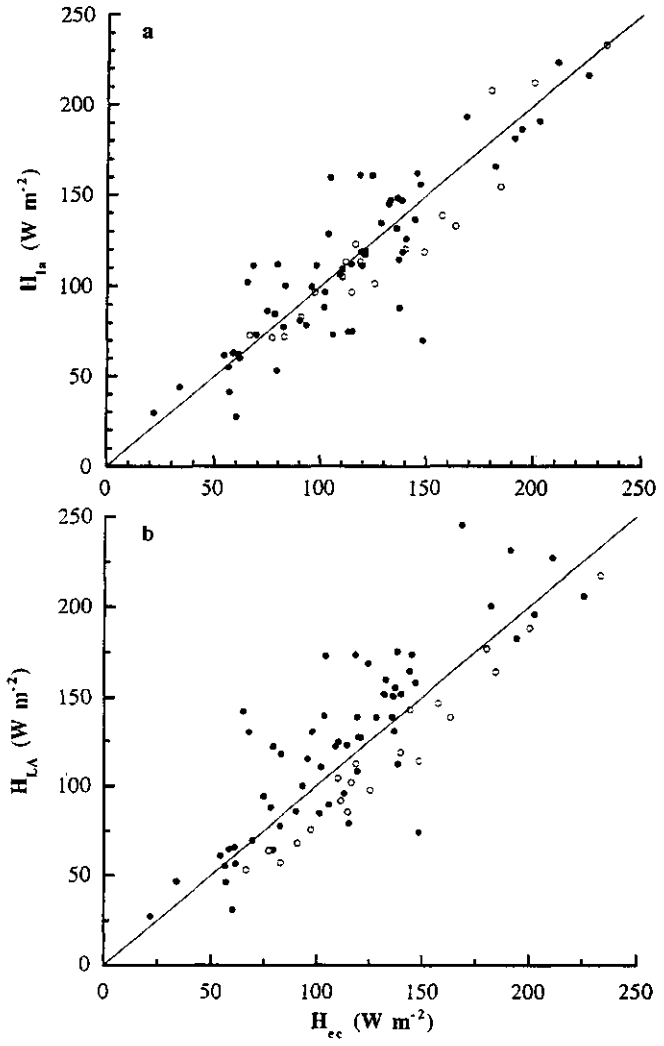

Figure (5.3). Sensible heat comparisons with the eddy covariance measurements for the laser (5.3a) and the LA (5.3b). Solid and open symbols represent cross-path and down-path wind data. Lines drawn indicate the 1:1 relations.

However, this contention is not supported by the data: for cross-path winds the scatter is similar for both instruments and, for the down-path case, and a lesser number of independent eddies sampled, Figure (5.3) indicates tighter correlations for either scintillometers with eddy covariance measurements.

Some other explanation is called. A further consideration is that the differences in H and hence C_n^2 seen by the two scintillometers are real and reflect slight variations in the surface energy budget across the field. Despite the visual impression of homogeneity, we can not rule out the possibility that local water and energy budgets varied spatially as much as 10 or 20% between the ends of the LAS path. In which case the different instruments would have weighted these varying source contributions in a different manner because of their unequal pathlengths.

When the wind blew down the path, the scintillation instruments lose some of their advantage of path-averaging over point measurements. That is to say that the shape of the footprints for the scintillometers should approach more closely that of eddy covariance instruments and we believe that this is the reason for the tighter correlation for these situations. Calculations using the formulations given by Schuepp et al. (1990) indicate that the peak sensitivity for the eddy covariance instruments was about 25 m upwind of the mast and for down-path conditions the tight correlation observed with either scintillometer is to be expected. More work is required to clarify this and, in future experiments, closer attention will be devoted to the performance of scintillometers vis-a-vis wind direction relative to the optical path.

5.4.2 Inner Scale Meter

A comparison of u_{*op} vs. u_{*ec} is given in Figure (5.4). Only cross-path conditions are shown as optical friction velocities calculated for down-path winds were often absurd ($u_{*op} >> u_{*ec}$) and, as such, discarded. Even so the scatter is much greater than when either scintillometer was used independently: regression analyses gave RSD values of 0.09 m s^{-1} for u_{*op} vs. u_{*ec} whereas the equivalent value using either the laser or the large aperture scintillometer in conjunction with a cup anemometer was 0.03 ms^{-1}. Comparison of Figure (5.2) and Figure (5.4) illustrates this point very clearly.

As indicated above, we believe the likely cause for such poor agreement with downpath winds is due to the systematic differences in the path-averaged C_n^2 seen by each scintillometer. Equation (5.5) and Equation (5.7) show that l_i is proportional to $(V_{la} - V_{LA})$ and any noise or systematic error in this value will be manifest as errors in u_{*op}. Even for lateral winds the agreement is poor, with u_{*op} often in error by a factor two. The only other published measurements of a similar nature are those of Hill et al. (1992) but their data for u_* are limited to very few points.

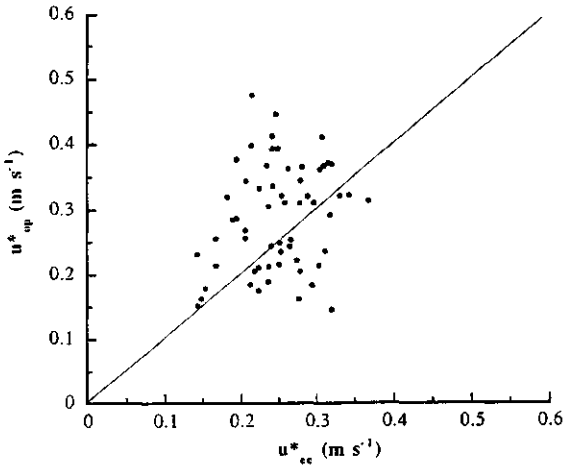

Figure (5.4). The ISM friction velocity compared to the eddy covariance measurements, only cross-path data are shown.

To overcome the problem we have selected data for the H_{op} and H_{ec} comparison when H_{LA} and H_{la} did not differ by more than 10% and under which conditions we have some confidence that the two scintillometers were affected by the same refractive turbulence albeit at different parts of the frequency spectrum. This selection includes some cases when the wind blew along the optical path from the SE and almost all of the cross-path data. It can be seen that the comparison is at least as good as the results obtained for H_{LA} and H_{la} (Figure 5.5). Regression statistics show a

slope of 1.02 (±0.05) and a RSD of 23 W m^{-2}. Hill et al. (1992a) also found satisfactory estimates for H_{op}.

The relative errors obtained for u_* and H are consistent with the analysis of Wyngaard and Clifford (1978) who show that the fractional momentum flux error is about twice that of the measured structure functions whereas scalar fluxes are much less sensitive. This is particularly the case under unstable conditions. Applying a similar analysis for ISM fluxes, it can be shown that the fractional error in u_* is three times more sensitive than H to absolute errors in the LAS voltage and that this difference in sensitivity increases with increasing instability.

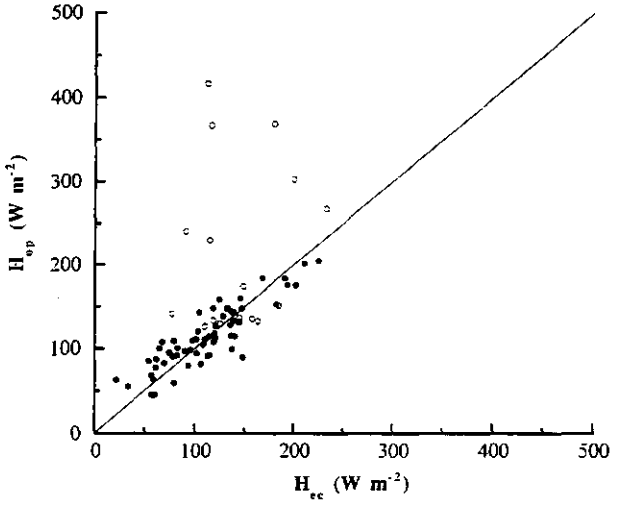

Figure (5.5). Sensible heat fluxes from the ISM compared to the eddy covariance instruments for conditions when H_{LA} and H_{la} agreed to within 10%. Symbols as in Figure (5.3).

Other errors considered by Wyngaard and Clifford (1978) such as uncertainties in various constants which appear in the equations and also the stability functions appear less serious given that these same constants and functions were successfully employed in the iterative process by which the fluxes were calculated from either scintillometer when used independently.

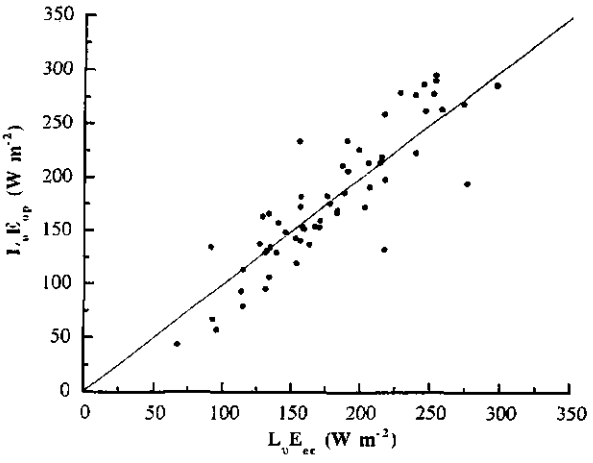

Figure (5.6). Comparison between the latent heat flux as calculated by difference between the available energy (R_n -G) and the cross-wind H_{opt}, and the directly measured eddy covariance value.

5.4.3 Latent heat flux

For completeness we show in Figure (5.6) a comparison between L_vE_{ec} and L_vE_{op}, the latter determined as a residual in the energy budget assuming that G constitutes 10% of R_n. Only crosswind data are presented. The result is not surprising as it faithfully reflects the sensible heat comparison of Figure (5.5). Similar results for L_vE determination were obtained from either the LA or laser scintillometer (data not shown).

5.5 Summary

Good agreement observed between reference eddy covariance sensible heat and momentum fluxes and those calculated from either scintillometer when employed independently provided further validation for this method of flux determination. However the LA measured systematically lower sensible heat fluxes when the wind blew down the optical path, a fact we believe is due to spatial differences in the surface energy budget and the different pathlengths employed for the two

scintillometers. While this did not seriously degrade H_{op} it translated to a serious overestimate of u_{*op} from the ISM for which the calculation is very sensitive to small errors in the difference in output voltages from the two scintillometers. Thus for our test of the ISM, data had to be discounted for most down-path winds as it invariably gave ridiculous values for the surface fluxes. Restricted to lateral winds or to occasions when H from either scintillometer used independently agreed within 10%, the ISM produced creditable sensible heat measurements with a similar accuracy to eddy correlation; however, the relative errors in u_* were still unacceptably high. We conclude that while the ISM provides another option for estimating either the path averaged sensible heat and/or latent heat fluxes, it yields an unsatisfactory measure of momentum flux.

6

Use of the scintillometer technique over a rice paddy[✓]

Abstract

Surface measurements of sensible heat flux (H) over rice paddies were made for several days using a large-aperture scintillometer (LAS) operating at near-infrared wavelengths. At these wavelengths temperature (T) fluctuations normally control refractive fluctuations and humidity (Q) fluctuations are considered a minor contributor. Under conditions of low Bowen-ratio, β encountered over the rice paddies the correlated T-Q fluctuations in theory will contribute to the refraction-index structure parameter, C_n^2. For low values of β and overcast skies, daytime C_n^2 fluctuated between 10^{-16} $m^{-2/3}$ and 10^{-14} $m^{-2/3}$. These values were smaller on average than observed nocturnal values but greater than the LAS signal-to-noise figure (10^{-17} $m^{-2/3}$ rms). Correcting the half-hour data for T-Q fluctuations did not improve a sensible heat flux comparison between the scintillometer and eddy covariance instruments over a small dynamic range of data ($-100 < H < 100$ Wm^{-2}).

6.1 Introduction

Throughout the Asian region traditional land usage has involved rice production. In Japan rice is grown in abundance in both small and larger holdings as an important local crop. Large volumes of water, a valuable resource in Japan are used to grow the rice. Knowing the aerial averaged water use of the rice paddies is needed for long-term sustainable agricultural production, as human activities demand more land and facilities for housing and industrialisation at the expense of food production. Understanding the energy balance dynamics of the rice paddy at scales close to the paddy footprint we can quantify and then optimise water usage throughout a region.

[✓] Green, A. E and Hayashi, Y., *Japanese J. Agric. Meteorol. 54 (3), 225-234, 1998*

Scintillometers can determine the surface fluxes of sensible heat, latent heat (E) and momentum at scales equivalent to the paddy sizes. To date, scintillometer research has concentrated on H measurements over drier surfaces. For instance Hill et al. (1992a) collected data over semi-arid desert in Colorado, De Bruin et al. (1995) measured over a valley of olive trees during the Crete summer and McAneney et al. (1995) used scintillometry over pasture in the New Zealand late summer. For all of these situations β has been greater than 0.5 and nowhere as low as values found over heavily irrigated vegetation ($\beta < 0.2$).

This study used a LAS developed by NOAA, Boulder, CO., (Ochs et al., 1980). The LAS has an operational advantage over laser scintillometers that it's signal does not saturate with increased refractive turbulence and it will transmit at least 5 km (De Bruin et al., 1995). It is not our intention to describe in detail the scintillometer design, as this has been discussed elsewhere (e.g. McAneney et al., 1995). Briefly though, the LAS transmitted a near-infrared beam across the surface under study. Atmospheric fluctuations in T and Q are linked to the surface fluxes H and E. These fluctuations altered the refractive-index (n) of the atmosphere causing the beam to scintillate. The amplitude modulation of the beam was caused by spatial variations in these scalar quantities, from which surface fluxes could be inferred. Homogeneity of the surface and stationarity of the atmosphere are required for the scintillometer method. The scintillations are caused by small-scale turbulence and the statistics quantifying these spatial variations are structure parameters. These parameters scale with height above the surface as dimensionless functions of atmospheric stability (Monin Obukhov similarity theory, MOST). The LAS offers the advantages of aerial path-averaging as opposed to more conventional measurement methods; short averaging periods (order of minutes) as turbulent information is extracted from the inertial subrange of eddy sizes; no requirement for absolute calibration as the log-intensity fluctuations of the received signal is measured simplicity of operation (essentially a Newtonian telescope) and a relatively low component cost (< NZ $2,000).

In recommending the suitability of the scintillometry technique to operation over well-watered surfaces it must first be tested under a variety of plant development and atmospheric conditions. Using a theoretical framework we explain the effect of correlated T-Q fluctuations on C_n^2. This is a similar explanation to that presented by

Wesley (1976a). In addition, the semi-empirical methodology for coupling the LAS measurement to the surface fluxes is outlined. The results of the experiment reported here focus on the final days prior to rice harvest. The paddies had been drained and plant growth had slowed. The soil was damp and soft with $\beta < 0.3$. The days were frequently cloudy, hot and humid with no visible scintillations. As a result low values of C_n^2 were experienced which was a test of the LAS to estimate small values of H. As a benchmark for the LAS performance, 30-minute averaged sensible heat fluxes were compared made to diurnal measurements taken using the eddy covariance method.

6.2 Theory

6.2.1 Relating fluctuations in temperature and humidity to the refractive index.

Spatial fluctuations in temperature, humidity and pressure about mean values $<T>$, $<Q>$ and $<P>$ within the inertial subrange of eddy sizes, cause fractional changes in the refractive index,

$$\frac{\partial n}{\langle n \rangle} = A_T \frac{\partial T}{\langle T \rangle} + A_Q \frac{\partial Q}{\langle Q \rangle} + A_P \frac{\partial P}{\langle P \rangle} \tag{6.1}$$

The wavelength (λ) dependent constants A_T, A_Q and A_P represent the contribution to $\partial n/\langle n \rangle$ from dry air, water vapour and atmospheric pressure respectively. For visible wavelengths the calculated ratio $A_T/A_Q \approx 4.6x10^{-3}$ (Hill et al., 1980). Anomalous dispersion of n about water vapour resonance is negligible at near-infrared wavelengths and is not considered in this analysis. In the atmospheric surface layer fractional changes in pressure, $\partial P/\langle P \rangle$ are generally much less than temperature and can be ignored. Unless fractional changes in humidity $\partial Q/\langle Q \rangle$ are substantially greater than temperature, $\partial T/\langle T \rangle$ (such as over wet surfaces) then fluctuations in atmospheric n will depend only on temperature at these wavelengths.

The refractive-index structure parameter, C_n^2 is often used to quantify the mean spatial variability of ∂n for separation distances (r) in the inertial subrange defined by,

$$C_n^2 = \left\langle \frac{\partial n}{r^{1/3}} \right\rangle^2 . \tag{6.2}$$

Substituting Equation (6.2) into Equation (6.1), assuming <n>=1, ignoring fractional pressure changes and expanding the quadratic gives,

$$C_n^2 = \frac{A_T^2 C_T^2}{\langle T \rangle^2} + 2\frac{A_T A_Q C_{TQ}}{\langle T \rangle \langle Q \rangle} + \frac{A_Q^2 C_Q^2}{\langle Q \rangle^2} \tag{6.3}$$

where, $C_T^2 = \left\langle \partial T / r^{1/3} \right\rangle^2$ (K^2 $m^{-2/3}$), $C_Q^2 = \left\langle \partial Q / r^{1/3} \right\rangle^2$ ((g m^{-3})^2 $m^{-2/3}$) and $C_{TQ} = \left\langle \partial T \partial Q / r^{2/3} \right\rangle$ (K g m^{-3} $m^{-2/3}$) are defined as the temperature, humidity and joint temperature-humidity structure parameters respectively. Note that C_T^2, C_Q^2, and C_{TQ} unlike C_n^2 are not wavelength dependent.

Temperature and humidity are usually strongly positively or negatively correlated in the inertial subrange of eddy sizes. Following Kohsiek (1982b), and Hill et al. (1988), we now apply the relationship,

$$C_{TQ} = \pm\sqrt{(C_T^2 C_Q^2)}, \tag{6.4}$$

and rearrange Equation (6.3) thus,

$$C_n^2 = \frac{A_T^2 C_T^2}{\langle T \rangle^2} \pm 2\frac{A_T A_Q C_T C_Q}{\langle T \rangle \langle Q \rangle} + \frac{A_Q^2 C_Q^2}{\langle Q \rangle^2} . \tag{6.5}$$

We separate terms to emphasise the importance of temperature fluctuations on C_n^2 at visible to near-infrared wavelengths.

$$C_n^2 = \left[\frac{A_T^2 C_T^2}{\langle T\rangle^2}\right]\left[1 \pm 2\frac{A_Q C_Q \langle T\rangle}{A_T C_T \langle Q\rangle} + \left(\frac{A_Q C_Q \langle T\rangle}{A_T C_T \langle Q\rangle}\right)^2\right]. \tag{6.6}$$

Measurement of C_T^2 and C_Q^2 provides a solution to C_n^2. Unfortunately this approach requires a microwave scintillometer which is sensitive to humidity fluctuations. Such equipment is sophisticated and expensive. Instead we introduce the relationship first applied experimentally by Weseley (1976a) and later verified by Kohsiek (1982b) that,

$$\beta = \left(\frac{\varrho\, C_p}{L_E}\right)\left(\frac{C_T}{C_Q}\right). \tag{6.7}$$

L_E is the latent heat of vaporisation of water, C_p the specific heat capacity of air at constant pressure and ρ the density of air. Equation (6.6) is now simplified further by substitution of Equation (6.7),

$$C_n^2 = \left[\frac{A_T^2 C_T^2}{\langle T\rangle^2}\right]\left[1 \pm 2\frac{A_Q \langle T\rangle \varrho\, C_p}{A_T \langle Q\rangle L_E \beta} + \left(\frac{A_Q \langle T\rangle \varrho\, C_p}{A_T \langle Q\rangle L_E \beta}\right)^2\right]. \tag{6.8}$$

This removes the need to measure C_n^2 directly. Further we define,

$$\Omega = \frac{A_Q \langle T\rangle \varrho\, C_p}{A_T \langle Q\rangle L_E \beta}.$$

Equation (6.8) now becomes,

$$C_n^2 = \left[\frac{A_T^2 C_T^2}{\langle T\rangle^2}\right]\left[1 \pm 2\frac{\Omega}{\beta} + \left(\frac{\Omega}{\beta}\right)^2\right]. \tag{6.9}$$

As the polarity of the *T-Q*, inertial subrange correlation coefficient is equivalent to the sign of β (Weseley et al., 1976a, Friehe et al., 1975 and Kohsiek, 1982b) then,

$$C_n^2 = \left(\frac{A_T^2 C_T^2}{\langle T \rangle^2} \right) \left(1 + \frac{\Omega}{\beta} \right)^2 \tag{6.10}$$

Weseley (1976) determined a value of $\Omega = 0.03$ for visible wavelengths which can be calculated by assuming values of; $<T> = 298$ K; a relative humidity of 80%; $\rho = 1.2$ kg m^{-3}; $C_p = 1.01$ kJ kg-1 K-1; $L_E = 2.45 \times 10^3$ kJ Kg-1; $A_T = 0.78 \times 10^{-6}$ (see Hill et al., 1980). Substitution into Equation (6.10) gives,

$$C_n^2 = C_T^2 \left(0.78 \times 10^{-6} \frac{\langle P \rangle}{\langle T \rangle^2} \right) \left(1 + \frac{0.03}{\beta} \right)^2 . \tag{6.11}$$

Equation (6.11) includes the combined effect of T-Q fluctuations on C_n^2 but represented through the inclusion of β. In this fashion measurements of C_{TQ} and C_Q^2 are not required. It is therefore expected Q fluctuations will increase C_n^2 if they are strongly coupled to T fluctuations in the inertial subrange. For example, if $\beta = 0.1$, then less than 60% of C_n^2 would be attributed to C_T^2, from which H_{sc} would ultimately be determined. A compromise in this method is combining a point measure of β with a path-averaged C_n^2. For dry surface conditions ($\beta > 0.6$) C_n^2 only depends on C_T^2 and Equation (6.11) reduces to a better-known form, rearranged in terms of C_T^2 thus,

$$C_T^2 = C_n^2 \times 10^{12} \left(\frac{\langle T \rangle^2}{0.78 \langle P \rangle} \right)^2 . \tag{6.12}$$

In practice, C_n^2 is obtained directly from the LAS receiver output and the average values of P (N m^{-2}) and T (K) are taken from slow-response sensors.

6.2.2 Equations for determining surface fluxes from structure parameters

Wyngaard and Clifford (1978) outlined the theory for linking the surface fluxes to the structure parameters. H is indirectly estimated from calculations of C_T^2 using MOST and a measurement of C_n^2, which is proportional to the log intensity variance of the received scintillometer signal, σ_I^2. This proportionality depends on the scintillometer aperture diameter D, and the propagation pathlength L (m). From Wang et al. (1978) we have,

$$\sigma_I^2 = 0.892 C_n^2 D^{-7/3} L^3. \tag{6.13}$$

Equation (6.13) requires equal transmitting and receiving apertures. The scintillometer is most sensitive to turbulent eddies that are of the same size as D (15 cm). Wang et al. (1978) designed the LAS to avoid the problem of signal saturation in strong turbulence as experienced by laser scintillometers (Clifford et al., 1974). The spatial, low-pass filtering of eddies smaller than D removes the dependence of the LAS determined C_n^2 on the microscale of refractive turbulence. σ_I^2 is measured at the scintillometer receiver. A scaled output is available in units of C_n^2 (Ochs et al., 1980). The bell-shaped, spatial weighting function for C_n^2 (Wang et al., 1978) has a maximum at $L/2$ and tapers to zero at the transmitter and receiver ends of the propagation path. A value of C_n^2 determined from the LAS is used to calculate C_T^2 using Equations (6.11) or (6.12), depending on surface wetness.

Having established a value for C_T^2 derivation of the sensible heat flux requires MOST. If C_T^2 is made dimensionless using units of temperature and length (see Equations (6.15) and (6.16)) it becomes a function of atmospheric stability ($\xi = z/L_{mo}$). Here z is the measurement height above the zero plane displacement height (d) and L_{mo} is the Obukhov length scale. Over a moist surface ξ is given by (Panofsky and Dutton, 1984) as,

$$\xi = -\frac{zg\kappa H(1+0.07/\beta)}{u_*^3 \varrho\, C_p \langle T \rangle}. \tag{6.14}$$

The constant g is gravitational acceleration (9.81 m s^{-2}), u_* is the friction velocity (m s^{-1}) and κ = 0.4 is von Karman's constant. From the 1968 Kansas experiments, Wyngaard (1973), we fit C_T^2 with the functional form for unstable conditions ($\xi \leq 0$),

$$f(\xi) = \frac{z^{2/3} C_T^2}{T_*^2} = 4.9\left(1+7|\xi|\right)^{-2/3}. \tag{6.15}$$

And,

$$f(\xi) = \frac{z^{2/3} C_T^2}{T_*^2} = 4.9\left(1+2.4(\xi)^{2/3}\right), \tag{6.16}$$

for stable conditions ($\xi \geq 0$). Here T_* is the temperature scaling parameter defined by,

$$T_* = -\frac{H_{sc}}{\varrho\, C_p u_*} \tag{6.17}$$

As C_T^2 is linked to H_{sc} via Equation (6.16) and Equation (6.17) any reduction in C_T^2 due to strongly correlated T-Q fluctuations over wet surfaces will reduce the calculated H_{sc}. Solving either Equation (6.15) or Equation (6.16) for T_* provides one way of determining H_{sc} from Equation (6.17). This process requires knowing ξ, u_* and maybe β.

A combination of a laser and a LAS can be used to measure the turbulent inner scale (Hill et al., 1992a, Green et al., 1997) from which u_* can be deduced. This was not attempted in this experiment as the technique is path-limited to short distances. The lack of available spatial measurements of u_* is overcome by using a measure of the average windspeed, V (cup anemometer) and an estimate of the surface roughness (z_o) then applying,

$$u_* = \frac{\kappa V}{ln\left[\left(\frac{z-d}{z_o}\right) - \Lambda(\xi)\right]} \qquad (6.18)$$

(Panofsky and Dutton, 1984). The integrated stability correction for the diabatic wind profile,

$$\Lambda(\xi) = ln\left\{\left((1+x^2)/2\right)\left((1+x)/2\right)^2\right\} + 2arctan(x) + \pi/2 \text{ , where } x = \left(1+16|\xi|\right)^{1/4},$$

for unstable conditions and $\Lambda(\xi) = -5\xi$ for stable conditions. A measure of the vegetation height h_v is usually sufficient to estimate z_o and d as for homogeneous canopies, $d \approx 0.65\ h_v$ and $z_o \approx 0.13\ h_v$ (McAneney et al., 1995). This procedure is complicated for sparse vegetation of varying crop height where it is unsure what h_v is appropriate.

To solve Equation (6.18) for u_* a value for ξ must be known. As ξ is not measured then an iterative procedure is used. A value of ξ is first guessed and substituted into Equation (6.18) to calculate u_*. Using the value of ξ and a measured C_T^2, T_* is calculated from either Equation (6.15) or Equation (6.16). H_{sc} is then calculated from Equation (6.17) using u_* and T_*. Finally, Equation (6.14) calculates a new value of ξ, which is substituted into Equation (6.18) and the process reiterated until convergence. If necessary β can also be deduced iteratively. Alternatively, if net radiation (R_n) is measured and a value for soil heat flux (G) assumed, then β ($=H/E$) is calculable by first solving for E using the Earth's energy budget equation,

$$E = R_n - G - H_{sc}$$

The success of this approach depends on the initial accuracy of H_{sc}.

6.3 Experimental Site and Conditions

In Japan rice paddies are spread out amongst housing and industrialised areas and it was difficult to discover a location near to the NIAES (National Institute of Agro-Environmental Sciences, Tsukuba) having sufficient fetch for the scintillation experiment. A block of commercially grown rice paddies at Yawara (lat. 140° 00' 59"; long. 36 ° 00' 30") 20 minutes by car SW of Tsukuba, was chosen as the best compromise of a flat site with homogeneity of canopy and a suitable fetch. These lowland fields were surrounded on their perimeter by the Yawara village and major roads. The most suitable wind direction was from the South (see Figure 6.1). The fields sloped gently to the East to assist a gravity feed irrigation system and were organised as rectangular plots orientated E-W roughly 100-200 m^2 in area and bounded by low concrete walls to retain the irrigation water. A series of three sequential plots were chosen for the scintillometer optical path which was orientated E-W over a distance of 320 m and average height above the rice canopy of 1.2 m.

The scintillometer beam crossed over a tar-sealed road and a drainage ditch at 100 and 200 m respectively from the scintillometer transmitter. The eddy covariance masts were not positioned at the midpoint but installed 100m from the scintillometer receiver, with the instrumentation orientated South into the dominant wind direction (which bisected the scintillometer beam). The farmer requested the rice crop was not disturbed so the eddy covariance instruments had to be extended over the canopy from the sides of an access causeway. The scintillometer receiver was set up on a roadside and the transmitter on the bank of an irrigation channel. Propagating the scintillometer beam across this water channel or having the receiver near to the constant traffic movement did not present a problem for the C_n^2 measurements as the path weighting tapers to zero at either end. Fetch was estimated to be at least 800 m over the homogeneous rice paddies to the distant motorway and urban area.

The experiment took place over several weeks in September 1996 prior to the rice harvest and towards the end of the Japanese summer. The rice had begun to yellow off and the fields had been drained of irrigation water. Soil conditions were however still very damp and soft underfoot. The days were frequently overcast, humid and hot with a light breeze. It was the typhoon season and the experiment was

postponed if rainy conditions threatened. The preferred southerly wind with its warm air and fine weather was evasive, making data collection sporadic.

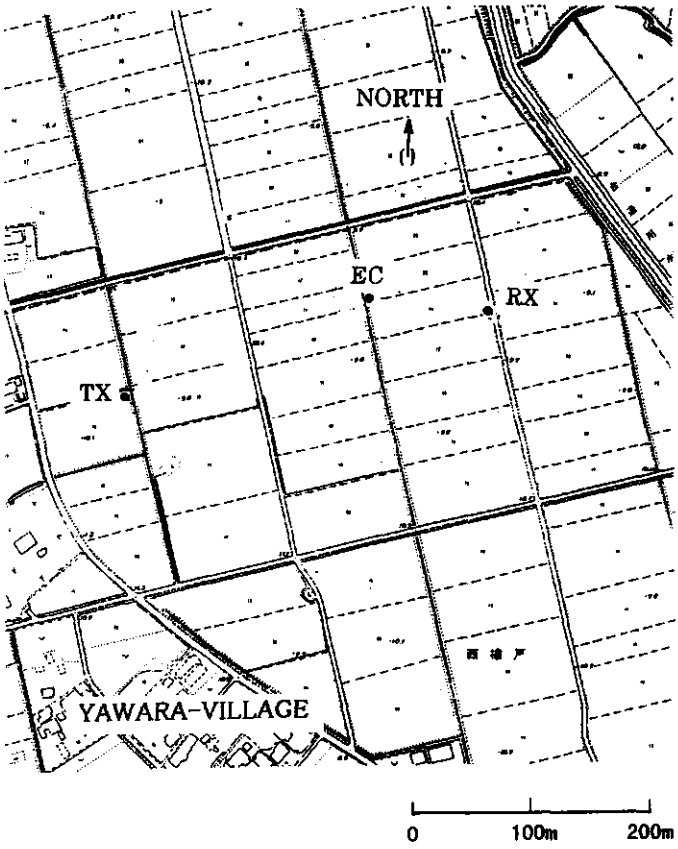

Figure (6.1). Experimental site for the scintillometer experiment. The LAS transmitter (TX) on the side of a drainage ditch propagates its near-infrared beam across 320 m of rice paddy to the LAS receiver (RX) just off the roadside. The eddy covariance instruments (EC) are mounted on masts accessed by a narrow causeway.

There were several varieties of rice being grown in this area and fortunately ours (Kinuhikari species) was the late maturity type, an advantage as the farmers were beginning preparations for a harvest which would quickly destroy the rice canopy. The vegetation height, $h_v \approx 80$ cm and z_o was set at 10.4 cm. The *honami* effect is characteristic of rice paddies on windy days. Turbulent eddies fluctuating at the

natural resonant frequency of the rice stalks flatten them into a patchwork pattern. Frequent periods of heavy rain also pushed clumps of rice stalks over. Fortunately measurements were completed before this weather and plant damage became too severe.

6.4 Instrumentation and data collection

A LAS spatial averaged the sensible heat flux over the 320 m. The transmitting and receiving units were mounted on metal surveyor tripods set to maximum extension (Figure 6.2). Vertical and lateral alignment of the units used telescopic sites to maximise receiver signal strength which was monitored by a portable oscilloscope. Each unit was covered with a thermal blanket to reduce mechanical expansion of the mountings and avoid scintillometer beam drift.

Average T (thermistor in heat shield) and V (sensitive cup anemometer) were measured at the LAS receiver position. The LAS electronics produced a filtered and scaled analogue output of C_n^2. The scintillation bandwidth was set at 0.03 to 400 Hz. The LAS output was sampled every 1 s and averaged for 30 min. using a 21X micrologger (CSI Inc., Logan Utah USA). The air temperature and windspeed were sampled at 60 s intervals and averaged over 30 min. using the same 21X. The cup anemometer was not positioned over the rice canopy and only served to indicate windspeed at the receiver position.

At the eddy covariance site (see Figure 6.1) instruments were mounted on several stayed masts and positioned over the rice canopy. A combination of windspeed and direction were recorded at 1.85 m above the surface using a Gill micro-vane (Model 1203/12305) and a 3-cup anemometer (Model 12012). Air temperature measurements were made using a naturally aspirated thermistor in a radiation shield (VAISALA DTR13) at z = 1.35 m. Solar radiation was measured using a solarimeter (EKO MS-62) set on a tripod at z = 1.2 m within the rice paddy perimeter. Dataloggers (Kona System Co., Ltd Japan, model KADEC-US) sampled these variables at 10 minute intervals, which were later averaged over 30 minutes. R_n (EKO MF11) was recorded at a height of 1.7 m, sampled every 60 seconds and averaged over 30 minutes using a 21X micrologger that also recorded a 2-D drag

anemometer (Green et al.), a 1-D sonic anemometer-thermometer (CSI Inc.) and a Krypton Hygrometer (CSI Inc.) at 0.1 s intervals.

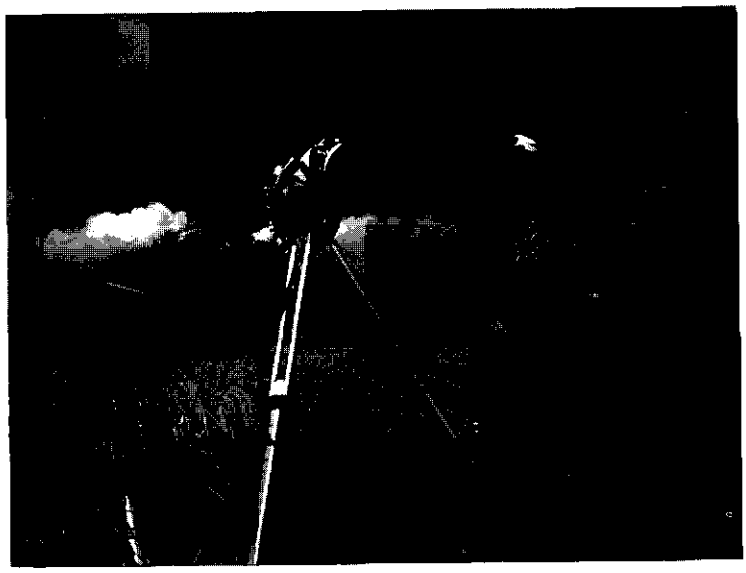

Figure (6.2). Standing beside the LAS instrumentation in the rice paddy at Yawara.

From these measurements, calculations of sensible heat flux, latent heat flux and friction velocity, were made using the eddy covariance technique. Auxillary eddy covariance equipment included a 3-D sonic anemometer (Kaijo Corp., model TR-90AH) set at 1.4 m over the rice canopy and connected to an analog signal conditioning unit (Kaijo Corp.) for 10 minute averages of sensible heat and momentum fluxes (Kona System datalogger).

6.5 Results and Discussion

Within the framework of the presented theory we wished to understand how the LAS performance was affected by having to path-average small values of H for wet surface conditions.

To this end a time series of scintillometer, eddy covariance and meteorological measurements were made for Julian day, J248 through to the early morning of J249. The LAS performance was compared for both unstable and stable atmospheric

conditions. Figure (6.3) presents the eddy covariance fluxes, H_{ec}, and (E_{ec}), friction velocity (u_*); δT , T and C_n^2 over this period. The afternoon of day J248 was cloudy/overcast with an average windspeed about 3.5 m s^{-1}. The wind blew from the preferred southerly direction.

In the first instance and as expected for the partitioning of the surface fluxes over a wet surface, $E_{ec} > H_{ec}$ ($0.1 < \beta < 0.3$) for most of the afternoon of J248 (Figure 6.3a). In the late afternoon of J248 E_{ec} and H_{ec} did not cross zero at the same time. H_{ec} went negative (1630 hrs, J248) long before R_n went to zero (not shown, 1800 hrs, J248) and sensible heat was being lost from the air to support the process of evaporation. About 2200 hrs (J248) both H_{ec} and E_{ec} approached zero flux.

Daytime air temperatures (Figure 6.3b) reached a maximum of 30 C by 1500 hrs (J248) and decreased to a still relatively high minimum value of 20 C by early morning (J249). An apparently oscillating friction velocity, u_* (Figure 6.3b) reached a maximum about 1700 hrs (J248) and then steadily decreased to near zero overnight.

Temperature fluctuations (Figure 6.3c) which are primarily responsible for C_n^2 were greatest during the daytime with peaks and troughs correlated to changes in H_{ec} and u_*. However values of C_n^2 measured over the wet canopy were smaller during the daytime than the nocturnal values. In explanation we note that Weseley and Alcaraz (1973) reported that conditions of wet surfaces and overcast skies reduced daytime C_n^2 below night-time C_n^2. Transitions in the magnitude of C_n^2 about dusk (1800 hrs, J248) and dawn (0700 hrs, J249) were caused by the atmosphere switching stability. The transition in C_n^2 at dusk appeared smoother than at dawn because this period included the overlapping effect of H_{ec} going zero then negative much earlier than R_n. The *hump* in C_n^2 from 1900-2200 hrs (J248) is caused by the negative H_{ec} extending past the point R_n went zero.

The observations made of the scintillometer C_n^2 and the behaviour of H_{ec} above the rice paddy are useful. As expected the scintillometer is unable to determine the direction of the sensible heat flux. Without supporting eddy covariance measurements or equivalent there is no way of knowing the polarity of the sensible

heat flux. If we assume H_{ec} is positive until R_n goes to zero then our selection of the appropriate MOST equations (Equation 6.15 versus Equation 6.16) would be flawed.

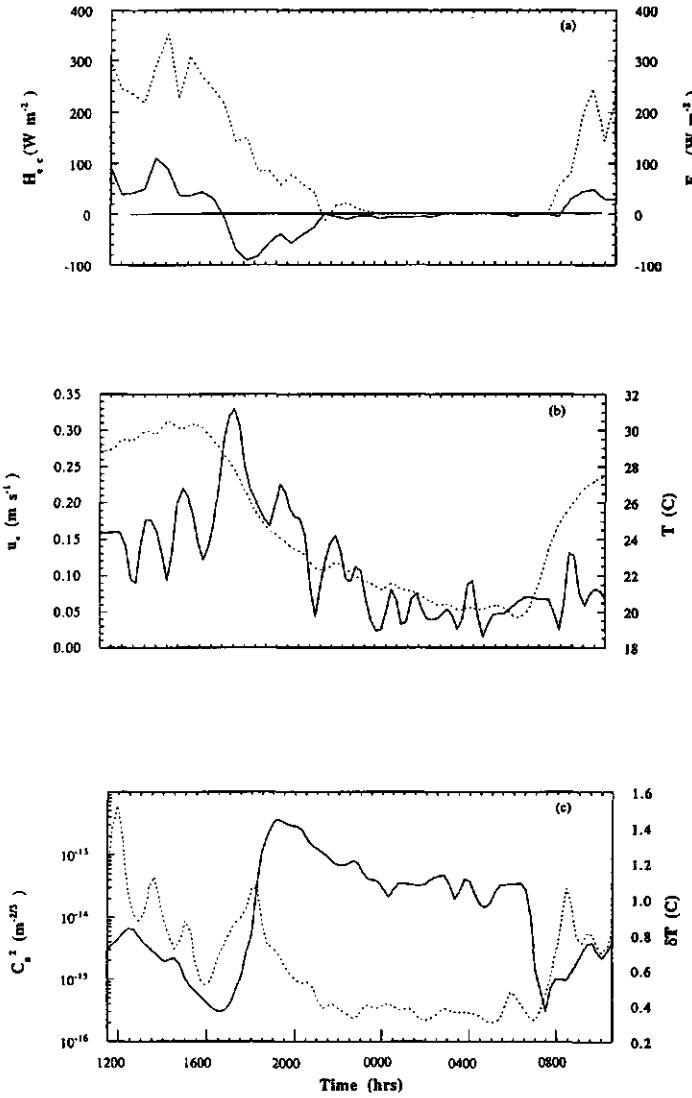

Figure (6.3). Time series of eddy covariance and the scintillometer data for Julian days J248 to J249. In Figure (6.3a) the --- indicates the E_{ec} plotted with H_{ec} (-). Air temperature (---) is shown with friction velocity (-) in Figure (6.3b) and Figure (6.3c) has fluctuations in air temperature (---) measured at the LAS beam height plotted with C_n^2 (-).

A time series of H_{sc} versus H_{ec} for the J248 and J249 emphasises this problem (Figure 6.4). Because H_{sc} is calculated assuming unstable conditions until R_n goes to zero (1800 hrs, J248) then H_{sc} is offset from H_{ec} for the period 1630-1800 hrs.

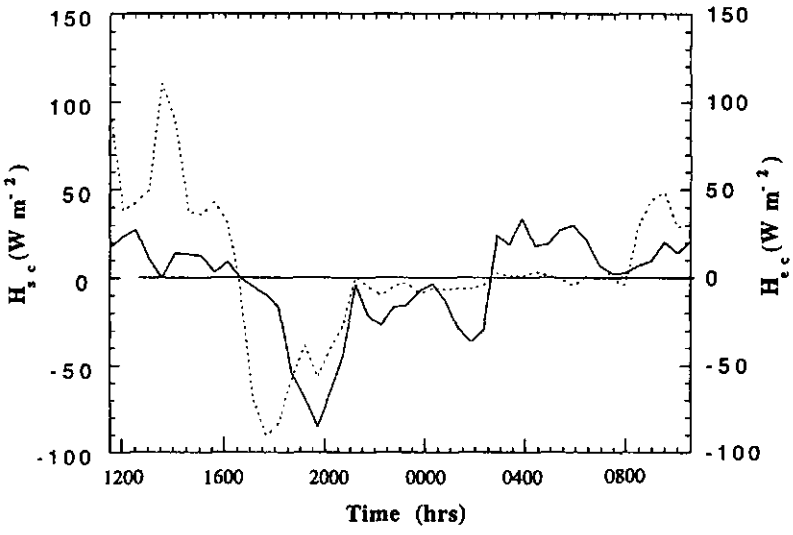

Figure (6.4). Time series of H_{sc} (-) and H_{ec} (---) over Julian days, J248 to J249.

From Figure (6.4), there is a trend for $H_{sc} < H_{ec}$ during the daytime hours. The night-time period has periods when $H_{sc} > H_{ec}$. We have no physical evidence to explain this behaviour. We are however aware that this LAS could record absorption scintillations at frequencies greater than 0.03 Hz (Nieveen et al., 1998). This effect is most pronounced during periods when the refractive scintillations contribute the least to C_n^2. Figure (6.3c) shows C_n^2 to be smallest about dusk and dawn and less than the night-time values. It is about these times we expect $H_{sc} > H_{ec}$ but with such low magnitudes of H recorded it is difficult to prove this unequivocally.

Concerned that the instruments performed properly the LAS was checked after the experiment. This involved injecting a known signal variance into the receiver opto-electronics which showed the LAS to be operating correctly. Prior comparison

of the 2-D drag and 1-D sonic combination to the 3-D sonic anemometer demonstrated a reasonable agreement for sensible heat flux comparison over a limited range. We were confident the eddy covariance instruments were also operating correctly.

The same data used in Figure (6.4) is plotted as a 1:1 comparison in Figure (6.5). As before there is a trend for $H_{sc} < H_{ec}$. The sensible heat fluxes are small

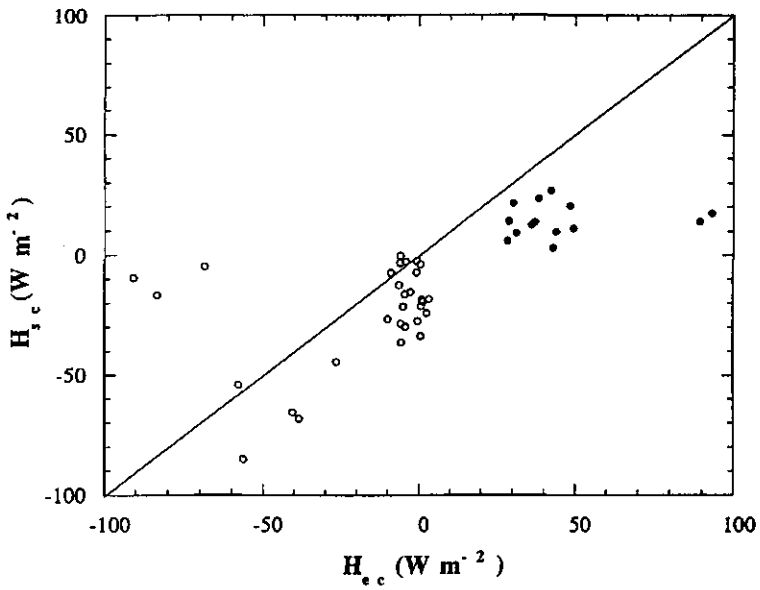

Figure (6.5). Comparison of 30 min averages of daytime (●) and night-time (o) values of H_{sc} versus H_{ec} over Julian days, J248 to J249.

and if E_{sc} is determined from H_{sc} and Equation (6.19) then the result will be greater on average than E_{ec}.

6.6 Summary

Low values of H_{ec} encountered over the rice paddies suggest the atmospheric scintillations will also be small. This is confirmed by small values of C_n^2 measured

for the daytime conditions (10^{-15}-10^{-14} $m^{-2/3}$). As the LAS signal-to-noise figure is 10^{-17} $m^{-2/3}$ rms (B. Heusinkveld, pers. comms.) the size of the measured signal variance may be of some concern for a low value of H_{sc}. For $\beta < 0.3$ the proportion of the LAS signal due to T-Q fluctuations is significant theoretically, which further reduces the calculated value of C_T^2. However it was not possible to observe this effect experimentally as this comparison of H_{sc} to H_{ec} involved measuring very small fluxes. Neither was the comparison improved by including the effect of a low β in calculations of C_T^2 as this further reduced H_{sc}. It is important that T and Q are well correlated in the inertial subrange. Confirming measurements were not undertaken at this spatial scale, rather a correlation coefficient was calculated for the eddy covariance H_{ec} and E_{ec}. From such data and the observed behaviour of H_{ec} in Figure (6.3a) there were periods during J248 when this correlation was less than unity and/or opposite in polarity.

With the available data collected we have no experimental evidence to explain why the daytime values of H_{sc} are less than H_{ec}. As dusk approaches and in the early morning the atmosphere is in a state of change so the output of the LAS is considered inaccurate during these times and it is accepted the two methods will not agree. The measured values of C_n^2 were small and humidity fluctuations presumably high over the rice canopy for the daily cycle. Recent measurements made by Nieveen et al. (1998) suggest the variance associated with absorption fluctuations may become significant (at frequencies within the scintillometer bandwidth) compared to the refraction, particularly for low values of C_n^2. Absorption scintillations would increase the value of C_n^2. Nieveen et al. (1998) suggests increasing the lower frequency cutoff of the scintillation filter to 0.5 Hz to avoid signal contamination by absorption fluctuations or operating the infrared source outside absorption wavelengths. Substantiation requires careful measurements of the spectral energy associated with the absorption and refractive mechanisms and as such will be incorporated into future investigation. Certainly more scintillation measurements over rice paddies and similar canopies will assist in extending this technique and methodology and should be encouraged.

水稲田上におけるシンチロメータ法の利用

アラン・エドウィン・グリーン*・林　陽生**
(*ニュージーランド園芸研究所・ケリケリ研究センター
**農業環境技術研究所・環境資源部)

要　約

近赤外線の揺らぎを測定して境界層の顕熱フラックスを評価する手法（シンチレーション法）と渦相関法を組み合わせ，水稲田における各種フラックスの観測を行った。シンチレーション法の最大の特徴は，近赤外線のパスを長く設定することによって，広範囲の地域を対象としたフラックスの測定が可能な点にある。本研究では，パスの長さを320m，高度を水稲群落上約1mに設定した。近赤外線の屈折を引き起こす要因は主に気温の不均一性であるが，水稲群落上のように湿潤な状態では湿度の効果が無視できない。始めに，湿度の効果について理論的に導いた。観測期間中の天候は晴れ時々曇りでボーエン比は0.3以下の非常に湿潤な状態であった。解析の結果，日中のリフラクティブ・インデックス（揺らぎの規模の指標）は夜間のそれより小さかった。観測結果を30分平均値に整理し，シンチレーション法と渦相関法による顕熱フラックスを日中と夜間について比較したところ，安定条件によって異なる関係が現れた。すなわち，シンチレーション法による値は日中の不安定条件下では過小評価となり，夜間の安定条件下では過大評価となった。これらの結果はWeseley(1976）の指摘と一致するものの，シンチレーション法においては水蒸気による近赤外線エネルギーの吸収効果の影響について今後考察する必要があると考えられた。

キーワード：顕熱フラックス，シンチレーション，水稲群落，低ボーエン比，リフラクティブ・インデックス

7

Path-averaged surface fluxes determined from infrared and microwave scintillometers[✓]

Abstract

Methods are needed to measure the surface fluxes of sensible (H) and latent heat (E) at large scales. A promising method is scintillometry. Over pasture a near-infrared scintillometer was most sensitive to temperature fluctuations whilst a microwave scintillometer was unduly affected by both humidity fluctuations and correlated temperature-humidity fluctuations. Slower changes in path-averaged humidity caused additional signal variance and an overestimation of H and E. Log-amplitude spectra of the microwave scintillometer signal showed inertial-convective subrange behavior. In combination, path-averaged E and H could be determined over 3 km.

Independent corroborative measurements of H and E were made at the path midpoint using the eddy covariance technique. For sensible heat, agreement was within 4% over a measured range of 0 to 300 W m^{-2}, with a residual standard deviation of 45 W m^{-2}. Latent heat agreed at best to within 12% over the range 0 – 450 W m^{-2} (residual standard deviation of 94 W m^{-2}) and an offset of 30 W m^{-2}.

7.1 Introduction

Scintillometers can determine path-averaged surface fluxes and have the potential to bridge the gap between local and regional scales. They path-average over kilometer distances providing ground-truth data that can be used to test global climate and regional hydrology models. Their spatial resolution is comparable with the pixel sizes of remote sensing satellite images and catchment scales. This path-averaging ability may be an advantage over conventional measurement methods, particularly in applications characterizing fluxes over patchwork surfaces. Scintillometers present a cheaper option

[✓] Green, A. E., Astill, M. S., McAneney, K. J. and Nieveen, J. P., *submitted Ag. & Forest Meteorol.*

to the low-flying aircraft flux-gathering systems. While versions of the visible and near-infrared scintillometers are now being commercialized and becoming a research tool of an increasing number of scientists, the microwave scintillometer remains, however, largely ignored, possibly due to the technical overhead, sophistication, and prohibitive cost (Hill, 1997). As a microwave scintillometer is primarily sensitive to humidity fluctuations and can be used to infer evapotranspiration, a close look at its ability to determine acceptable flux measurements is required.

The operation of a scintillometer is straightforward. A scintillometer transmitter propagates electromagnetic radiation through the turbulent atmosphere to a receiver sited some distance away. The receiver measures the log-intensity variance of the signal σ_I^2 (dimensionless) caused by turbulent-induced fluctuations in the refractive-index of air. The refractive-index is primarily affected by temperature T (K) and humidity Q (g m^{-3}) fluctuations which are driven by H (W m^{-2}), E (W m^{-2}) and the wind shear. The signal variance is proportional to C_n^2 ($m^{-2/3}$) a measure of the strength of the path-averaged refractive turbulence. C_n^2 is related to the structure parameters of temperature C_T^2 (K^2 $m^{-2/3}$), humidity C_Q^2 ((g m^{-3})^2 $m^{-2/3}$) and the T-Q structure parameter C_{TQ} (K g m^{-3} $m^{-2/3}$) by (Hill et al., 1980),

$$C_n^2 = \frac{A_T^2 C_T^2}{\overline{T}^2} + 2\left(\frac{A_T A_Q C_{TQ}}{\overline{T}\,\overline{Q}}\right) + \frac{A_Q^2 C_Q^2}{\overline{Q}^2}. \tag{7.1}$$

Overbars indicate temporal averages. Constants A_T and A_Q are functions of wavelength λ (m), $\overline{T}$, $\overline{Q}$ and average pressure $\overline{P}$ (N m^{-2}), (Hill et al., 1980). C_n^2 depends on the weightings of C_T^2, C_Q^2 and C_{TQ}. The scintillation determined surface fluxes H_{sc} (W m^{-2}) and E_{sc} (W m^{-2}) are calculated from normalized values of the structure parameters and Monin-Obukhov similarity theory. Unless the atmosphere is very unstable the friction velocity u_* (m s^{-1}) is also required for such calculations.

The first reported attempt to calculate E_{sc} was published by Kohsiek and Herben (1983). They used a single microwave scintillometer (λ = 1 cm) over a distance, L = 8.2 km and at a height, z = 60 m and compared their results to micrometeorological point-measurements scaled up from z = 10 m. They concluded that E_{sc} could be calculated

using a single microwave scintillometer, provided that simplifying assumptions based on micrometeorological observations were incorporated into the method. At approximately the same time, McMillan et al. (1983) measured C_T^2, C_{TQ} and C_Q^2 using scintillometry and compared them to micrometeorological estimates. They demonstrated good agreement. In their experiment, a large-aperture infrared scintillometer (λ = 0.94 μm) designed by the Wave Propagation Laboratory (NOAA, Boulder, CO.) and a microwave scintillometer (λ = 1.7 mm) were employed over flat farmland for, L = 1.374 km and z = 3.7 m (Flatville, Illinois, USA). A second paper was published comparing H_{sc} and E_{sc} with micrometeorological measurements (Hill et al., 1988) and discussed the deficiencies in this method. Firstly, an eddy covariance value for u_* was used in the calculations. Some progress has since been made to provide a path-average u_* (Hill et al., 1992, Green et al., 1996 and Nieveen and Green, 1999) but these techniques have limitations. Secondly, as C_{TQ} was not measured directly it was assumed that, $C_{TQ} = \pm\sqrt{C_T^2 C_Q^2}$ (Hill et al., 1988).

Andreas (1988) performed a sensitivity analysis to select the best λ combination for determining surface fluxes. A combination of infrared and microwave scintillometers were found to have the highest sensitivity and capable of approximately the same accuracy as eddy covariance measurements ($\pm$ 12%). Scintillometers provide reliable statistical data after several minutes (Wyngaard and Clifford, 1978) and because they do not require an absolute calibration they may be continuously operated. There is an expectation by researchers that scintillometers will determine H_{sc} and E_{sc} over non-homogeneous terrain. To date this expectation has only been addressed by a simple experiment; a step-change from maize to fallow, along the scintillometer transect (Lagouarde et al., 1996). An independent reviewer suggests, operation over non-homogeneous terrain may prove to be the greatest stumbling block to the future progress of the scintillometer method but it is also the greatest challenge. Similarity theory empirically linking the structure parameters to H and E was developed over and is valid for homogeneous terrain. Departures from similarity theory are due to large-scale atmospheric processes like entrainment. In the absence of a similar theory for non-homogeneous terrain the approach currently is to experiment with the scintillation technique over semi-homogeneous terrain.

In the experiment reported here, and in a fashion similar to Hill et al. (1988) a microwave and a large-aperture, near-infrared scintillometer (henceforth referred to as the infrared scintillometer) are used to determine path-average values of H_{sc} and E_{sc} over L = 3.1 km and at z = 10 m. The infrared scintillometer deployed a single transmitter but used dual receivers to test for system noise. Half-hour averaged surface fluxes from the scintillometers were compared with eddy covariance measurements. Unlike Hill et al. (1988) the value of $u*$ was estimated using a cup anemometer and a measure of the average canopy height, h_c (m). Our interest was as follows; to operate both scintillometers together and ascertain whether they can effectively estimate H_{sc} and E_{sc}; to explain how these fluxes are calculated and discuss some assumptions and limitations of the scintillometer method; to explore the effect that T and Q fluctuations have on each scintillometer and importantly report on the first experimental test of this microwave scintillometer.

7.2 Theory

7.2.1 Extracting C_T^2 and C_Q^2 from the scintillometer signals

A general solution describing the relationship between σ_I^2 and C_n^2 for a given λ and L is (Lawrence and Strobehn, 1970),

$$\sigma_I^2 = 0.5 C_n^2 K^{7/6} L^{11/6}, \qquad l_o < F < L_o. \tag{7.2}$$

$K = 2\pi/\lambda$ (m^{-1}), is the propagation wave-number and $F = \sqrt{\lambda L}$ (m) is the first Fresnel size of diffractional spreading. The inner-scale length l_o (m) and the outer-scale length L_o (m) define the upper and lower spatial limits respectively, for the inertial-convective turbulence described by C_n^2. Microwave scintillometers satisfy the criterion, $l_o < F < L_o$. Scintillometers that operate at visible through to infrared wavelengths have $F \approx l_o$ and will require correction for the effect of l_o and possible signal saturation (Hill and Clifford, 1978).

Wang et al. (1978) designed an infrared scintillometer to be independent of signal saturation and inner scale effects using an aperture diameter D (m) much greater than F.

Spatial filtering of the smaller turbulent Fresnel sized eddies by the aperture modified Equation (7.2) to (Wang et al., 1978),

$$\sigma_I^2 = 0.892 C_n^2 D^{-7/3} L^3, \qquad l_o < F < D < L_o. \tag{7.3}$$

Equations (7.2) and (7.3) are used to calculate C_n^2 for the microwave or infrared scintillometers respectively. σ_I^2 has a combined wavenumber and path-ordinate weighting function. The weighting function approximates a bell-shaped curve with a maximum contribution to σ_I^2 at $L/2$ where Fresnel sized eddies are the most effective at diffracting the signal. The weighting tapers to zero at either end of the propagation path.

Both scintillometers measured σ_I^2 directly and provided scaled analog outputs proportional to $C_{n_{mw}}^2$ and $C_{n_{ir}}^2$. The subscripts $_{mw}$ and $_{ir}$ denote the microwave or the near-infrared scintillometer respectively.

Applying the assumption, $C_{TQ} = \pm\sqrt{C_T^2 C_Q^2}$ to Equation (7.1) Hill et al. (1988) determined C_T^2 and C_Q^2 from measured $C_{n_{mw}}^2$ and $C_{n_{ir}}^2$,

$$C_Q^2 = \left[A_{T_{mw}}^2 C_{n_{ir}}^2 + A_{T_{ir}}^2 C_{n_{mw}}^2 + 2S\, A_{T_{mw}} A_{T_{ir}} \sqrt{C_{n_{mw}}^2 C_{n_{ir}}^2} \right] / \left(\overline{T}\Pi\right)^2 \tag{7.4}$$

$$C_T^2 = \left[A_{Q_{mw}}^2 C_{n_{ir}}^2 + A_{Q_{ir}}^2 C_{n_{mw}}^2 + 2S\, A_{Q_{mw}} A_{Q_{ir}} \sqrt{C_{n_{mw}}^2 C_{n_{ir}}^2} \right] / \left(\overline{Q}\Pi\right)^2. \tag{7.5}$$

$\Pi = \left[A_{T_{mw}} A_{Q_{ir}} - A_{T_{ir}} A_{Q_{mw}}\right]\overline{TQ}$ and S is the sign ($\pm$) of the T-Q correlation.

7.2.2 Linking the structure parameters to surface fluxes

Monin-Obukhov similarity theory (MOST) is used to empirically link C_T^2 and C_Q^2 to H_{sc} and E_{sc}. Wyngaard (1973), fitted the same functional form of atmospheric stability, $f(z/L_{mo})$ to normalized values of C_T^2 and C_Q^2 using data collected during the 1968 Kansas experiment.

For unstable atmospheric conditions $(z/L_{mo} \le 0)$ this function is described by,

$$f\left(\frac{z}{L_{mo}}\right) = \frac{C_T^2 z^{2/3}}{T_*^2} = \frac{C_Q^2 z^{2/3}}{Q_*^2} = 4.9\left(1 + 7\left|\frac{z}{L_{mo}}\right|\right)^{-2/3}. \tag{7.7}$$

Similarly for stable conditions $(z/L_{mo} > 0)$,

$$f\left(\frac{z}{L_{mo}}\right) = \frac{C_T^2 z^{2/3}}{T_*^2} = \frac{C_Q^2 z^{2/3}}{Q_*^2} = 4.9\left(1+2.4\left(\frac{z}{L_{mo}}\right)^{2/3}\right). \tag{7.8}$$

L_{mo} (m) is the Obuhkov length scale. If we include the buoyancy correction for humidity fluctuations then,

$$L_{mo} = -\frac{u_*^2 \overline{T}}{g\kappa\, T_*\left(1+0.07/\beta\right)}. \tag{7.9}$$

g = 9.81 m s^{-2} and is the gravitational acceleration, κ = 0.4 (dimensionless) is von Karman's constant. $\beta = H_{sc}/E_{sc}$ is the path-averaged Bowen-ratio defined by (Kohsiek, 1982),

$$\beta = \left(\frac{\varrho\, C_P}{L_v}\right)\left(\frac{C_T}{C_Q}\right). \tag{7.10}$$

The constants ϱ , C_P, and L_v are the density of air (kg m^{-3}), the specific heat capacity of air at constant pressure (J kg^{-1} K^{-1}), and the latent-heat of vaporization of water (J kg^{-1}), respectively. The surface-layer temperature and humidity scaling parameters, T_* (K) and Q_* (kg m^{-3}) are given as,

$$T_* = -\frac{H_{sc}}{\varrho\, C_P u_*} \qquad \text{and} \qquad Q_* = -\frac{E_{sc}}{L_v u_*}. \tag{7.11}$$

Equations (7.7) or (7.8) provide path-averaged values of T_* and Q_* from scintillometer determined C_T^2 and C_Q^2. These values are combined with a path-averaged u_* to calculate H_{sc} and E_{sc} using Equation (7.11).

Before extending the scintillometer method over non-homogeneous surfaces we must first test it over homogeneous terrain where H, E and u_* should obey MOST. It is preferable to use a path-averaged value of u_* because this measurement would be needed for a slightly non-homogeneous surface. In its absence we used instead the average windspeed, u_c (m s^{-1}) obtained from a cup anemometer mounted at z = 10 m. The motivation was to simplify the supporting instrumentation required for scintillation measurements despite having an available eddy covariance value for u_*. A previous

scintillation experiment (McAneney et al., 1995) using a single infrared scintillometer and a cup anemometer produced credible estimates of u_*.

The diabatic wind profile in the first tens of meters of the surface-layer is described by,

$$u_c = u_* ln\left[\left(\frac{z-d}{z_o}\right) - \Lambda\left(\frac{z}{L_{mo}}\right)\right] \Big/ \kappa \qquad (7.12)$$

The stability correction expansion $\Lambda(z/L_{mo})$ for unstable and stable atmospheric conditions can be found in Panofsky and Dutton (1984). The displacement height, d (m) and the surface roughness, z_o (m) are estimated from h_c using $d \approx 0.65 h_c$ and $z_o \approx 0.13 h_c$ (McAneney et al., 1995). When measuring 10 m over pasture, then $z >> h_c$, and d may be ignored (De Bruin et al., 1995) to simplify Equation (7.11). There is the functional dependence of z_o on the surface geometry to consider and the authors acknowledge the above estimations are a rule-of-thumb approach in the absence of direct measurements (see Garratt, 1992). Other propagationists (Hill et al., 1992 and De Bruin et al., 1995) have inferred z_o using the eddy covariance method and then assumed it to be a constant in Equation (7.12).

Determination of H_{sc} and E_{sc} follows an iterative procedure (Hill et al., 1992). The measured parameters include $\overline{T}$, $\overline{Q}$, $C^2_{n_{mw}}$, $C^2_{n_{ir}}$, h_c and u_c. Equations (7.4), (7.5) and (7.10) calculate C_Q^2, C_T^2 and β respectively. A first *guess* for (z/L_{mo}) is required to solve $f(z/L_{mo})$ and then calculate T_* and Q_* using Equation (7.7) or Equation (7.8). The same value of (z/L_{mo}) calculates u_* using Equation (12). (z/L_{mo}) is now *calculated* using Equation (7.9) and the new values of T_*, u_* and β. The procedure is repeated until convergence of (z/L_{mo}). In practice as little as four iterations are required after which H_{sc} and E_{sc} are calculated using Equation (7.11).

7.3 Experimental details

7.3.1 Site and weather conditions

The experiment took place in the 1996 summer. Measurements began on February the 14th but due to several days of rain and mechanical problems stabilising the scintillometer towers, the majority of data were collected on the 25th February through to the 2nd of March, termed Days 56 - 62. Measurements were made continuously for a range of unstable daytime conditions, $-1.0 \leq (z/L_{mo}) \leq -0.05$ and stable nighttime values, $0 < (z/L_{mo}) \leq 0.05$. Data was recorded using micro-loggers mounted in weather-proof enclosures at the base of each tower. Weather conditions varied with days of overcast skies and high winds and days of brilliantly clear blue skies. The wind direction was not constant, wind blew across, as well as up and down, the scintillometer transect.

The scintillometer transect was established across flat, homogeneous pastoral country between Kaitaia township and the small coastal settlement of Ahipara in the far-North of New Zealand (Figure 7.1). A professional surveyor measured the scintillometer transect at 3.1 km (compass bearing of 320° magnetic). This area is reclaimed coastal swamp approximately 10 km west inland from from the Tasman Sea with flat relief (verified from topographical maps and an aerial survey). The scintillometer beams were therefore considered to be parallel to the surface. The landscape was bereft of buildings, people, and bisecting roads. It was composed of paddocks used primarily for grazing cattle and dairy cows. None of these paddocks was irrigated during the experiment. Surface cover was mainly Kikuyu grass (*Pennisetium clandestinum* Hochst. ex Chiov) broken by occasional clumps of Pennyroyal weeds (*Mentha pulegium* L.). At approximately the midpoint of the scintillometer transect a large, 4 m wide drainage ditch, the Tangonge Drain broke the surface. Smaller drainage ditches encompassed some paddock perimeters. At this time of year these drains were dry and there was no free-water evaporation to effect the scintillometer signals. Within 500 m of the transmitter tower grew patches of blackberries (*Rubus fruiticosus* agg.), bulrushes (*Juncus* sp L.) and Scotch thistles (*Cirsium vulgare* (Savi) Ten.).

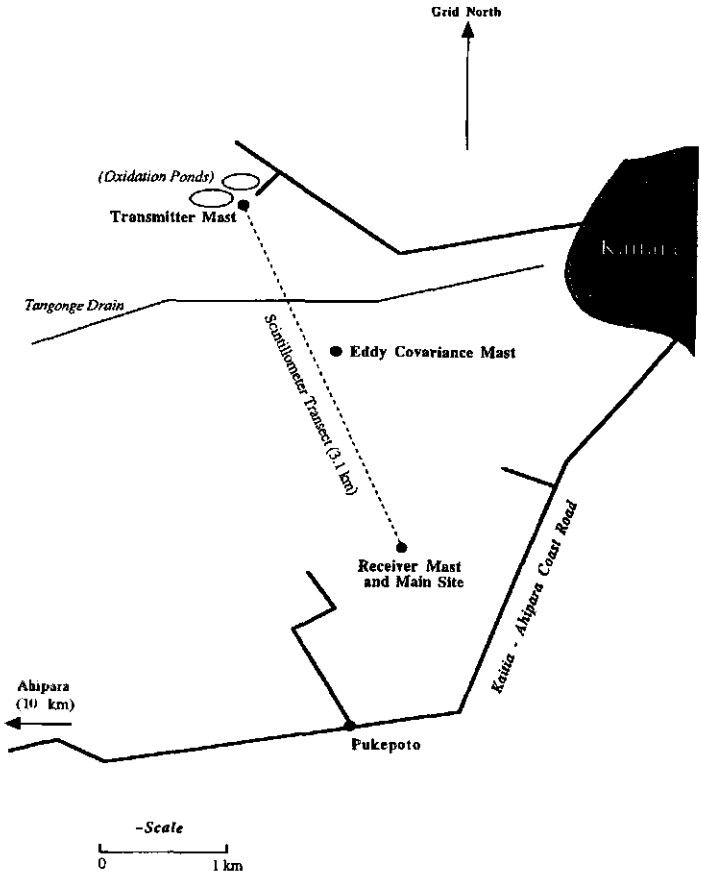

Figure (7.1). Site detail, showing the orientation of the scintillometer transect across the flat pastoral land close to the Kaitaia township, in the far-North of New Zealand.

The C_n^2 path-weighting attributes little influence to turbulence at either end of the transect. Consequently the change in surface cover at the transmitter end or the evaporating water from the sewerage ponds, was considered to have a negligible effect on $C_{n_{nw}}^2$ or $C_{n_{ir}}^2$. The average vegetation height was estimated at, $h_c \approx 0.15$ m. The scintillometer transmitters were positioned at the Kaitaia Council oxidation ponds. The site was chosen for the availability of mains power and the easy access road. The

receiver tower was installed in a pasture close to the Kaitaia-Ahipara coastal road. Access to this end of the scintillometer transect was via farm livestock-vehicle paths. A portable, petrol generator supplied mains power. A shed and tent housed the data acquisition equipment and provided shelter from the weather. The photograph of Figure (7.2) shows the receiver end of the scintillometer transect with the microwave dish and the two adjacent infrared scintillometer receiver units mounted on top of a 9 m stayed, triangular, open-lattice tower. A similar tower was positioned at 1.6 km from the transmitter tower (longitude 173° 15', latitude 35° 08'). Eddy covariance instruments were mounted at the top of this tower to calculate H_{ec}, E_{ec} and u_*. A sensitive cup anemometer recorded u_c at z = 10 m. A wind-vane (continuous 360° angle), a combination slow-response T-Q sensor and a net radiometer were also installed at this height.

7.3.2. The microwave scintillometer

The microwave dishes were mounted with their centers at z = 10 m. Mechanical alignment was possible using a coarse and fine azimuth and elevation adjustments. Telescopic rifle sights mounted on top of each microwave dish gave coarse visual alignment. The microwave dishes were panned in the horizontal and vertical planes until maximum signal strength and carrier frequency lock were achieved at the receiver. The allocated frequency for the microwave transmitter was, f = 27 GHz. The microwave receiver was an analog power meter producing a continuous signal output in decibel (dB) scaled to millivolt units. The received microwave signal was low-pass filtered at f = 10 Hz and sampled at f = 20 Hz.

7.3.3 The infrared scintillometer

The transmitting scintillometer was mounted adjacent to the microwave dish with the center of its infrared beam at z = 10 m. The magnitude of the infrared scintillometer signal was observed to decrease with increases in path-averaged Q. In the early morning, heavy dew on the perspex spacers used to support the transmitter source and receiver opto-electronics reduced the signal strength at the receiver sensors and caused unequal illumination on the mirror surfaces. Electronic band-pass filtering of the

received scintillometer signal confined measurable scintillations to a frequency range of 0.03 - 400 Hz.

Figure (7.2). *Photograph of the scintillometer tower at the receiver site showing the microwave dish mounted alongside two infrared scintillometer receivers. Wire stays are used to stabilize the tower and prevent the scintillometer beams shifting out of alignment.*

Sources of low frequency drift that could affect the signal, such as a varying power supply, were removed by this filter. The equal diameters (D = 0.15 m) of the scintillometer's transmitter and receivers ensured a symmetrical path-weighting function about the midpoint of the scintillometer transect. The two identical infrared scintillometer receivers were mounted adjacent to the microwave scintillometer receiver dish, centered at z = 10 m and separated by a distance of 0.2 m. The use of these identical receivers allowed a comparison of $C_{n_{ir}}^2$ and examination of the system noise. These two signals were recorded at, f = 1 Hz.

7.3.4 Eddy covariance instruments

For the purpose of surface flux comparisons a 9 m tower was stationed at approximately the midpoint of the scintillometer transect. It was instrumented with a 1-D sonic anemometer-thermometer, SAT (Model CA27, Campell Scientific Inc., Utah), a 2-D drag anemometer (Green et al., 1991), and a Krypton hygrometer (Model KH20, Campell Scientific Inc., Utah). These instruments were mounted at the z = 10 m. Half-hour calculations of H_{ec}, E_{ec} and $u*$ were made using the eddy covariance technique. The site was chosen because maximum path weighting of $C_{n_{mw}}^2$ and $C_{n_{ir}}^2$ occurred at $L/2$. At one quarter or three quarters the distance along L the relative weighting reduces to approximately 40% of the midpoint value and there was no advantage in placing multiple towers along a homogeneous transect for comparison purposes.

The eddy covariance instruments required reorientation for major wind-shifts. If these instruments had not been corrected for changing wind direction, the acceptance-angle for the sonic and drag anemometers were compromised through flow distortion caused by the instruments and the tower. The Krypton hygrometer windows were cleaned daily with distilled water to prevent scaling and accumulation of dust on the surface. The fine thermocouple (12 μm diameter wires) of the SAT was changed every other day as a precaution against salt deposits from any afternoon sea breezes.

7.4 Results & discussion

7.4.1 The spectra of $C^2_{n_{mw}}$

The temporal, spectral density for the log-amplitude scintillations $S(f)$ ($dB^2\ Hz^{-1}$), of a received microwave scintillometer signal is characterized by $f^{-8/3}$ behavior in the inertial-convective subrange of frequencies (Ott and Thompson, 1978).

Half-hour averaged, temporal spectra were constructed from the microwave scintillometer signal. The spectrum of $S(f)$ versus f, from 1230 to 1300 hours on Day 60 is shown in Figure (7.3) and is similar to spectra obtained for other microwave scintillometers (e.g., Ho et al., 1979).

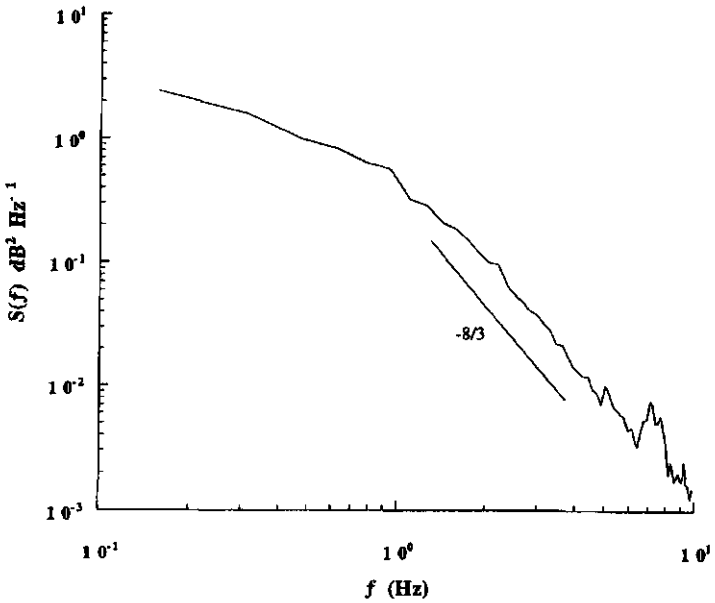

Figure (7.3). The temporal, power density spectrum of the log-amplitude fluctuations of the microwave scintillometer signal, $S(f)$ ($dB^2\ Hz^{-1}$). Obtained over a half-hour period, Day 60, 1966, the spectrum displays inertial-convective subrange behaviour for a frequency f, (Hz) range extending from 1-10 Hz.

Over this particular half-hour period the sky was clear with u_c = 4.9 m s^{-1} and winds blew from the NE. Figure (7.3) displays a well defined -8/3 slope in a frequency range 1-10 Hz at the high frequency refractive end of the scintillometer spectrum. This result implies the microwave scintillometer was measuring within the inertial-convective subrange and can determine $C^2_{n_{mw}}$.

It became apparent from additional spectra of $S(f)$ the greater percentage of refractive energy existed at lower frequencies ($f \leq 0.1$ Hz) and absorption fluctuations originating from changes in path-averaged Q about this frequency increased σ_I^2. The microwave scintillometer signal was not filtered at very low frequencies. Moulsley and Vilar (1982) suggested a suitable cut-off frequency was, f = 0.01 Hz. Instead we accepted half-hour values of $C^2_{n_{mw}}$ when Q changed less than ± 0.1 g m^{-3} between periods. This filtering procedure albeit somewhat arbitrary, was based on the observation that these were the periods when $S(f)$ lacked significant energy about f = 0.01 Hz. This filtering process reduced the microwave scintillometer data set. With the microwave being unable to differentiate between refraction and absorption fluctuations, interpreting what effect this had on σ_I^2 and ultimately H_{sc} and E_{sc} was complicated.

Two small peaks in the spectrum of Figure (7.3) occurred about f = 7 Hz and corresponded to the resonant frequencies of the supporting towers. This vibration energy contributed little to σ_I^2 as it was of a relatively small amplitude compared to the energy associated with the spectral peak ($f \approx 0.1$ Hz). We believe the vibration energy was accentuated by the wind blowing on the microwave dishes as $S(f)$ was observed to increase in magnitude about f = 7 Hz with increased windspeed. Efforts to stabilize the towers to reduce the vibration did not eliminate the resonant energy.

7.4.2 The effect of fluctuating Q on $C_{n_{mw}}^2$ and $C_{n_{ir}}^2$

The atmospheric absorption of microwave signals by water vapor is strong at f = 27 GHz and without filtering the microwave scintillometer will be affected by low frequency fluctuations in path-averaged Q. Absorption scintillations will combine with refractive scintillations and increase $C_{n_{mw}}^2$. The infrared scintillometer emits an envelope of radiation overlapping the wavelengths of strongly absorbing water vapor lines (Nieveen et al., 1998).

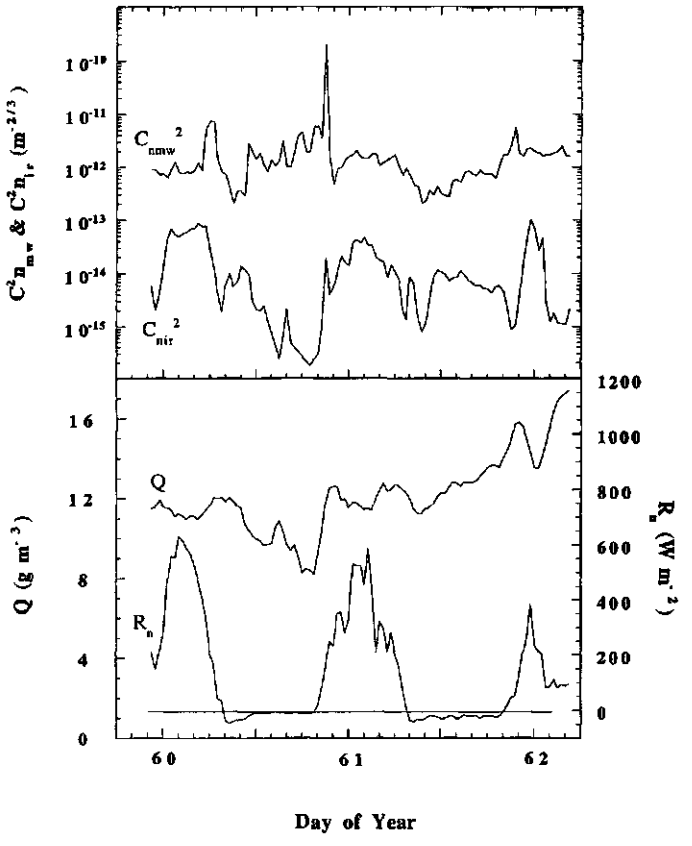

Figure (7.4). A combined time series of the refractive-index structure parameters for the microwave and large aperture scintillometers, $C_{n_{mw}}^2$ ($m^{-2/3}$) and $C_{n_{ir}}^2$ ($m^{-2/3}$), the average humidity, Q (g m^{-3}) and net radiation, R_n (W m^{-2}) for Days 60, 61 and 62, 1966.

Despite band-pass filtering of the infrared scintillometer signal, Nieveen et al. (1998) observed that absorption fluctuations increased $C^2_{n_{mw}}$ for $f \geq 0.03$ Hz. The effect being most noticeable during dusk when refractive scintillations decreased in strength relative to absorption scintillations. Any unwarranted increase in $C^2_{n_{mw}}$ and $C^2_{n_{ir}}$ can lead to an overestimate of H_{sc} and E_{sc} and a failure of the scintillation method.

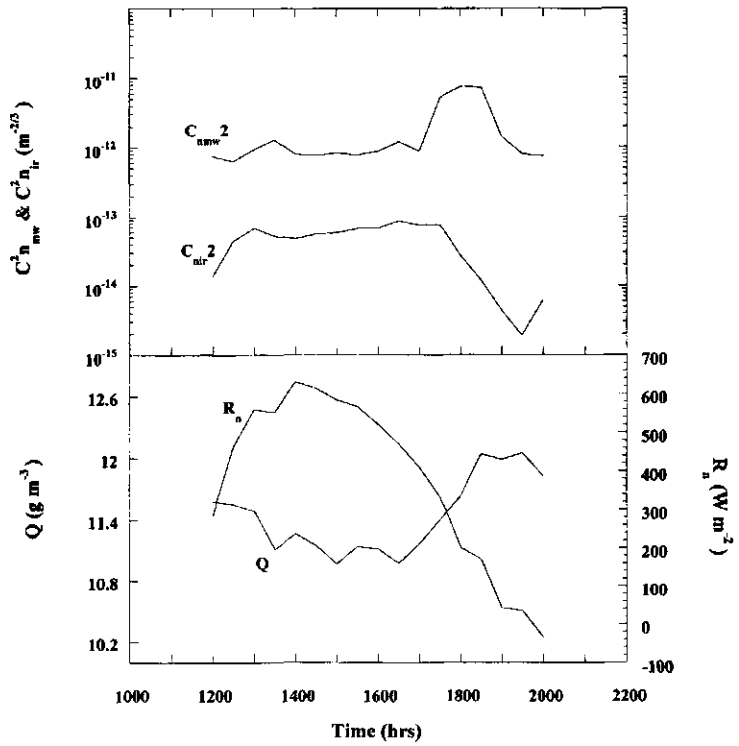

Figure (7.5). A combined time series of the refractive-index structure parameters for the microwave and large aperture scintillometers, $C^2_{n_{mw}}$ ($m^{-2/3}$) and $C^2_{n_{ir}}$ ($m^{-2/3}$), the average humidity, Q (g m^{-3}) and net radiation, R_n (W m^{-2}) for Day 60, 1966.

Fluctuations in T and Q in the inertial-convective subrange cause the refractive scintillations. Low-frequency fluctuations in path-averaged Q in the variance-

containing subrange can cause absorption scintillations. Temporal trends in the magnitude of Q and net radiation R_n (W m^{-2}) are correlated to changes in the magnitude of $C^2_{n_{mw}}$ and $C^2_{n_{ir}}$. We present all these parameters in a time series (Figure 7.4) for Days of the year 60, 61 and 62.

R_n shows Day 60 to be cloudy in the early morning particularly about 1100 hours but clearing in the early afternoon. Day 61 experienced intermittent cloud cover and Day 62 was overcast and became very bleak with the approach of several days of rain. Over this period Q fluctuated about a mean value of 11 g m^{-3} then steadily increased on the morning of Day 62 with the approach of a wet front.

The effect of absorption scintillations is identified by the behavior of $C^2_{n_{mw}}$ and $C^2_{n_{ir}}$ during the late afternoon of Day 60 (Figure 7.5). A prominent increase in $C^2_{n_{mw}}$ from 10^{-12} $m^{-2/3}$ (1700 hours) to 10^{-11} $m^{-2/3}$ (1800 hours) coincided with an increasing Q (11 g m^{-3} to 12 g m^{-3}). After 1830 hours Q maintained a rough plateau until 2000 hrs but $C^2_{n_{mw}}$ decreased as R_n approached zero. In contrast $C^2_{n_{ir}}$ did not demonstrate any obvious dependence on Q and remained relatively constant in value about 10^{-13} $m^{-2/3}$ between 1600 and 1730 hours before steadily decreasing in magnitude an hour earlier than $C^2_{n_{mw}}$.

This behavior is explained by the percentage of unfiltered absorption scintillations included with refractive scintillations. Path-averaged fluctuations in Q have a weaker influence on the infrared scintillometer signal than do refractive fluctuations at this time of the day (Nieveen et al., 1998) and $C^2_{n_{ir}}$ generally follows the behavior of R_n. At microwave wavelengths a continuum of water absorption lines means path-averaged Q fluctuations can contribute significantly to $C^2_{n_{mw}}$. Consequently, changes in $C^2_{n_{mw}}$ are more pronounced than $C^2_{n_{ir}}$ (Figure 7.5). As fluctuations in Q decrease then R_n determines the behavior of $C^2_{n_{mw}}$.

7.4.3 The wavelength dependence of C_{nmw}^2 and C_{nir}^2

Equation (1) gives the relationship between C_n^2 and the structure parameters C_T^2, C_{TQ} and C_Q^2. The relative contribution each structure parameter makes to C_{nmw}^2 and C_{nir}^2 is rarely, if ever, tabulated. Table 1 contains a selection of half-hourly averaged values of C_T^2, C_{TQ} and C_Q^2 weighted by the constants A_T, A_Q, $\overline{Q}$ and $\overline{T}$ and equated to C_{nmw}^2 and C_{nir}^2.

It is clear from Table 1 that, $C_{nmw}^2 > C_{nir}^2$ and the component structure parameters are weighted differently. We first consider the behavior of the infrared scintillometer. The term in Table 1 containing C_Q^2 does not contribute significantly to C_{nir}^2 because Q fluctuations have little effect on C_{nir}^2 at infrared wavelengths. As expected the C_T^2 term is the largest as fluctuations in T are generally the most effective at causing refractive-index fluctuations at infrared wavelengths. Table 1 shows C_{TQ} to be a significant component of C_{nir}^2 and decreasing in magnitude with increasing β. At 1100 hours, β = 0.21 and 31% of C_{nir}^2 is attributable to C_{TQ}. For the late afternoon (1700 hours) the surface is drier and β = 0.72, but C_{TQ} is still a significant 9% of C_{nir}^2. The use of an infrared scintillometer over irrigated crops will require a measurement of C_{TQ} to account for its effect on C_{nir}^2. As the surface dries the C_{TQ} component decreases and the C_T^2 component dominates C_{nir}^2. A single infrared scintillometer is then sufficient to calculate H_{sc}.

Table 1 shows the C_Q^2 term to be the largest component of C_{nmw}^2 and that the C_T^2 term is several magnitudes smaller. Humidity fluctuations dominate refractive-index fluctuations at microwave wavelengths. The C_{TQ} component acts to significantly decrease C_{nmw}^2 as the combined T-Q fluctuations increase. This is the opposite behavior found for C_{nir}^2 and is caused by the negative polarity of A_T at microwave wavelengths. C_{TQ} is an important component of C_{nmw}^2 and requires a measure of both C_Q^2 and C_T^2 to be calculated.

Time	Scintillometer	C_n^2	=	$\frac{A_T^2 C_T^2}{\overline{T}^2}$	$\pm$	$2\frac{A_T A_Q C_{TQ}}{\overline{TQ}}$	+	$\frac{A_Q^2 C_Q^2}{\overline{Q}^2}$
(hrs)		($m^{-2/3}$)		($m^{-2/3}$)		($m^{-2/3}$)		($m^{-2/3}$)
1100	microwave	8.84×10^{-13}	$\equiv$	2.69×10^{-15}	-	0.89×10^{-13}	+	9.71×10^{-13}
	infrared	2.04×10^{-15}	$\equiv$	1.55×10^{-15}	+	0.78×10^{-15}	+	9.90×10^{-17}
1200	microwave	7.44×10^{-13}	$\equiv$	1.89×10^{-14}	-	2.30×10^{-13}	+	9.59×10^{-13}
	infrared	1.36×10^{-14}	$\equiv$	1.21×10^{-14}	+	0.28×10^{-14}	+	9.88×10^{-17}
1300	microwave	9.38×10^{-13}	$\equiv$	9.81×10^{-14}	-	0.69×10^{-12}	+	1.51×10^{-12}
	infrared	6.89×10^{-14}	$\equiv$	6.28×10^{-14}	+	0.63×10^{-14}	+	1.57×10^{-16}
1400	microwave	8.01×10^{-13}	$\equiv$	6.71×10^{-14}	-	0.50×10^{-12}	+	1.23×10^{-12}
	infrared	4.80×10^{-14}	$\equiv$	4.44×10^{-14}	+	0.47×10^{-14}	+	1.29×10^{-16}
1500	microwave	8.29×10^{-13}	$\equiv$	8.22×10^{-14}	-	0.57×10^{-12}	+	1.32×10^{-12}
	infrared	5.85×10^{-14}	$\equiv$	5.37×10^{-14}	+	0.54×10^{-14}	+	1.38×10^{-16}
1600	microwave	8.73×10^{-13}	$\equiv$	9.75×10^{-14}	-	0.65×10^{-12}	+	1.42×10^{-12}
	infrared	6.88×10^{-14}	$\equiv$	6.34×10^{-14}	+	0.61×10^{-14}	+	1.46×10^{-16}
1700	microwave	8.83×10^{-13}	$\equiv$	0.10×10^{-12}	-	0.68×10^{-12}	+	1.46×10^{-12}
	infrared	7.52×10^{-14}	$\equiv$	6.93×10^{-14}	+	0.65×10^{-14}	+	1.52×10^{-16}

Table (7.1). The relative contributions of the structure parameters to C_n^2 at microwave and infrared wavelengths for selected average half-hour values on Day 60.

There is a trend for the relative contribution made by the C_T^2 component to increase $C_{n_{mw}}^2$ with drier surface conditions (1700 hours). As the relative magnitude of the T

fluctuations become very much greater than the Q fluctuations, the C_T^2 component begins to influence $C_{n_{mw}}^2$. At microwave frequencies at least C_Q^2 and C_{TQ}, and at times C_T^2 are required to calculate $C_{n_{mw}}^2$. Calculation of E_{sc} will require a two-wavelength scintillometer combination.

7.4.4 Comparing the scintillation surface flux densities

7.4.4.1 Time series

The eddy covariance instruments provide half-hour averages of H_{ec} and E_{ec}. These types of measurements are routinely presented in a time series format. For long-term monitoring a similar capability from scintillometers is needed.

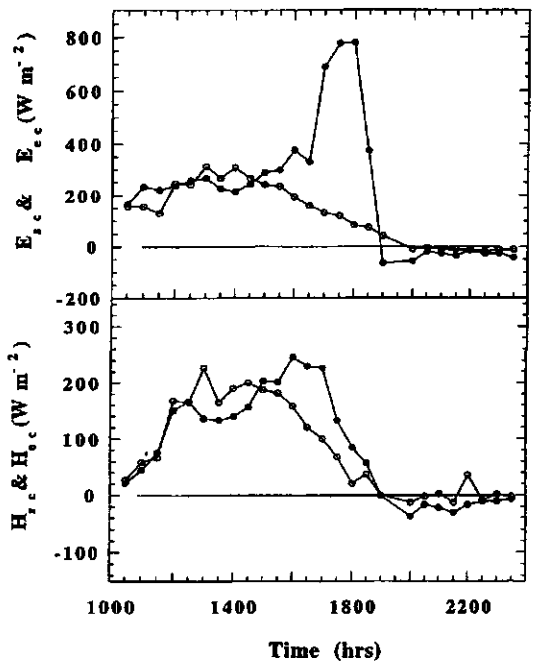

Figure (7.6). A time series for Day 60, 1966, of the latent and sensible heat flux calculated from the combination of microwave and infrared scintillometers, E_{sc} (W m^{-2}) and H_{sc} (W m^{-2}) with the eddy covariance method, E_{ec} (W m^{-2}), (o) and H_{ec} (W m^{-2}) (o).

For a comparison of H_{sc} to H_{ec} and E_{sc} to E_{ec}, two time series for Day 60 (1030 to 2330 hours) are presented in Figure (7.6). There is reasonable agreement between the eddy covariance and scintillometer methods until the steady onset of increasing Q at approximately 1600 hours (see Figure 7.5). By reasonable it is meant not more than a 50 W m^{-2} difference over any half-hour period, which is within the error of $\pm 12\%$ proposed by Andreas (1988). Following 1600 hours both H_{sc} and E_{sc} overestimate H_{ec} and E_{ec}. This behavior follows from the explanation given in Section (7.4.2) for the observed increase in C^2_{nmw}.

7.4.4.2 Half-hour comparison

Half-hour averaged calculations of H_{sc} and E_{sc} were compared to eddy covariance values (Figures 7.7 and 7.8). Data was compared when, 1) closure of the surface energy budget calculated using H_{ec} and E_{ec} plus an assumed value for ground heat flux (~ 10% R_n) came close to unity; 2) the wind direction was within ± 45% of the stream-wise component of the drag anemometer; 3) fluctuations in Q did not exceed the filtering criteria established in Section 7.4.1; 4) rain intervals and smoke in the scintillation path from farm burnoffs did not occur; 5) the krypton hygrometer windows were not covered in dew; and 6) general maintenance of equipment was not necessary.

H_{sc} and E_{sc} were calculated using Equation (7.11). A regression analysis of the data gave the relationship between sensible heat fluxes as,

$$H_{sc} = 0.96(\pm 0.10)H_{ec}. \qquad r^2 = 0.67$$

The offset was non-significant. The residual standard deviation was 45 W m^{-2}. A similar comparison for latent heat flux gave,

$$E_{sc} = 0.79(\pm 0.09)E_{ec} + 51.8(\pm 21.3), \qquad r^2 = 0.71$$

with a residual standard deviation of 94 W m^{-2}. Both comparisons showed a similar spread of data and correlation coefficients, r^2.

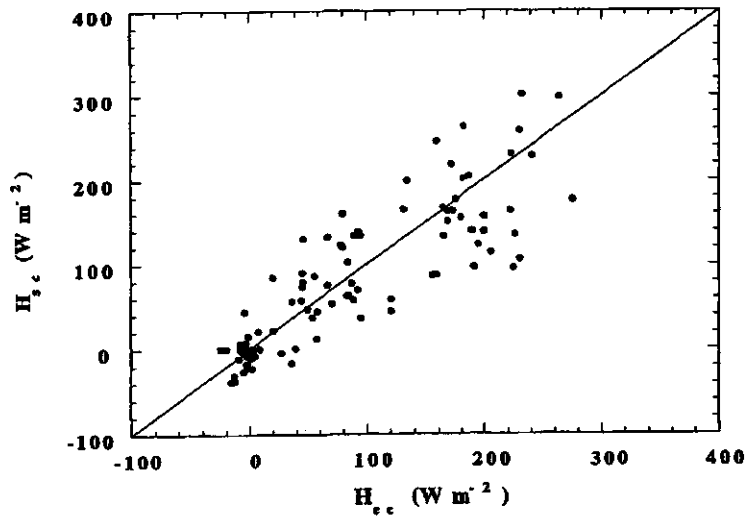

Figure (7.7). Half-hour comparisons of H_{sc} (W m^{-2}), and H_{ec} (W m^{-2}), for a selection of daily data.

Comparison of data obtained at different spatial scales can complicate interpretation. Structure parameters are spatial averages but are presented here as ensemble averages. The scintillometer method does not consider the effect of local turbulent intermittency on C_n^2 (Peltier and Wyngaard, 1995) which will produce differences between point and path-averaged measurements along the 3.1 km. For truly homogeneous cover we would expect an 'on average' agreement between the scintillometer and eddy covariance methods. A larger data set obtained by appropriate filtering of the microwave scintillometer signal would produce more robust statistics for comparison.

An experiment recently conducted over a vineyard during the summer of 1997-1998 in the South Island of New Zealand (Green et al., 2000), indicated that some of the problems associated with fluctuations in path-averaged Q have been eliminated and continuous surface flux measurements are possible.

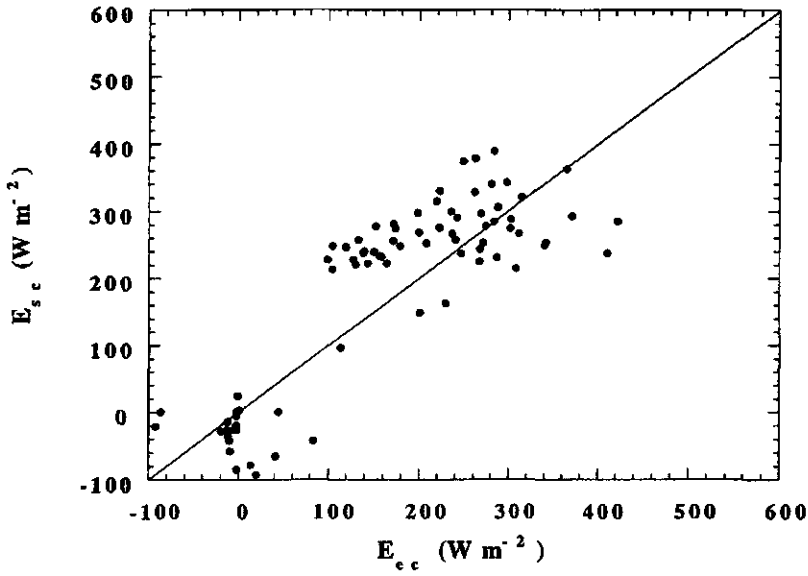

Figure (7.8). Half-hour comparisons of E_{sc} (W m^{-2}), and E_{cc} (W m^{-2}) for a selection of daily data.

The performance of both types of scintillometer was excellent. There were no malfunctions at any stage of the experiment. Tower vibration and condensation on the perspex spacers of the infrared scintillometer are problems easily remedied.

7.5 Summary

The infrared scintillometer and microwave scintillometer combination successfully estimated path-averaged values of H and E over pasture. The microwave scintillometer signal requires low-pass filtering to remove absorption scintillations due to changing path-averaged Q. In such cases both H and E were unrealistically large compared to eddy covariance measurements. When correlated T-Q fluctuations are insignificant compared to T fluctuations at infrared wavelengths then a single infrared scintillometer can determine H. However calculation of E requires the scintillometer combination as T-Q fluctuations are shown to be as equally important as Q fluctuations at microwave wavelengths.

8

Estimating latent heat flux from a vineyard using scintillometry[1]

Abstract

The combination of a near-infrared and a microwave scintillometer were used to estimate the line-averaged, latent heat flux (λE_s) from a well-irrigated, vineyard valley during summer. The 2 km scintillometer beam passed over the valley floor at a height, z = 30 m. Eddy covariance towers instrumented at 3 m above the valley surface provided an independent check of vineyard evaporation. A formula for free convective λE_s compared favourably to the eddy covariance values, λE_e at low wind speeds and under clear skies. As the convective boundary layer (CBL) developed and passed through the scintillometer beam it caused additional scintillations, in which case $\lambda E_s >> \lambda E_e$. During unstable conditions the comparisons were in close agreement. However λE_s tended to overestimate λE_e as the wind speed increased. For near-neutral conditions the scintillometer gave unrealistically large values of λE_s. The additional scintillations originated from the strong entrainment of advected dry and warm air into the newly formed surface boundary layer. During calm overcast days, cold days and during the early morning periods when the surface fluxes were small, the signal strength of the infrared scintillometer approached the system noise.

8.1 Introduction

Over the last ten years several experiments have used a combination of a microwave and near-infrared scintillometer to determine the line-averaged fluxes of the sensible heat H_s (W m^{-2}) and the latent heat λE_s (W m^{-2}), directly above the Earth's surface. Notable is the experiment of Hill et al. (1988) who used scintillometers operating at

[1] Green A. E., Green, S. R., Astill, M. S. and Caspari, H. W., *J. Terres., Atmos. & Ocean. Sci., 11, 525-542*

millimeter and micrometer wavelengths. They were the first to outline the methodology for determining H_s and λE_s and produce what Hill described as 'a reasonable agreement with those values from micrometeorological measurements'. The next recorded experiment using multiple scintillometers was Green et al. (2000) who found H_s and λE_s compared favourably to eddy covariance measurements made at the midpoint of the scintillometer transect. This latter experiment confirmed that the recently designed microwave scintillometer was operational and sensitive to inertial sized eddies of heat and water vapour. This research also highlighted the effect of line-averaged, low frequency humidity fluctuations and their detrimental effect on the scintillometer signals. In both these experiments the surface was flat, expansive and homogeneous in surface coverage with the scintillometer beam close to the canopy ($z < 10$ m).

There are provisos for the scintillometer method because it is indirect in its approach, relying upon similarity theory to scale the temperature structure parameter, C_T^2 ($K^2\ m^{-2/3}$) and the humidity structure parameter, C_Q^2 ($[g\ m^{-3}]^2\ m^{-2/3}$) as functions of atmospheric stability. In practice, these parameters are first calculated from the scintillometer signals then incorporated into similarity functions to determine H_s and λE_s. To satisfy the prerequisites of similarity theory, scintillometer experiments should be conducted over a flat and homogeneous landscape under a relatively stationary atmosphere. This satisfies the empirical linking (albeit at times tenuous) of the scintillometer beam-intensity perturbations with the surface generated eddies of heat and moisture.

If there is to be an acceptance of the scintillometer method, comprehensive experimental verification and testing over a variety of terrain and atmospheric conditions is mandatory. It is our intent in this paper to contribute an improved understanding of the scintillometer method from initial experience gained with this scintillometer combination (Green et al., 1999). We present here results using a microwave and near-infrared scintillometer propagating across a vineyard valley. Our approach is somewhat different than other close to the canopy scintillometer experiments. A vineyard has been studied previously using an near-infrared scintillometer (De Bruin et al., 1995) however the scintillometer beam was very close to the canopy ($z = 3.3$ m) and the soil-plant conditions were dry. Here we examine the scintillometer capability to measure the surface evaporation across an irrigated

valley and at a beam height much greater than previously attempted for this two-scintillometer combination. Operating at height is necessary to cover the large distances (up to 10 km). The surrounding farmland was drought stricken. We suspected the contrast in soil-water conditions would cause additional scintillations if dry air advected into the valley. The scintillometers were installed at z = 30 m above the valley floor by placing them on opposing and exposed ridges (see Figure 7.1). Within the vineyard at two locations eddy covariance instruments monitored H_e and λE_e. These measurements provided a measure of the vineyard energy balance and a benchmark for the scintillometer determined fluxes. The valley floor had no significant undulations and the canopy was of a consistent roughness about the center of the scintillometer beam (maximum scintillometer weighting). Based on past experience (Green et al., 2000) it was believed possible to estimate half hourly λE_s. The preferred wind direction was from the NW, because this was the wind that blew up the valley and across substantial grape planting before intersecting the scintillometer beam. If the wind blew into the valley from across the surrounding hill-sides this could adversely effect the scintillometer performance and λE_s was treated with scepticism.

8.2 Theory

Scintillometers provide a wavelength-dependent, line-averaged measurement of the refractive-index structure parameter, C_n^2 ($m^{-2/3}$). Embedded within each value of C_n^2 reside the weighted spatial effects of temperature and humidity fluctuations that have affected the scintillometer beam along its entirety. Each received scintillometer signal is time integrated within a bandwidth that encompasses the inertial subrange of turbulent eddies. These conditioned scintillometer signals provide the first step in determining H_s and λE_s.

8.2.1 Structure parameters C_T^2 and C_Q^2

Through assuming these structure parameters obey Monin-Obukhov Similarity Theory (MOST) Hill et al. (1988), provide the values of C_T^2 and C_Q^2 obtained for a

dual scintillometer operating at microwave and near-infrared wavelengths (denoted by subscripts $_m$ and $_i$ respectively) as,

$$C_Q^2 = \left[A_{T,m}^2 C_{n,i}^2 + A_{T,i}^2 C_{n,m}^2 + 2S\, A_{T,m} A_{T,i} \sqrt{C_{n,m}^2 C_{n,i}^2} \right] / (TD)^2 \tag{8.1}$$

$$C_T^2 = \left[A_{Q,m}^2 C_{n,i}^2 + A_{Q,i}^2 C_{n,m}^2 + 2S\, A_{Q,m} A_{Q,i} \sqrt{C_{n,m}^2 C_{n,i}^2} \right] / (QD)^2 \tag{8.2}$$

A_T^2 and A_Q^2 are parameters (Hill et al., 1980) that are influenced by the operating wavelength of the scintillometer, absolute temperature T (K), pressure P (N m^{-2}) and humidity Q (g m^{-3}).

The factor D expands to,

$$D = \left[A_{T,m} A_{Q,i} - A_{T,i} A_{Q,m} \right] TQ \tag{8.3}$$

One significant consequence of MOST is that S, the T-Q correlation coefficient takes a value of +1 for unstable conditions (Hill, 1989). Such a correlation has not always been observed in scintillation experiments. For instance Kohsiek (1982b) found an average S of 0.75 while Hill et al. (1988) found S to be much closer to unity (S = 0.99).

8.2.2 Sensible and latent heat fluxes

Our primary interest in scintillometers is determining line-averaged values of H, and λE, at kilometre scales. To infer these fluxes across large areas scintillation measurements must be made over long horizontal paths. In this experiment the scintillometer averages over a horizontal distance of 2 km. λE, is our main surface flux of interest because of its potential for irrigation scheduling. Operating over such distances or greater is acceptable provided the scintillometer pathlength is a small fraction of the boundary layer height. For instance Kohsiek (1985) operated a CO_2 laser scintillometer over 5.9 km and z = 40 m. At such heights slight non-uniformity in the surface maybe from ditches or roads, cloud cover or canopy cover are *blended*

with the surrounding surfaces if there is some mechanical mixing of the boundary layer. Because this scintillometer process is one of line-averaging, a single spatial anomaly at the surface would need to cause a very significant difference in surface flux to produce a measurable signal change at the scintillometer receiver. In such cases it would be unwise to select an experimental site that wasn't fairly uniform. The scintillation method can be considered a form of low-pass filtering whereby small spatial and temporal changes are smoothed by the average signal. Further, as the weighting function of the scintillometer method is symmetrically bell shaped, the scintillometer can be positioned to minimize the effect of any significant change in surface conditions from the normal cover underlying the beam.

Currently MOST provides the only framework for indirectly predicting H_s and λE_s from C_T^2 and C_Q^2. As has been previously discussed the ideal situation for such experiments is a flat and homogeneous site having a stationary atmosphere. Such was the case in the Kansas Plain Experiment from where the original MOST algorithms were derived (Wyngaard, 1973). In this experiment we assumed MOST was applicable in the vineyard and C_Q^2 and C_T^2 would scale to the scintillometer beam height as functions of atmospheric stability (z/L_o).

We use the empirical scaling relationship of Hill et al. (1988) for unstable conditions,

$$g\left(\frac{z}{L_o}\right)=4.9\left(1+7\left|\frac{z}{L_o}\right|\right)^{2/3}=\frac{C_Q^2 z^{2/3}}{Q_*^2}=\frac{C_T^2 z^{2/3}}{T_*^2} \qquad , z/L_o<0 \tag{8.4}$$

L_o (m) is the buoyancy length scale, which includes a correction for humidity fluctuations and is defined by,

$$L_o=-\frac{u_*^2 T}{g\kappa T_*\left(1+0.07/\beta\right)} \tag{8.5}$$

$\kappa = 0.4$ is von Karman's constant, T_* (K) is the temperature scaling parameter, g = 9.81 m s^{-2} is gravitational acceleration and $\beta = H_s/\lambda E_s$ we have called the line-averaged Bowen-ratio. Kohsiek (1982b) notes that β is proportional to the ratio C_T/C_Q which are two of the structure parameters derived from this experimental

scintillometer. The humidity scaling parameter Q_* (g m^{-3}) and the velocity scale u_* (m s^{-1}) combine to give a value for λE_s as,

$$\lambda E_s = -L_v u_* Q_* \tag{8.6}$$

The latent heat of vaporisation of water L_v is taken here as 2.45 x 10^3 kJ kg^{-1}.

Obtaining a reliable line-averaged u_* for inclusion in Equation (7.6) is difficult to achieve and other options are favoured. Over a homogeneous surface a line-averaged u_* is preferred to that obtained from either an eddy covariance measurement or that estimated from the windspeed profile and a surface roughness measurement. Neither of the latter approaches will spatial average u_* at the length scale of the scintillometer transect. It is impractical to measure u_* at the scintillometer beam height of 30 m and position of maximum signal weighting (the midpoint of the beam). Instead, conventional meteorological instruments placed at z = 3 m estimate u_* which is then taken as being equivalent at z = 30 m because a constant flux layer is assumed.

For near-neutral conditions, typically characterized by overcast skies, strong surface winds and low values for surface fluxes, (z/L_o) approaches zero as mechanical turbulence dominates. The wind profile is logarithmic with z and u_* can be determined from an average windspeed u_c (m s^{-1}) at z = 3 m, the canopy displacement height d (m) and surface roughness z_o (m) using,

$$u_* = \frac{\kappa\, u_c}{ln(z - d/z_o)} \tag{8.7}$$

An empirical calculation of z_o is made assuming z_o/h_c = 0.13 and d/h_c = 0.7 (Sene, 1994). This requires an estimate of the average canopy height, h_c (m). Deviation from the log-law increases for unstable conditions requiring a modification of Equation (8.7) to become,

$$u_* = \frac{\kappa\, u_c}{ln(z - d/z_o) - \Psi(z/L_o)} \tag{8.8}$$

The full expression for the function $\Psi(z/L_o)$ can be found in Panofsky and Dutton (1984). An iterative solution to Equation (8.8) is obtained by first assuming an initial value for (z/L_o) then calculating u_*. From Equation (8.5) a new (z/L_o) is determined and substituted into Equation (8.8), the process repeating until convergence. In the author's experience this procedure is fairly robust, requiring on average, just three to four iterations to complete.

For a very unstable atmosphere, the free convective situation, when $(z/L_o) < -1$, mechanical mixing is not significant permitting a simplification of Equation (8.4) using the prior the expressions for L_o and λE_s. This rearrangement expresses C_Q^2 as,

$$C_Q^2 = 2.5\left(\frac{\lambda E_s}{L_v}\right)^{4/3} z^{-4/3}\left(\frac{TQ_*}{gT_*}\right)^{2/3} \tag{8.9}$$

From Equation (8.9) there is a decrease of C_Q^2 with height. In reality this is observed as a rapidly diminishing scintillometer signal. Scintillometers are placed at greater heights to reduce the risk of signal saturation and to obtain greater scales of spatial integration. In so doing the resolution of the scintillometer may be compromised.

Continuing with our derivation of λE_s under free convection, from Equation (8.4),

$$\frac{Q_*}{T_*} = \frac{C_Q}{C_T} \tag{8.10}$$

By the substitution of Equation (8.10) into Equation (8.9),

$$\lambda E_s = L_v z\left(\frac{C_Q^2}{2.5}\right)^{3/4}\left(\frac{gC_T}{TC_Q}\right)^{1/2}. \tag{8.11}$$

This is a similar result to the free convective form given by Hill et al. (1988). Note that both C_T and C_Q are needed to estimate λE_s and so the technique requires at

least two different wavelength scintillometers. In contrast the free convective, sensible heat flux only requires a value for C_T which can be provided by a single near-infrared scintillometer (Panofsky and Dutton, 1984).

8.3 Experimental

8.3.1 Site description and instrumentation

The Brancott Estate situated in the fluvial Fairhall Valley at the foothills of the Southern Ranges is found on the outskirts of Blenheim (Marlborough region, South Island of New Zealand). The Estate was chosen as the experimental site, being one of the largest vineyards in this country encompassing some 240 ha of vines stretching across the valley floor and bounded by low hills (schematic Figure 8.1). These hillsides provided a convenient solution to mounting the scintillometers sufficiently high so the beams could *see* the valley-floor and line-average the vineyard λE_v. Using a laser theodolite the scintillometer transect was established as 1,969 m at an average height of 30.3 m above the valley floor. The grade was 1:248 from the transmitter end on the hillside above the dry Fairhall riverbed to the receiver end, 'Rob's Knob'. For the purposes of this experiment the scintillometer beam was treated as parallel to the ground surface. The scintillometer beam crossed the central portion of the vineyard in an EW direction from transmitter to receiver. The preferred wind direction was from the NW because it was from this direction that the wind blew up the valley and across the irrigated grapes (a fetch of more than one kilometre) before intersecting the scintillometer beam. Downwind of the vineyard were further grape plantings (Fairhall Estate) but to the NE was the beginning of a dry scrub-land interspersed with barren land (local civilian and military airport) and some scattered olive plantings. This surrounding drier farming terrain then extended many kilometres to the base of the Nelson foothills (Richmond Range) having more vineyards on either side of the distant Wairau River. Because of a prolonged drought the irrigated Brancott Estate was for all practical purposes an oasis.

The scintillometers were the same microwave (1.1 cm wavelength) and near-infrared (0.94 μm wavelength) types as described by Green et al. (1999) and were

mounted on short 1 m towers, themselves cemented into concrete bases at either end of the scintillometer transect.

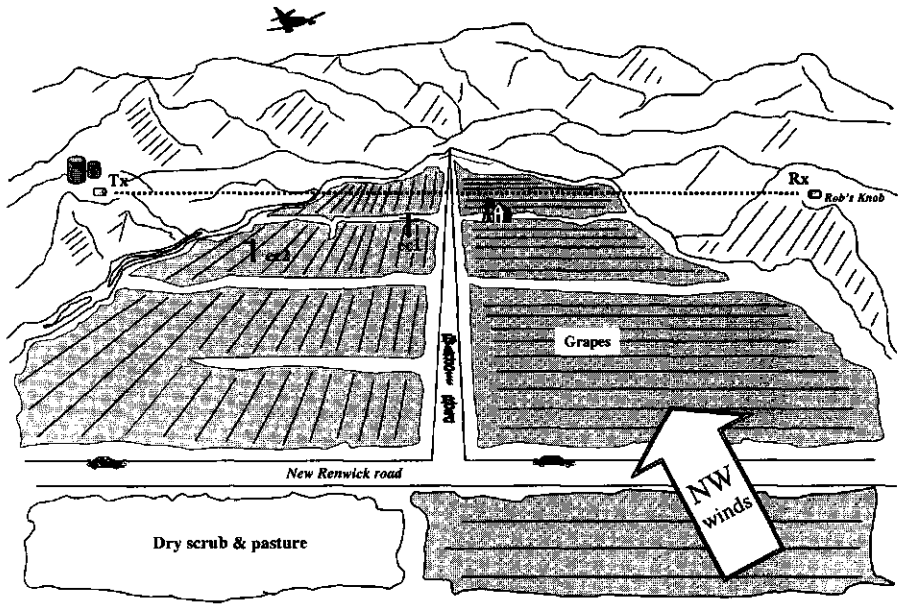

Figure (8.1). A simplified schematic of the Brancott Valley showing the positions of the scintillometer and eddy covariance instruments.

A plywood cover was built around each scintillometer to protect against wind vibration and the weather. At a later date, clear acrylic covers were added across the front openings as it was suspected the wind shear on the microwave dishes could cause unwanted *mechanical* scintillations. Acrylic is transparent at the scintillometer wavelengths. Following this experiment the scintillometers are now permanently housed in 1 m^3, aluminium cubes with portable power systems and telemetry capability. This new construction greatly simplifies installation and is ideal for transportation and weatherproofing.

The Brancott Road running NS separated the Estate into eastern and western sections characterized by the grape-rows orientated NS on the eastern side and EW on the western side. In most cases the vines were planted 1.8 m apart in rows spaced at 3 m but planting age varied from 1 through to 25 years. The vines were trellised and h_c was estimated as 1.5 m, though some vines at the centre of the scintillometer beam

were 2 m in height. The eastern side was planted in predominantly the Sauvignon Blanc variety with the canopy touching the ground. In comparison the vines on the western side were sparser and were pruned below 1 m. The vineyard relied on irrigation to meet the water requirements with all vines receiving water via drip emitters. In contrast the inter-rows were dry and devoid of plant cover due to the enduring drought.

Two, 3 meter high, open-lattice towers were instrumented with rapid response 1-D sonic anemometer-thermometers and krypton hygrometers. Half-hourly values of λE_e and H_e were calculated using the eddy covariance technique. Other slower sensors included sensitive cup anemometers, a net radiometer R_n (W m^{-2}) and a combination temperature-relative humidity sensor. One tower was placed in the mature canopy on the eastern side almost directly under the centre of the scintillometer beams (designated the road site) and the other tower near to the Fairhall river and the much younger vines (the river site). Wind speed, temperature and the relative humidity were recorded by data-loggers on Rob's Knob.

8.3.2 Weather conditions and data collection

The experiment started in late summer, February 1998, during an extreme drought. There had been no significant rainfall in the Marlborough region during the previous winter-spring period. The surrounding hillsides and pastures were brown and dry with little if any growth. In contrast, the canopy of the vineyard was green and lush. Data collection first began on the afternoon of the 21st February (day of the year, D51) and was continuous for the next three days until the monthly average rainfall (~ 35 mm) was experienced over the intervening days, D54 and D55. As the ground was baked hard very little of the rain penetrated the surface soil and most disappeared as runoff. Throughout days D51, D52 and D53 strong winds, mainly N-NW drove up the valley and through the scintillometer beam. Days D52 and D53 were overcast. These days had relatively low H_e and λE_e. By day D56 the rain had stopped and the sky was clear and the early morning winds were a cold SW blowing across the surrounding hills and through the scintillometer beam. In the afternoon the wind direction shifted around to the NE and was accompanied by intermittent cloud cover and an increasing air temperature. Day D57 had a clear sky with low windspeeds in

the morning. By the early afternoon of D57 the windspeed had increased from a northerly direction. D58 started with a brilliantly clear morning, which quickly degenerated into overcast conditions with SW wind. The final day of the experiment, D59, began the morning with strong SW winds and overcast skies followed by rain in the late afternoon.

Data from the eddy covariance and the scintillometer instruments was recorded using Campbell Scientific Inc. 21x micro-loggers programmed for 10 minute and half-hour averages. The data was retrieved daily by portable computer and analysed using a software spreadsheet. Supporting micrometeorological data were recorded using a standard met station located beside the eddy covariance instruments.

8.4 Results and discussion

8.4.1 Near-neutral and advective conditions

Day D51 had a clear sky with strong N-NW winds. In contrast days D52 and D53 were characterized by overcast skies but still with strong N-NW winds (see Figure 8.2) that blew up the valley almost perpendicular to the scintillometer beam. For instance at 1200 hrs the windspeed at 30 m was estimated to be $u_{c30m} \sim 24$ m s^{-1}. The calculation of u_{c30m} assumed a logarithmic wind profile under near-neutral conditions. Subsequent calculations of u_* at $z = 3$ m were taken as the same value at $z = 30$ m.

Over the days D51, D52 and D53 and during daytime periods of high windspeed ($u_{c3m} > 8$ ms^{-1}) both the microwave and near-infrared scintillometer signals had very large signal variances. Values of λE_s were at least an order of magnitude greater than λE_e. The eddy covariance values of H_e and λE_e are credible (Figure 8.2). Figure (8.3) compares the two methods for half-hour averages of λE selected over these three days. The 20:1 line offers a coarse indication of the disparity between the two methods.

The fluctuations measured by the scintillometer can not be due to the surface fluxes alone. The origin of these additional perturbations must lie elsewhere and were somehow related to the high wind-speeds at the scintillometer beam height ($u_c > 20$ m s^{-1}). There is the effect of the terrain to consider, as several kilometres upwind of the well-irrigated vineyard valley the landscape is mainly dry pasture and scrub. This

situation describes a transition from dry to wet surfaces effectively the strong advection of dry air into the well-irrigated valley. De Bruin et al. (1991) and De Bruin et al. (1993) made a study of surface fluxes over non-uniform terrain under advective conditions, using both the variance and eddy covariance techniques and found H to be significantly overestimated using the former method.

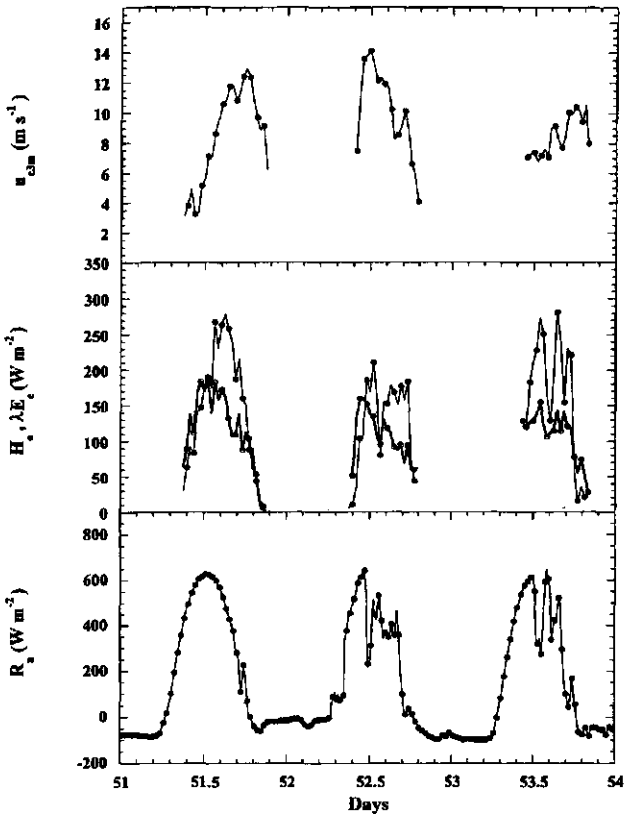

Figure (8.2). Time series of eddy covariance determined fluxes H_c (●) and λE_c (○) along with net radiation, R_n and the average windspeed at z = 3m, u_{c3m} for near neutral days D51, D52 and D53.

These extra temperature fluctuations were attributed to the entrainment of the upwind dry and warm air into the newly formed internal moist boundary layer (De Bruin, pers comms.) This is a plausible explanation for the observed increased variance in the scintillometer signals. However, because the scintillometer can not

differentiate or separate the *source* of this increased scintillation the derivation of C_T^2 and C_Q^2 is invalid and the scintillation method is flawed.

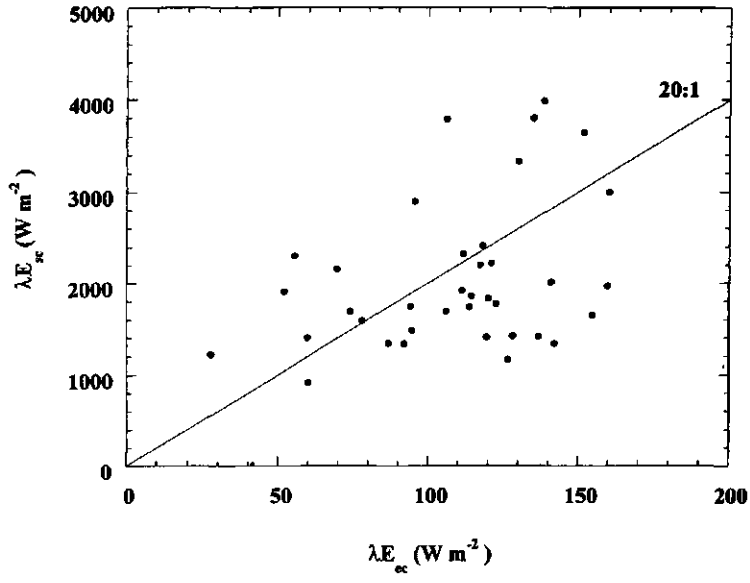

Figure (8.3). A comparison of half hour averages of λE_s and λE_e obtained under near-neutral and strongly advective conditions.

Also contributing to the additional signal variance may be wind turbulence generated by the valley slopes and the ridges where the scintillometers are positioned. Although the scintillometer path weighting is minimal at the transect extremes (Wang et al., 1978), additional mixing of the atmosphere by these physical barriers could have created unwanted fluctuations in T and Q within the valley. It is expected this effect would be particularly evident at the ridge height rather than near the valley floor as the wind accelerates upwards towards the crest of the hillsides (Kaimal and Finnigan, 1994). For the N-NW wind direction this meant the wind would strike the eastern ridge at an angle of approximately 45 degrees. The scintillometer data collected at height and under the combination of very strong advective N-NW winds taking place within this valley, remains unusable in its present form.

8.4.2 Unstable conditions

Constant heavy rain over days D54 and D55 meant all instrumentation had been turned off during this period to protect against failure. The experiment was restarted at 0900 hrs on day D56. As Figure (8.4) shows, the morning of day D56 was characterised by a clear sky and air temperature around 12 C. R_n steadily increased to a 700 W m^{-2} maximum at 1230 hrs followed by intermittent cloud cover over the afternoon.

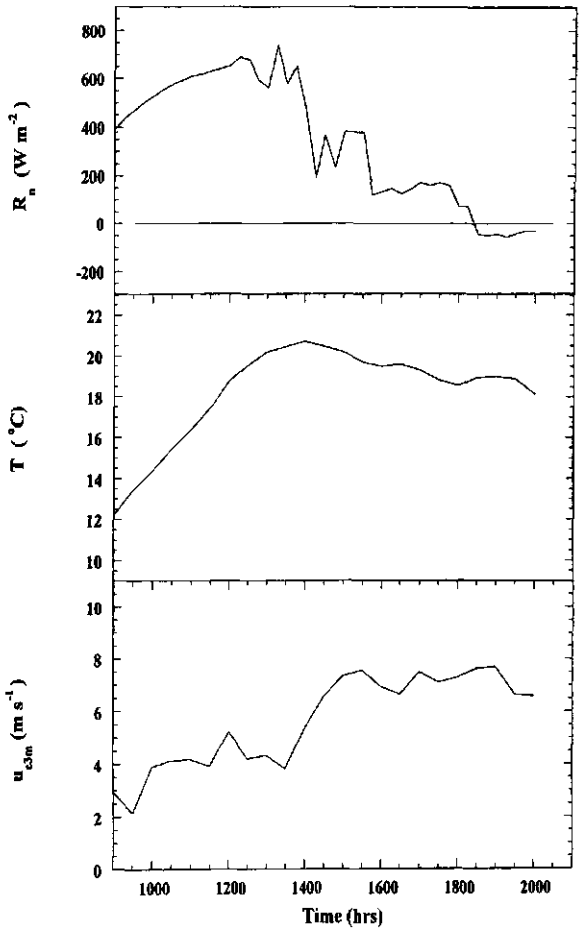

Figure (8.4). Average wind-speed at z = 3m, u_{c3m}, Temperature (T) and net radiation R_n during the unstable conditions of day, D56.

Light SW winds (u_{c3m} ~ 4 m s^{-1}) passed through the scintillometer beam but after midday the wind began to shift direction rotating 180 degrees towards the NE. Over the next 3 hours as the wind increased in speed to (u_{c3m} ~ 7.5 m s^{-1}, 1500 hrs) it blew first EW down the scintillometer beam before finally settling into a NE direction (~ 1500 hrs).

A time trace of daily half hourly averaged values of λE_s and λE_e is presented in Figure (8.5). The transition in wind direction during this period has been indicated on Figure (8.5) using the notation, SW, EW and NE. Until 1200 hrs (SW wind) the comparison between λE_s and λE_e was reasonable. In the afternoon when the wind shifted direction to the EW to blow over the east-ridge and down the scintillometer beam there was a marked underestimation by λE_s. On several occasions during the early afternoon transition in wind shift the structure parameter C_T^2 was observed to vary by more than an order of magnitude over 10 minute periods. Following Hill et al. (1992a) we have classified these periods as *non-stationary*. The atmospheric conditions prevented the application of MOST. By mid afternoon (~ 1500 hrs) agreement between λE_s and λE_e had improved.

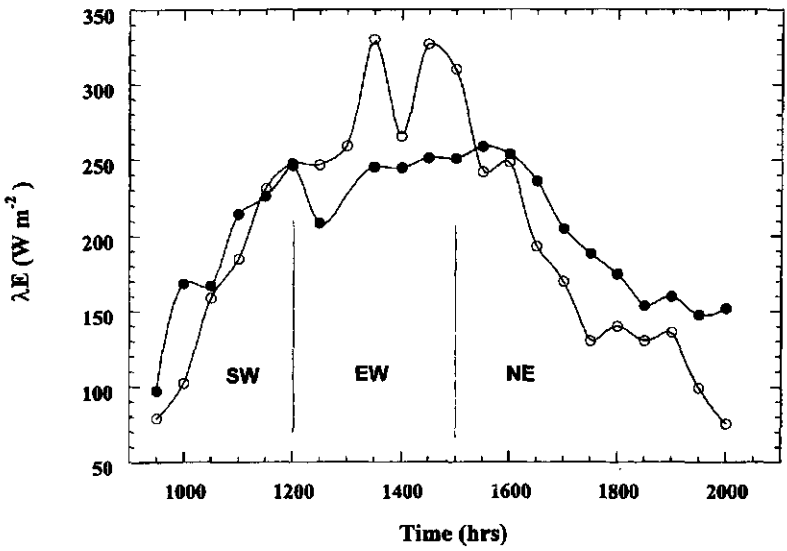

Figure (8.5). A time series of λE_s (●) and λE_e (o) for D56, a day of unstable atmospheric conditions with shifting wind direction.

Drier winds that blew from the NE apparently advected sufficient dry air into the valley so there was a trend for $\lambda E_s > \lambda E_e$. The D56 behaviour of λE_{sc} can be demarcated roughly into three temporal transitions caused by a 180-degree change in wind direction. The results suggest the successful comparison of the scintillometer and eddy covariance methods is dependent on the strength and the direction of the wind, the surrounding topography and their relation to the scintillometer beam orientation.

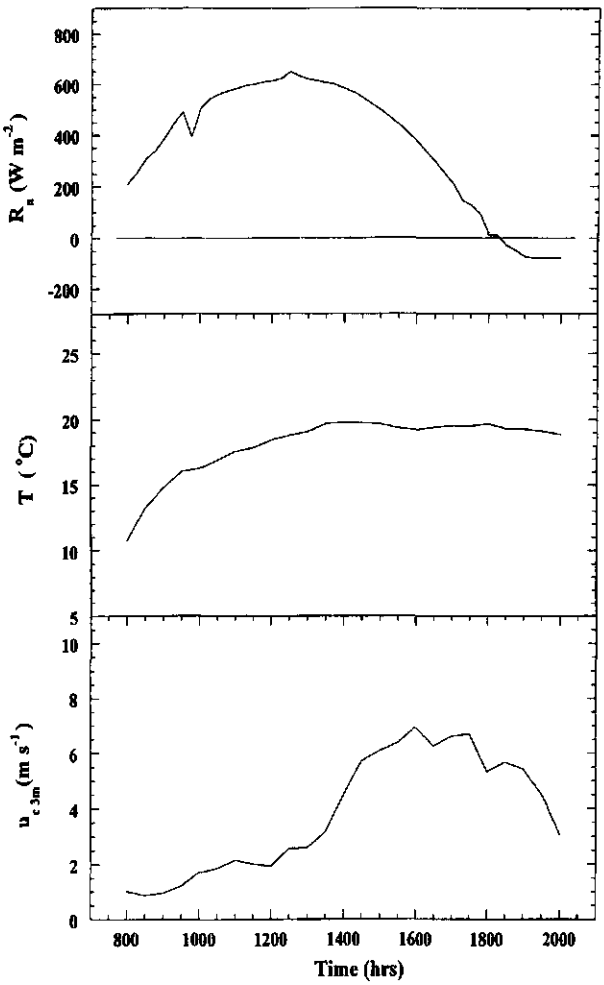

Figure (8.6). Air temperature, T, average wind-speed at z = 3m, u_{c3m} and net radiation, R_n for day, D57 which experienced very unstable conditions in the morning period.

During the morning of day D57 the atmosphere tended towards highly unstable conditions to provide a data set with which to test the effectiveness of Equation (8.11). Average wind-speed was low during the first part of the day ($u_{c3m} < 1.5$ m s^{-1}) and the sky was clear throughout the previous night and extended over the morning of D57 (Figure 8.6). By noon the air temperature had climbed to 19 C from an early morning low of 10 C (0800 hrs). From noon the wind-speed increased from $u_{c3m} \sim 2$ m s^{-1} to $u_{c3m} \sim 7$ m s^{-1} by 1600 hrs and from a northerly direction. As significant mechanical mixing was now occurring in the boundary layer Equation (8.11) was no longer valid.

Figure (8.7) is a time series comparison between λE_s and λE_e for D57. In the period between 0800 and 1330 hrs λE_s has been calculated using Equation (8.11) assuming very unstable conditions. From 1400 hrs onwards and with the increasing wind-speed, λE_s is determined using the iterative method as described for unstable conditions. In the first instance and in contrast to λE_e, the values of λE_s lying between 0800 and 1030 hrs are larger than believable as $R_n < 450$ W m^{-2}.

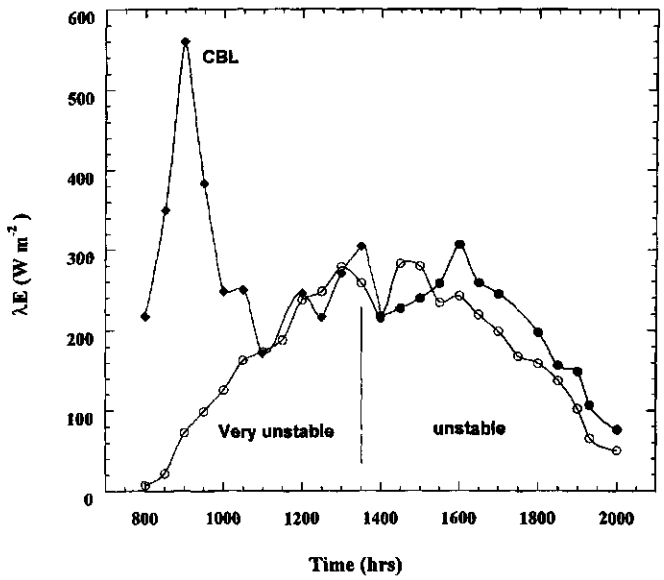

Figure (8.7). A time series for day D57 showing the effect of the CBL passing through the scintillometer beam mid-morning and the reasonable agreement obtained between very unstable λE_s (◆) and unstable λE_s (●) with values of λE_e (o).

During this period the values of C_T^2 and C_Q^2 (Figure 8.8) experienced an increase in magnitude peaking at 0900 hrs. Calculated λE_s was then very much greater than expected from a surface latent heat flux. Both the microwave and large aperture infrared scintillometer signals independently showed additional signal variance. In explanation it is proposed these peaks are indicative of the evolution of the CBL (as indicated on Figure 8.7) growing in height in response to surface heating. Stull (1988) describes the depth of the CBL increasing slowly, under calm situations, from several tens of metres controlled by the strong nocturnal stable layer capping the CBL. We believe that as the air temperature rose in the mid-morning, the top of the CBL moved upward and passed through the scintillometer beam. The transition in air density as the warmer air moved through the beam caused additional fluctuations to be recorded by the scintillometer, but these went unseen by the eddy covariance instruments. Kohsiek and Herben (1983) infer this behaviour in their paper when describing evaporation made by measurements of radio wave scintillation.

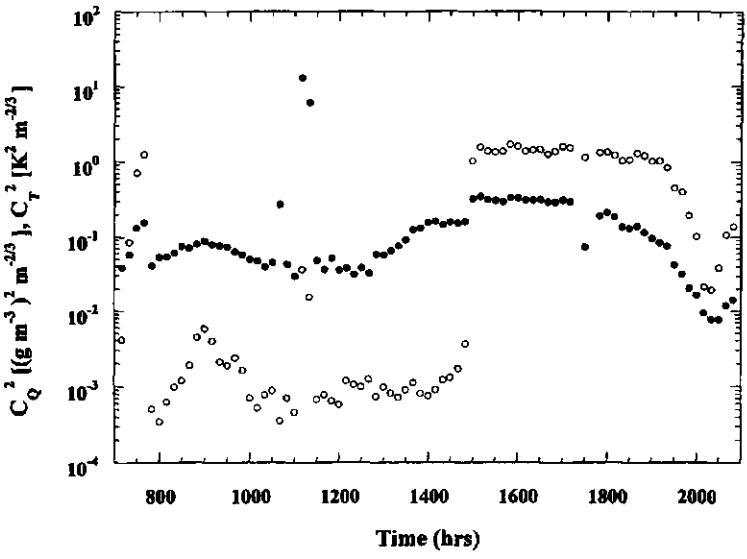

Figure (8.8). The behaviour of the structure parameters C_T^2 (o) and C_Q^2 (●) for day, D57. Each of the spikes in the time traces are periods when reliable data is unavailable. This is due either to obstruction of the beam or the behaviour of the atmosphere as it undergoes various transitions.

Additionally, Wyngaard and LeMone (1980) discuss the behaviour of C_T^2 and C_Q^2 in the CBL and observed that these values can be several orders of magnitude greater near the inversion height than expected through that generated by surface fluxes.

By late morning (1100 hrs) the height of the CBL had grown beyond both the scintillometer and eddy covariance instruments and the fluxes recorded by both instruments was contained within the convective surface layer. Application of Equation (8.11) for free convective conditions was valid and demonstrated extremely pleasing agreement between λE_s and λE_e from 1100 to 1330 hrs (Figure 8.7). At 1130 hrs an acrylic screen was placed over the scintillometer transmitter. A similar screen was erected at the scintillometer receiver about 1730 hrs. The screens were designed to prevent mechanical oscillations by heavy winds moving the scintillometers. This modification to the enclosures caused peaks in C_T^2 and C_Q^2 about 1130 and 1730 hrs (Figure 8.8) as the scintillometer beam was broken. There is no evidence there was an improvement in the scintillometers performance by the placement of these screens. From 1400 hrs onwards the free convective formula was discarded in favour of the unstable approach. Calculations of λE_s constantly overestimate λE_e in a manner similar to the results of day, D56. The sudden jump in magnitude of both C_T^2 and C_Q^2 around 1430 hrs (Figure 8. 8) from one plateau to another occurs with increased wind-speed (see u_{c3m}, Figure 8.6).

During the very unstable conditions the signal from the near-infrared scintillometer was very close to the instrument noise. Some discussion on this problem is warranted because the scintillation method relies on accurate measurements of $C_{n,i}^2$. During very unstable conditions simple theory states that both C_T^2 and C_Q^2 are proportional to $z^{-4/3}$ within the surface boundary layer. In practical terms this means the magnitude of C_T^2 or C_Q^2 measured by a scintillometer placed at a height of z = 30 m will be only 5 % of that measured by the same instrument placed at z = 3 m above the valley floor. This reduction in signal strength becomes problematic for low values of evaporation as the scintillometers must be capable of a suitable signal resolution without approaching their own noise limit. During the convective conditions, C_T^2 was three orders of magnitude less than the values measured over the unstable mid-afternoon situation (Figure 8.8). The other two peaks in C_T^2 and C_Q^2

occurring in the early morning and the early evening (0700 – 0800 hrs and 2000 – 2100 hrs) represent the transition between the unstable and stable atmospheric states. During these periods C_T^2 and C_Q^2 are indeterminable as will be λE_s.

The final days of the experiment, D58 and D59, are not discussed in detail here as both were overcast, cold and with strong winds blowing NW down the scintillometer transect making data interpretation difficult. During this period the signal output from the infrared scintillometer was observed to approach its own noise limit ($C_n^2 < 10^{-17}$ $m^{-2/3}$). However the clear early morning of day, D58, provided several half-hour data points which although not presented had λE_s and λE_e in close agreement.

The issue of improving the signal strength of the near-infrared scintillometer is currently being addressed through the use of a more powerful radiation source. It is noted the microwave scintillometer signal strength was always adequate.

8.5 Conclusion

The purpose of this research was to identify whether the scintillometer method could be used to estimate evaporation from a vineyard valley and be capable of providing figures for daily irrigation scheduling and the management of water resources. The scintillometer was placed on opposing valley ridges to propagate its beam across and well above the valley floor. In calculating λE_s it was assumed that similarity theory was 'workable' for the valley situation and the scintillations were caused by the surface fluxes of heat and moisture.

The results demonstrate the success of these λE_s measurements when compared with eddy covariance data depend on the prevailing atmospheric conditions and surrounding terrain. Operating scintillometers at $z = 30$ m creates additional problems not encountered when the beam is closer to the canopy. These problems are extraordinary scintillations and much weaker signals whose symptoms are an excessive intensity variance and reduced signal-to-noise ratio. The cases identified to date include the entrainment of warm dry air under advective conditions and the development of the CBL as it passes through the scintillometer beam. Confirmation of these phenomena is a next experimental step. Excessive wind-speed contributed to the overestimation of λE_s relative to λE_e during unstable conditions. The difference

became extreme for near-neutral conditions with a dry-to-wet transition downwind. There is no evidence to suggest the scintillometer combination will not perform well when operated at this height and under near-neutral conditions over uniform terrain. The free convection formula gave good results for the small data set collected.

In summary the results presented indicate the scintillation method can produce credible estimations of λE_s from an irrigated valley. The scintillometer performed best under unstable to very unstable atmospheric conditions. The reasonable comparison between the scintillometer and eddy covariance time series suggests the application of similarity theory was appropriate. Scintillometers need to be mounted at greater heights than conventional instruments in order to obtain an unobstructed propagation of their beams across kilometer distances and to compensate for curvature of the Earth. As a result they may encounter some of the unwanted effects reported in this experiment.

Summary

This thesis has collated one review chapter and five experiments concerned with addressing the question, *'how successful is the scintillometer method in determining the surface fluxes of heat, moisture and momentum and under what circumstances does it appear to fail?'* Answering this question is important as a workable scintillation method provides the meteorologist with spatial integrated measurements of the surface fluxes at kilometre scales. With such a tool, ground-truth validation of remote sensing systems is possible, water balance studies can be conducted at catchment scales and energy balance experiments extended over slightly non-homogeneous terrain. Using electromagnetic scintillation to infer turbulence quantities is a fairly recent development. Although our interest lies in estimating the surface fluxes Chapter 3 makes it very clear that the foundation of the scintillation method is deeply rooted in at times questionable combination of turbulence and wave propagation theory. The novice must appreciate the important steps and assumptions in the scintillation method. Purchasing a scintillometer *off-the-shelf* is no guarantee of reliable measurements.

How well this thesis has answered the treatise depends to an extent on the relative performance of the scintillometer method against some benchmark. For these scintillation experiments this benchmark was the eddy covariance method, selected for convenience and familiarity. In many ways this selection is a compromise as different temporal and spatial band-widths are used by each method. Scintillation measures the ensemble average of spatial fluctuations in the refractive-index along the propagation path. The eddy covariance technique makes measurements at one point in space as a function of time. The time average of the eddy covariance method is considered to be an ensemble average. Depending on atmospheric stability the eddy covariance method may require several tens of minutes to integrate the energy from all eddy scales contributing to the surface fluxes. In comparison, the scintillometer can provide statistically stable data within minutes because it only measures in the

inertial-convective subrange of frequencies. In light of such differences any comparison between methods should be made with a *tongue-in-cheek* approach with the state of the atmosphere and surface conditions carefully scrutinised to explain any discrepancies. The strength of using the eddy covariance technique as a comparison is because it identifies any marked deviations from the norm experienced by the scintillation method. Success is in comprehending what caused these deviations not through obtaining the perfect half-hour correlation between methods. The five experiments in this thesis table such deviations and propose explanations for their particular scintillometer type and application. What follows, are the salient facts gleamed from this research.

The experiments using the inner scale meter and the semiconductor laser diode highlighted the pluses and minuses of l_o dependence for laser scintillometers. This dependence required a correction to the measured signal variance using the spectra of Hill (1978), but it also provided information on the magnitude of l_o and ultimately a measure of u_*. In the case of the semiconductor laser diode scintillometer, l_o was indirectly determined using a measurement of average windspeed and crop height. This approach proved successful in the calculation of H_{sc}. In contrast, the inner scale meter measured l_o using the difference in received signal variances between a gas laser and a large aperture scintillometer having little l_o dependence. This latter approach was particularly sensitive to small signal differences and caused considerable scatter in the u_* comparisons. Despite a coarse result for u_*, H_{sc} still compared favourably to H_{cc}. In addition to the l_o dependence the laser scintillometers suffered from signal saturation in the presence of strong turbulence. This path limited the laser scintillometers and consequently the inner scale meter to operation over short distances (L < 100 m). This limitation was less than attractive for the purposes of path averaging fluxes at catchment scale.

The near-infrared large aperture scintillometer was designed to overcome the shortcomings of the laser scintillometers. It is most suited to calculations of H_{sc} and it successfully did so as a component of the inner scale meter. This scintillometer however performed poorly for the rice paddy experiment. Here $H_{sc} < E_{sc}$ and at times up to 40% of the received signal variance could be attributed to correlated T-Q fluctuations. The rice paddy experiment highlighted the effect of absorption

scintillations on the large aperture signal variance. This effect was also apparent in the test of the two-wavelength scintillometer at Ahipara (Chapter 7). Subsequent modification to the scintillometer's electronic filtering alleviated this problem. If large aperture near-infrared scintillometers are still being built based on the original design of Ochs and Cartwright (1980) then the C_n^2 output signal may contain the effect of absorption fluctuations in addition to refractive fluctuations.

The optical wavelength scintillometers, whether they are the laser or the large aperture types, struggled to provide a measurement of E_{sc} because they are less sensitive to humidity fluctuations than temperature fluctuations. This was confirmed by observations of the relative contributions made by C_T^2, C_{TQ}, and C_Q^2 to C_n^2 at visible to near-infrared wavelengths. The opposite was shown to be true at microwave wavelengths and so measuring E_{sc} requires a microwave scintillometer. The two-wavelength combination of microwave and large aperture scintillometers proved successful in calculating both E_{sc} and H_{sc}, provided the effect of low frequency path-averaged humidity fluctuations was filtered from the scintillometer signals. The microwave scintillometer was shown to be sensitive to inertial-convective fluctuations and capable of calculating C_n^2.

When mechanical turbulence is minimal and one is interested in unstable atmospheric conditions then the free convection formula developed for the two-wavelength scintillometer provided a reasonable estimate of E_{sc}. However measuring at height and under very unstable conditions means the scintillometer signal variance can be corrupted by the passage of the growing CBL. Because $C_n^2 \propto z^{-4/3}$, the scintillometer signal variance can become very small and possibly undetectable from signal noise. Unpublished data from the Ahipara experiment showed the large aperture scintillometer operated at 10 m and can provide reliable estimates of H_{sc} by also using a free convective scaling formula (De Bruin et al., 1995). This result is in-line with the observations of De Bruin et al. (1995) who also showed coarse measurements of u_* were sufficient to ensure reasonable calculations of H_{sc} and E_{sc}.

Until microwave scintillometers were used in these experiments measurements were confined close to the ground. Microwave technology required installing the

scintillometer at some minimum height to avoid surface reflection of the propagated signal. With increased height and distance so grew the requirements to preserve MOST. The valley experiment at Brancott was the first time the effect of advection was observed on the scintillation measurements. The scintillometer footprint was sensitive to the effects of the dry-to-wet transition and the entrainment of the dry and warm air into the newly formed surface boundary layer. Under these conditions the scintillometers could not distinguish the source of the additional signal variance and the scintillometer method failed. It was also highly unlikely under these circumstances the *T-Q* correlation held at the scintillometer beam height.

In light of these summarised results we present here some recommendations.

- Laser scintillometers or scintillometers which incorporate lasers such as the inner scale meter are only useful over short distances as they are limited by signal saturation and a dependence on l_o. Theoretical advances in describing the scintillometer signal variance in strong turbulence will still require a powerful and stable laser scintillometer to implement such advances if operation over kilometre distances is required.
- The near-infrared large aperture scintillometer is simple and inexpensive to construct. It has minimal dependence on l_o and it can operate over kilometre distances without signal saturation. It probably is not suited to measurements over well-irrigated surfaces because it is most sensitive to temperature fluctuations. This scintillometer performs well in unstable conditions using free convective scaling.
- The microwave scintillometer and large aperture near-infrared scintillometer combination can provide reliable estimates of H_{sc} and E_{sc}. They should be used over reasonable homogeneous terrain with sufficient fetch to guarantee reliable measurements. This two-wavelength combination can estimate both H_{sc} and E_{sc} under unstable conditions using free convective scaling.

Samenvatting

Dit proefschrift geeft een theoretisch overzicht en het resultaat van vijf veldexperimenten met betrekking tot de vragen: '*hoe succesvol is de scintillatiemethode in het bepalen van de oppervlaktefluxen van warmte, waterdamp en impuls en onder welke omstandigheden is de methode niet toereikend*'. Het antwoord op deze vragen is belangrijk omdat de methode meteorologen kan voorzien van ruimtelijk geïntegreerde metingen van de oppervlaktefluxen op een schaal van kilometers. Met dit hulpmiddel is validatie van satellietwaarnemingen mogelijk, kunnen waterbalansstudies uitgevoerd worden op de schaal van een stroomgebied of energiebalansexperimenten worden uitgevoerd boven lichtelijk niet-homogeen terrein. Het gebruik van elektromagnetische scintillatie om turbulente kwantiteiten af te leiden is een tamelijk nieuwe ontwikkeling. Hoewel onze interesse ligt bij het schatten van de oppervlaktefluxen, maakt Hoofdstuk 3 duidelijk dat de fundering van scintillatiemethode diep geworteld is in de bij tijden twijfelachtige golftheorie. Een beginner moet deze belangrijke stappen en aannamen in de scintillatiemethode waarderen en begrijpen, want de aanschaf van een kant-en-klare scintillometer is géén garantie voor betrouwbare metingen.

Hoe goed dit proefschrift antwoord geeft op de bovengestelde vragen is in hoge mate afhankelijk van de relatieve prestatie van de scintillatiemethode ten opzichte van een standaardmethode. Uit gemak en ervaring is de eddy-covariantietechniek als standaard voor de scintillatiemethode gekozen. In vele opzichten is deze keuze een compromis, omdat de methoden gebruik maken van verschillende tijds- en ruimtelijke schalen. De scintillatiemethode meet een ensemble gemiddelde van de ruimtelijke fluctuaties in de atmosferische brekingsindex langs het optische pad. De eddy-covariantiemethode daarentegen, is een puntmeting in de ruimte als functie van de tijd. De tijdsgemiddelde eddy-covariantiemeting wordt hierbij beschouwd als ensemble gemiddelde. Afhankelijk van de atmosferische stabiliteit zijn er veelal tientallen minuten nodig om alle energie van de eddy-schalen die bijdragen aan de

oppervlaktefluxen te integreren. De scintillatiemethode biedt echter na enkele minuten al statistisch betrouwbare data omdat de methode slechts meet in de inertiële-convectieve frequentiegebied.

Met deze verschillen in ons achterhoofd moet een vergelijking van deze methoden met enig voorbehoud benaderd worden, waarbij de toestand van de atmosfeer en het oppervlak nauwlettend moeten worden bestudeerd om bepaalde discrepanties te kunnen verklaren. De kracht van de vergelijking met eddy-covariantietechniek wordt bepaald door de identificatie van markante afwijkingen van de 'normaal' bij gebruik van de scintillatiemethode. Succes is, het begrijpen van de oorzaken van deze afwijkingen en niet het bereiken van de perfecte correlatie tussen de twee methoden. De vijf experimenten beschreven in dit proefschrift belichten dergelijke anomalieën en stellen verklaringen voor, afhankelijk van het type scintillometer en toepassingsgebied. Wat volgt zijn opvallende feiten die voortvloeien uit dit onderzoek.

De experimenten waarin de 'inner scale' meter en de semi-conductor laserscintillometer gebruikt werden accentueerden de positieve en negatieve kant van de l_o afhankelijkheid van laserscintillometers. Deze afhankelijkheid maakte een correctie met behulp van de spectra van Hill (1978) op de gemeten signaalvariantie noodzakelijk, maar gaven tegelijkertijd ook informatie over de grootte van l_o en uiteindelijk van u_*. In het geval van de semi-conductor laserscintillometer, werd l_o bepaald met behulp van een indirecte meting van de gemiddelde windsnelheid en de gewashoogte. Deze benadering is succesvol gebleken bij de berekening van H_{sc}. In tegenstelling tot het voorgaande, bepaalde de 'inner scale' meter l_o uit verschil in de ontvangen signaalvarianties van een laserscintillometer en een scintillometer met grote openingshoek die weinig afhankelijk is van l_o. Deze laatste methode was bijzonder gevoelig voor kleine signaalverschillen en veroorzaakte daardoor aanzienlijke spreiding bij de vergelijking van u_*. Ondanks dit resultaat voor u_*, kwamen H_{sc} en H_{ec} toch goed overeen. Naast de afhankelijkheid van l_o van de laser scintillometers trad er bovendien verzadiging op van het signaal onder sterk turbulente omstandigheden. Dit beperkte het gebruik van de laserscintillometer en daarmee de 'inner scale' meter tot korte padlengten ($L < 100$ m).

De nabij infrarode scintillometer met grote openingshoek werd ontworpen om de tekortkomingen van de laserscintillometer te overwinnen. Deze scintillometer is zeer geschikt om H_{sc} te bereken werd hiervoor ook succesvol ingezet als onderdeel van de 'inner scale' meter. Deze scintillometer presteerde echter slecht tijdens het rijstveldexperiment. In dit geval was $H_{sc} < E_{sc}$ en soms kon 40% van het ontvangen signaalvariantie worden toegeschreven aan de gecorreleerde T-Q fluctuaties. Dit rijsveldexperiment heeft wederom het effect van absorptiefluctuaties op de variantie van het signaal van deze scintillometer laten zien. Dit was ook duidelijk aanwezig tijdens het experiment met de twee golflengten scintillometers in Ahipara, Nieuw Zeeland (Hoofdstuk 7). Door het aanpassen van de elektronische filtering van de scintillometer werd dit probleem verholpen. Als er echter scintillometers gebouwd worden volgens het ontwerp van Ochs en Cartwright (1980) dan zou het output signaal, C_n^2, beïnvloed kunnen worden door het effect van absorptiefluctuaties bovenop de fluctuaties ten gevolge van refractie.

De optische scintillometers, lasers of met grote openingshoek, waren niet in staat E_{sc} te bepalen, omdat deze typen gevoeliger zijn voor temperatuur- dan voor vochtfluctuaties. Dit werd bevestigd door waarnemingen van de relatieve bijdragen van C_T^2, C_{TQ} en C_Q^2 aan C_n^2 voor zichtbare- en nabij infrarode golflengten. Het tegenovergestelde werd echter aangetoond bij het gebruik van microgolfen. Voor het bepalen van E_{sc} is dus een microgolfscintillometer nodig. Een combinatie van een microgolfscintillometer en een scintillometer met grote openingshoek bleek succesvol te zijn bij het bepalen van zowel E_{sc} als H_{sc}, aangenomen dat het effect van padgemiddelde, laagfrequente vochtfluctuaties uit het scintillometersignaal gefilterd werd. De microgolfscintillometer toonde aan gevoelig te zijn voor inertiële convectieve fluctuaties en in staat te zijn om C_n^2 te bepalen.

Onder onstabiel omstandigheden met minimale mechanische turbulentie voldeed de vrije convectie formule ontwikkeld voor de twee golflengten scintillometer en gaf daardoor een redelijke schatting van E_{sc}. Echter metingen op grotere hoogte onder zeer onstabiele omstandigheden betekenden dat de variantie van het signaal van de scintillometers verstoord werd door de passage van een groeiende grenslaag. Omdat $C_n^2 \propto z^{-4/3}$ kon het variantiesignaal zo klein worden dat deze

mogelijk niet te onderscheiden was van de signaalruis. Ongepubliseerde data van het Ahipara experiment lieten zien dat voor een scintillometer met grote opening, geplaatst op 10 m hoogte, de vrije convectie formule (De Bruin et al., 1995) betrouwbare waarden voor H_{sc} opleverde. Dit resultaat correspondeert met waarnemingen van De Bruin et al. (1995), die ook lieten zien dat grove metingen van u_* voldoende waren om een redelijke berekening te maken van H_{sc} en E_{sc}.

Tot het moment dat microgolfscintillometers hun intrede deden, werden experimenten vlak boven de grond gedaan. Microgolventechnologie vereiste een minimale afstand van het oppervlak om reflecties van het golfsignaal te voorkomen. Met de groter wordende hoogte en afstand groeide ook het belang van het behoud van MOST. Het Brancott vallei experiment liet voor het eerst het effect van advectie zien op metingen met een scintillometer. De voetafdruk van de scintillometer was gevoelig voor droog naar nat overgangen en voor menging van droge en warme lucht in de nieuw gevormde oppervlaktegrenslaag. Onder deze omstandigheden was de scintillometer niet in staat de bron van de toegevoegde signaalvariantie te onderscheiden, waardoor de scintillometermethode faalde. Het was bovendien hoogst onwaarschijnlijk dat onder deze omstandigheden de T-Q correlatie in takt bleef op de hoogte van de stralingsbundel.

In het licht van de samengevatte resultaten volgen hier enkele voorzichtige aanbevelingen:

- Laserscintillomers of gecombineerde scintillometers die lasers gebruiken, zoals de 'inner scale' meter zijn alleen bruikbaar over relatief korte afstanden, omdat deze beperkt zijn door signaalverzadiging en de afhankelijkheid van l_o. Om de theoretische vooruitgang bij het beschrijven van de signaalvariantie van de scintillometer onder sterk turbulente omstandigheden te implementeren vereist, indien er op kilometer schaal gewerkt moet worden, een krachtige en stabiele laserscintillometer vereist.
- De nabij infrarode scintillometer met een grote openingshoek vereist relatief simpel en goedkoop te construeren. De afhankelijkheid van l_o is minimaal en kan zonder verzadiging over enkele kilometers meten. Het instrument is waarschijnlijk niet geschikt om betrouwbare metingen te verrichten boven goed geïrrigeerde oppervlakten omdat op deze golflengte refractie vooral

veroorzaakt wordt door temperatuurfluctuaties. Deze scintillometer geeft goede resultaten met vrije convectie schaling onder zeer onstabiele omstandigheden.

- Een combinatie van een microgolfscintillometer en een nabij infrarode scintillometer met een grote openingshoek geeft betrouwbare schattingen van zowel H_{sc} als E_{sc}. De combinatie moet worden ingezet boven homogeen terrein met voldoende ongestoorde aanstroming om betrouwbare metingen te garanderen. Vrije convectie schaling geeft ook hier een goede schatting van H_{sc} en E_{sc}.

References

Abbott, M.B., Bathurst, J.C., Cunge, J.A., O'Connell, P.E., and Rasmussen, J., 1986. An introduction to the European Hydrological System - Systeme Hydrologique Europeen, "SHE", 1. History and philosophy of a physically-based, distributed modelling system. Journal of Hydrology, **87**, 45-59.

Andreas, E. L., 1987. On the Kolomogorov constants for the temperature-humidity cospectrum and the refractive-index spectrum. J. Atmos. Sci., **44**, 2399-2406.

Andreas, E. L., 1989. Two-wavelength method of measuring path-averaged turbulent surface heat fluxes. J. Atm. Ocean. Tech., **6**, 280-292.

Andreas, E. L.(ed.), 1990. *Selected papers on turbulence in a refractive medium, SPIE Milestone Series*, **25**, Society of Photo-Optical Instrumentation Engineers, Bellingham WA.

Andreas, E. L., Hill, R. J., Gosz, J. R., Moore, D. I., Otto, W. D. and Samra, A. D., 1996. Statistics of surface-layer turbulence and evaluations of eddy-accumulation coefficients over terrain with meter-scale heterogeneity. Boundary-Layer Meterolo. **86**, 379-408.

Batchelor, C.H., Cain, J.D., Farquharson, F.A.K., and Roberts, J.M. 1998. Improving water utilisation from a catchment perspective. SWIM Paper 4.

Beljaars, A.C.M. and Viterbo, P., 1998. Role of the Boundary Layer in a Numerical Weather Prediction Model, in: *'Clear and Cloudy Boundary Layers'* Holtslag, A.A.M. and Duynkerke, P.G. Eds, 287-322.

Beven, K., 1989. Changing ideas in hydrology - The case of physically-based models. Journal of Hydrology, **105**, 157-172.

Beyrich, F, Richter, S.H., Weisensee, U., Kohsiek, W., Bosveld, F., Lohse, H., De Bruin, H.A.R., Hartogensis, O., Bange, J. and R. Vogt, 2000a. The LITFASS-98 Experiment: Fluxes over a heterogeneous land surface, Proc. 14th Symposium on Boundary Layer and Turbulence, 5-9.

Beyrich, F., De Bruin, H.A.R. and Schipper, H., 2000b. Experiences from one-year continuous operation of a large aperture scintillometerover heterogeneous land surface, Proc. 14th Symposium on Boundary Layer and Turbulence, 175-177.

Bloschl, G. and Sivapalan, M., 1995. Scale issues in hydrological modelling: A review. In: Kalma, J.D. and Sivapalan, M. (Eds.). Scale issues in hydrological modelling. John Wiley and Sons, Chichester, pp. 9-48.

CASES-99: http://www.colorado-research.com/cases/CASES-99.html

Champagne, F. H., Friehe, C. A., LaRue, J. C. and Wyngaard, J. C., 1972. Flux measurements, flux estimation techniques, and fine-scale turbulence measurements in the unstable surface layer over land. J. Atmos. Sci., **34**, 515-530.

Chehbouni, A., Kerr, Y. H., Watts, C., Hartogensis, O., Goodrich,D., Scott, R., Schieldge, J., Lee, K., Shuttleworth, W. J., Dedieu, G. and De Bruin,H. A. R., 1999. Estimation of area-averaged sensible heat flux using a large-aperture scintillometer during the Semi-Arid Land-Surface-Atmosphere (SALSA) experiment, 1999: Water Res. Res., **35** No 8, 2505-2511.

Churnside, J. H., Lataitis, R. J. and Lawrence, R. S., 1988. Localized measurements of refractive turbulence using spatial filtering of scintillations. Applied Optics, **27**, 2199-2213.

Churnside, J. H., 1990. A spectrum of refractive turbulence in the turbulent atmosphere. J. Modern Optics, **37**, 13-16.

Churnside, J. H., 1992. Optical remote sensing. *Wave propagation in a random media (scintillation)*., Tatarskii, V. I., Ishimaru, A., Zavorotny, V. U. (eds.), SPIE, Bellington, WA.

Clifford, S. F. and Strohbehn, J. W., 1970. The theory of microwave line-of-sight propagation through a turbulent atmosphere. IEEE Trans. Antennas. And Prop., **AP-18**, 264-274.

Clifford, S. F., Ochs, G. R. and Lawrence, R. S., 1974. Saturation of optical scintillation by strong turbulence. J. Opt. Soc. Am., **64**, 148-154.

Commission of the European Communities. 1996. Commmission proposal for a Council Directive establishing a framework for a European Community Water Policy. Consultation draft. Luxembourg, Office for Official Publications of the European Communities, 70 pp.

Coppin, P. A., 1982. An examination of cup anemometer overspeeding. Meteorlo. Rdsch., **35**, 1-11.

Corrsin, S., 1951. On the spectrum of isotropic temperature fluctuations in an isotropic turbulence. J. Applied Physics, **22**, 469-473.

De Bruin, H. A. R., Bink, N. J. and Kroon, L. J. M., 1991. Land Surface Evaporation: Fluxes in the Surface Layer Under Advective Conditions. Schmugge and Andre, (ed).

De Bruin, H. A. R., Kohsiek, W. and van den Hurk, B. J. J. M., 1993: A verification of some methods to determine the fluxes of momentum, sensible heat, and water vapour using standard deviation and structure parameter of scalar meteorological quantities. *Boundary-Layer Meteorol.* **63**, 231-257.

De Bruin, H. A. R., van den Hurk, B. J. J. M. and Kohsiek, W., 1995. The scintillation method tested over a dry vineyard area. *Boundary-Layer Meteorol.* **76**, 25-40.

De Bruin, H. A. R., Nieveen, J. P., de Wekker, S. F.J. and Heusinkveld, B. G., 1996. Large aperture scintillometry over a 4.8 km path for measuring areal-average sensible heat flux. Published in the 22nd Conference on Agricultural and Forest Meteorology.

De Bruin, H. A. R, 1998. A long-path scintillometer for measuring areal-average sensible heat flux, in: Proc. WMO Commission CIMO , Casablanca, Maroc.

De Bruin, H. A. R., van den Hurk, B.J.J.M.; Kroon, L.J.M.; 1999. On the temperature-humidity correlation and similarity. Boundary-Layer Meteorol., **93**, 453-468

Fairhall, C. W., Edson, J. B., Larsen, S. E. and Mestayer, P. G., 1980. Inertial dissipation air-sea flux measurements: A protype system using realtime spectral computations. J. Atmos. Ocean. Tech., **7**, 425-453.

Friehe, C. A., Larue, J. C., Champagne, F. H., Gibson, C. H. and Dreyer, G. F., 1975. Ffects of temperature and humidity fluctuations on the optical refractive-index in the marine boundary layer. J. Opt. Soc. Am., **65**, 221-230.

Frehlich, R. G. and Ochs, G. R., 1990. Effects of saturation on the optical scintillometer. Applied Optics, **29**, 548-553.

Garratt, J. R., 1992. The atmospheric boundary layer. Cambridge University Press, ISBN 0 521 38052 9.

Green, A. E., Judd, M. J., McAneney, K. J., Astill, M. S. and Prendergast, P. T., 1991. A rapid-response, 2-D drag anemometer for atmospheric turbulence measurements. Boundary-Layer Meteorol. **57**, 1-15.

Green, A. E, McAneney, K. J. and Astill, M. S., 1994. Surface layer scintillation measurements of daytime and heat and momentum fluxes. Boundary-Layer Meteorol., **68**, 357-373.

Green, A. E, McAneney, K. J and Lagouarde, J-P., 1997. Sensible heat and momentum flux measurement with an optical inner scale meter. Agric. For. Meteorol. **85**, 259-267.

Green, A. E., Astill, M. S. and Nieveen, J. P., 1999: Path-averaged surface fluxes determined from infrared and microwave scintillometers. Submitted *Ag. and Forest Meteorol.*

Green, A. E., Green, S. R., Astill, M. S. and Caspari, H., 2000. Estimating latent heat flux from a vineyard valley using scintillometry. J. Terrestrial, Atmos. and Oceanic Sci. **11**.

Hartogensis, O., 1997. Measuring areal-averaged sensible heat flux with a large aperture scintillometer, MS-Thesis,. Wageningen University and Research Center, Meteorology and Air Quality Group,47 pp.

Holtslag, A.A.M. and Duynkerke, P.G. Eds, *'Clear and Cloudy Boundary Layers'*, Royal Neth. Academy of Art and Sciences. pp 372.

Hill, R. J., 1978a. Models of the scalar spectrum for turbulent advection. J. Fluid Mechanics, **88**, 541-562.

Hill, R. J. and Clifford, S. F., 1978b. Modified spectrum of atmospheric temperature fluctuations and its application to optical propagation, **68**, 892-899.

Hill, R. J., Clifford, S. F. and Lawerence, R. S., 1980. Refractive-index and absorption fluctuations in the infrared caused by temperature, humidity and pressure fluctuations. J. Opt. Soc. Am., **70**, 1192-1205.

Hill, R. J., Bohlander, R. A., Clifford, S. F., McMillan, R. W., Priestley, J. T. and Schoenfeld, W. P., 1988. Turbulence-induced millimetre-wave scintillation compared with micrometeorological measurements. IEEE Trans. on Geosci. and Remote Sensing, **26**, 330-341.

Hill, R. J., 1989. Implications of Monin-Obukhov similarity theory for scalar quantities. J. Atm. Sci., **46**, 2236-2244.

Hill, R. J., Clifford, S. F, Lataitis, R. J. and Sarma, A. D., 1990. Scintillation of millimeter-wave intensity and phase caused by turbulence and precipitation. Atmospheric propagation in the UV, visible, IR and MM-wave region and related systems aspects. AGARD conference proceed. 454, Copenhagen, Denmark.

Hill, R. J., Ochs, G. R. and Wilson, J. J, 1992a. Measuring surface-layer fluxes of heat and momentum using optical scintillation. Boundary-Layer Meteorol., **58**, 391-408.

Hill, R. J., 1992b. Review of optical scintillation methods of measuring the refractive-index spectrum, inner scale and surface fluxes. Waves in Random Media, **2**, 179-201.

Hill, R. J., 1997. Algorithms for obtaining atmospheric surface-layer fluxes from scintillation measurements. J. Atmos. Ocean. Tech. **14**, 456-467.

Ho, K. L., Mavrokoukoulakis, N. D. and Cole, R. S., 1979. Propagation studies on a line-of-sight microwave link at 36 GHz and 110 GHz. Microwave Optics and Acoustics, **3**, 93-98.

Hoedjes, J.C.B. and R.M. Zuurbier, 1999. Measuring areal-averaged surface fluxes over heterogenous terrain and the influence of moisture- and temperature correction terms using Scintillometers, MS-Thesis,. Wageningen University and Research, Meteorology and Air Quality Group Center., 47 pp.

Hoedjes, J.C.B. and Zuurbier, R.M, 2000. Measuring surface fluxes over an irrigated wheat field using a Large Aperture Scintillometer and determination of universal functions using structure parameters and variance methods, Ms-Thesis Wageningen University Research Centre, Dept. Environmental Sciences, Meteorology and Air Quality Group.

Hojstrup, J., 1981. A simple model for adjustment of velocity spectra in unstable conditions downstream of an abrupt change in roughness and heat flux. Boundary-Layer Meteorol., **21**, 341-356.

Hufnagel, R. E. and Stanley, N. R., 1964. Modulation transfer function associated with image transmission through turbulent media. J. Optical Soc. Am., **54**, 52-61.

Lawrence R.. S. and Strohbehn, J. W., 1970. A survey of clear-air propagation effects relevant to optical communications. Proceedings of the IEEE, **58**, 1523-1545.

Kaimal, J. C., Wyngaard, J. C., Izumi, Y. and Cote, O. R., 1972. Spectral characteristics of surface-layer turbulence. Quart. J. R. Met. Soc., **98**, 563-589.

Kaimal, J. C., Wyngaard, J. C., Haugen, D. A., Cote, O. R. and Izumu, ., 1976. Turbulence structure in the convective boundary layer. J. Atmos. Sci., **33**, 2152-2169.

Kaimal, J. C. and Finnigan, J. J., 1994. Atmospheric Boundary Layer Flows: Their Structure and Measurement. Oxford University Press Inc., New York.

Kohsiek, W., 1982a. Optical and in situ measuring of structure parameters relevant to temperature and humidity and their application to the measuring of sensible and latent heat flux. NOAA tech. Mem. ERL WPL-96.

Kohsiek, W., 1982b. Measuring C_T^2, C_Q^2, and C_{TQ} in the unstable surface layer, and relation to the vertical fluxes of heat and moisture. *Boundary-Layer Meteorol.*, **24**, 89-107.

Kohsiek, W. and Herben, M. H. A. J., 1983. Evaporation derived from optical and radio wave scintillation. Appl. Opt., **22**, 629-633.

Kohsiek, W., 1984. Inertial subrange correlation between temperature and humidity fluctuations in the unstable surface layer above vegetated surfaces. Boundary-Layer Meterolo., **29**, 211-224.

Kohsiek, W., 1985. A comparison between line-averaged observation of C_n^2 from scintillation of a laser beam and time-averaged in situ observations. *J. Climate and Appl. Meteorol.*, **24**, 1099-1102.

Kolmogorov, A. N., 1941. Dissipation of energy in locally isotropic turbulence. Doklady Akad. Nauk. SSSR, **32**, 16.

Kunkel, K. E. and Walters, D. L., 1983. Modelling the diurnal dependence of the optical refractive index structure parameter. J. Geophys. Res., **88** (C15), 10999-11004.

Lagouarde, J-P. and McAneney, K. J., 1992. Daily sensible heat flux estimation from a single measureemnt of surface temperature and maximum air temperature. Boundary-Layer Meterol., **59**, 341-362.

Lagouarde, J-P, McAneney, K. J and Green, A. E., 1996. Scintillometer measurements of sensible heat flux over heterogeneous surfaces. In: J. B. Stewart, E. T. Engman, R. A. Feddes and Y. Kerr (Editors), Scaling up in

hydrology using remote sensing. Institute of Hydrology, Wallingford, U.K., pp. 147-160.

Lawrence, R. S. and Strobehn, J. W., 1970. A survey of clear-air propagation effects relevant to optical communications. Proceedings of the IEEE ,**58**, 1523-1545.

McAneney, K. J., Green, A. E. and Astill, M. S., 1995. Large-aperture scintillometry: the homogeneous case. Agric. For. Meteorol., **76**, 149-162.

McMillan, R. W., Bohlander, R. A., Ochs, G. R., Hill, R. J. and Clifford, S. F., 1983. Millimetre wave atmospheric turbulence measurements: preliminary results and instrumentation for future measurements. J. Opt. Eng., **22**, 32-39.

Meininger, W. M. L. and De Bruin, H. A. R., 2000. The sensible heat fluxes over irrigated areas in Western Turkey determined with a large aperture scintillometer. J. Hydrology, **229**, 42-49.

Meininger, W.M. L., 2001. In preparation.

Moeng, C-H., 1998. Large-eddy Simulation of the Atmospheric Boundary Layers, in *'Clear and Cloudy Boundary Layers'*, Holtslag, A.A.M. and Duynkerke, P.G. Eds., 67-83.

Monin, A. C. and Obukhov, A. M., 1954. Basic laws of turbulent mixing in the atmosphere near the ground. Trudy, Akademiia Nauk SSSR, Geofizicheskogo Instituta.

Moulsley, T. J. and Vilar, E., 1982. Experimental and theoretical statistics of microwave amplitude scintillations on satellite down-links. IEEE Trans. on Antennas and Propagation, **30**, 1099-1106.

Nappo, C.J. and Johansson, P-E., 1999. Summary of the Lövånger International Workshop on Turbulence and Diffusion in the Stably Stratified Planetary Boundary Layer. Boundary-Layer Meteorol., **90**, 345-374.

Nieveen, J. P., Green, A. E. and Kohsiek, W., 1998. Using a large-aperture scintillometer to measure absorption and refractive index fluctuations. Boundary-Layer Meteorol., **87**, 101-116.

Nieveen, J. P. and Green, A. E., 1999. Measuring sensible heat flux density over pasture using the C_T^2 -profile method. Boundary-Layer Meteorol., **91**, 23-35.

NOPEX-WINTEX: http://www.hyd.uu.se/nopex.

Ochs, G. R. and Cartwright, W. D., 1980. Optical system IV for space-averaged wind and C_n^2 measurements. NOAA Tech, Memo. ERL WPL-52, NOAA, Bo., CO, 31 pp.

Ochs, G. R., Holler, J. K. and Wilson, J. J., 1990. An optical inner scale meter. NOAA Tech. Memo. ERL-183, NOAA WPL, Bo. CO., 18 pp.

Ott, R. H. and Thompson, M. C., 1978. Atmospheric amplitude spectra in an absorption region. Trans. on Antenn. and Prop., **AP-26**, 329-332.

Panofsky, H. A. and Dutton, J. A., 1984. Atmospheric turbulence: Models and methods for engineering applications. Wiley, New york, 397 pp.

Peltier, L. J. and Wyngaard, J. C., 1995. Structure-function parameters in the convective boundary layer from large-eddy simulation. J. Atmos. Sci., **52**, 3641-3660.

Priestey, C. H. B. and Taylor, R. J., 1972. On the assessment of surface heat flux and evaporation using large scale parameters. Mon. Weather Rev., **100**, 81-92.

Priestley, J. T. and Hill, R. J., 1985. Measuring high-frequency humidity, temperature and radio refractive index in the surface layer. J. Atmos. and Oceanic Tech., **2** (2), 233-251.

Schuepp,P. H., Leclerc, M. Y., Macpherson, J. I. and Desjardins, R. L., 1990. Footprint prediction of scalar fluxes from analytical solutions of the diffusion equation. Boundary-Layer Metorol., **50**, 355-373.

Sene, K. J., 1994: Parameterizations for energy transfers from a sparse vine crop. *Ag. and Forest Meteorol.*, **71**, 1-18.

Sequin, B., Assad, E., Imbernon, J. P., Kerr, Y. and Lagouarde, J-P., 1989. Use of meteorological satellites for water balance monitorong in Sahelian regions. Int. J. remote sensing., **10**, 1101-1117.

Stanhill, G., 1969. A simple instrument for the field measurement of turbulent diffusion flux. J. Applied Meteorlo., **8**, 509-513.

Stewart, J. B., Engman, E. T., Feddes, R. A. and Kerr, Y. (eds), 1996. Scaling up in hydrology using remote sensing. Wiley, Chichester, 255 pp.

Strohbeln, J. W., 1968. Line-of-sight wave propagation through the turbulent atmosphere. Proceedings of the IEEE, **57**, 703-704.

Stull, R. B., 1988: An Introduction to Boundary Layer Meteorology. Kluwer Academic Publishers, The Netherlands.

Roerink, G.J.,Su, Z. and Menenti, M., 1999. *S-SEBI*: A Simple Remote Sensing ALgorithm to Estimate the Surface Energy Balance, Phy.Che. Earth (B), Vol. 25,no2, 147-157.

Tanner, C. B. and Pelton, W. L., 1960. Potential evapotranspiration estimates by the approximate energy balance method of Penman. J. Geophys. Res., **65**, 3391-3413.

Tanner, B. D., Tanner, M. S., Dugas, W. A., Campbell, E. C. and Bland, B. L., 1985. Evaluation of an operational eddy correlation system for evapotranspiration measurements. National Conference on Advances in Evapotranspiration American Society of Agricultural Engineers, Chicago, IL, Decemeber 16-17.

Tatarskii, V. I., 1961. *Wave propagation in a turbulent medium.* McGraw-Hill, NY.

Tatarskii, V. I., 1993. Review of scintillation phenomena. In: V. I. Tatarskii, A. Ishimaru and V. U. Zavorotny (eds), Wave propagation in random media (scintillation). Co-published by SPIE, Bellingham, Washington, USA.

Tennekes, H. and Lumley, J. L., 1972. *A first course in turbulence.* MIT Press, Cambridge, Mass., 300 pp.

Thiermann, V. and Azoulay, E., 1989. Modelling of structure constants and inner scale of refractive-index fluctuations – an experimental investigation. Proc. SPIE, **1115**, 124-135.

Thiermann, V. and Grassl, H., 1992a. The measurement of turbulent surface-layer fluxes by use of bichromatic scintillation. Boundary-Layer Meteorol., **58**, 367-389.

Thiermann, V., 1992b. A displaced beam scintillometer for line-averaged measurements of surface layer turbulence. Tenth Symposium on Turbulence and Diffusion, Am. Meteorol. Soc., Portland, OR., Sept. 29th-Oct. 2nd.

Time, N. S., 1972. Estimation of the turbulence spectrum in the dissipation range from measurements of laser-light fluctuations. J. Atmos. Ocean. Phys., **8**, 48-59.

Wang, Ting-i, Ochs, G. R. and Clifford, S. F., 1978. A saturation-resistant optical scintillometer to measure C_n^2. J. Opt. Soc. Am., **68**, 334-338.

Weseley, M. L. and Alcaraz, E. C., 1973. Diurnal cycles of the refractive index structure function coefficient. J. Geophysical Research., **78**, 6224-6232.

Weseley, M. L., 1976a. A comparison of two optical methods for measuring line averages of thermal exchanges above warm surfaces. J. Appl.. Meteorol., **15**, 1177-1188.

Weseley, M. L., 1976b. The combined effect of temperature and humidity fluctuations on refractive index. J. Appl. Meteorol., **15**, 43-49.

Wieringa, J., 1986. Roughness-dependant geographical interpolation of surface wind speed averages, Quart. J. R. Meteorol. Soc., **112**, 867-889.

Williams, R. M and Paulson, C. A., 1977. Microscale temperature and velocity spectra in the atmospheric boundary layer. J. Fluid Mechanics, **83**, 547-567.

Wyngaard, J. C., Izumi, Y. and Collins, S. A., 1971a. Behaviour of the refractive-index structure parameter near the ground. J. Opt. Soc. Am., **61**, 1646-1650.

Wyngaard, J. C. and Cote, O. R., 1971b. The budgets of turbulent kinetic energy and temperature varaiance in the atmospheric surface layer. J. Atmos. Sci., **28**, 190-201.

Wyngaard, J. C. , 1973. On surface layer turbulence. Workshop on micrometeorology, Am. Meteorol. Soc., Boston, MA: 101-148.

Wyngaard, J. C. and Clifford, S. F., 1978. Estimating momentum, heat and moisture fluxes from structure parameters. J. Atm. Sci., **35**, 1204-1211.

Wyngaard, J. C and LeMone, M. A., 1980: Behaviour of the refractive index structure parameter in the entraining convective boundary layer. *J. Atm. Sci.*, **37**, 1573-1585.

Curriculum Vitae

Geboren op 15 december 1955 in Auckland, Nieuw Zeeland. Groeide op in de plattelands steden Taupo en Taradale en genoot tussen 1969 en 1973 zijn middelbareschoolopleiding aan de 'Napier Boys High School'. Haalde in 1976 zijn BSc graad in de fysica en een postdoctoraal diploma in de landbouw wetenschappen aan de Massey University in Palmerston North. Werkte van 1977 tot 1983 voor de landbouwfysische groep van het DSIR. In 1983 verhuisde hij naar Auckland en werkte daar tot 1988 voor verschillende elektronica firma's. In 1988 verhuisde hij naar Kerikeri en ontwikkelde daar snelle instrumenten om turbulente grootheden te meten voor het Ministerie van Landbouw. Verkaste in 1992 naar de Horticultural and Food Research Institute of New Zealand alwaar hij uitgebreid aan scintillometers werkte. Tijdens buitenlandse avontuurtjes werkte hij bij het KNMI en Wageningen Universiteit in Nederland en het NIAES in Japan. Tegenwoordig is hij technisch directeur van MicroMet Scientific.